Fourth International Colloquium on

Nonlinear Dynamics and Control of Deep Drilling Systems

Stavanger, May 14-16, 2018

Pulpit Rock

Proceedings edited by

U.J.F. Aarsnes
E. Detournay
N. van de Wouw
V. Denoël

IRIS

Fourth International Colloquium on

Nonlinear Dynamics and Control of Deep Drilling Systems

Ulf Jakob Flø Aarsnes,
Nathan van de Wouw,
Emmanuel Detournay,
Vincent Denoël
Editors

Stavanger, Norway
May 14-16th, 2018

Cover Photo: Shutterstock

Rectification:

This version of these proceedings are a rectified version of an earlier version of the proceedings. The abstract EFFECTIVENESS ANALYSIS OF ANTI STICK-SLIP TOOLS has been removed from the proceedings as it did not carry the full consent of all partners involved in the research project from which the abstract resulted. Authors agreed that some of the outcomes of the paper require further investigations and clarifications.

Foreword

This Colloquium is a follow-up of the meetings on the same topics, held at the University of Liége, Belgium, in 2009, at the Eindhoven University of Technology, The Netherlands, in 2012 and at the University of Minnesota, U.S.A., in 2014. The "control" part of the name was added at the second Colloquium to underline the two main themes.

For this Colloquium, four main domain themes were specified:

- Underbalanced Operations & Managed Pressure Drilling (UBO/MPD)
- Drill String Vibrations & Drilling Mechanics
- Geosteering & Borehole Propagation
- Drilling Automation & ROP Optimization

In keeping with the previous incarnations, however, most submissions have been focused on drill-string vibrations.

It has been the aim of the organizing committee to strive for the correct blend between industry and academia participation, and between the theoretical depth and the practical relevance of the submissions. This to ensure that the colloquium can provide an arena where the practitioners can learn what relevant theoretical tools are available, while providing feedback so as to keep the research focused and relevant to applications where it can provide value. Judging from the content of these proceedings, we believe we have succeeded in this goal. It contains both descriptions of problems encountered in the field, new developments on known problems, as well as proposing novel solutions through employment of sophisticated mathematical methods. Together, these proceedings, we truly believe, reflect the state of the art of Nonlinear Dynamics and Control of Deep Drilling Systems.

Ulf Jakob Flø Aarsnes, Nathan van de Wouw,
Emmanuel Detournay and Vincent Denoël

Acknowledgements

We gratefully acknowledge financial support for this colloquium by TOMAX, Schlumberger, Sperry Drilling, ExonMobil and Halliburton Drill Bits & Services. We are also indebted Mette Stokseth Myhre for help with logistics and financial matters and Mona Winge for her help with the Colloquium website.

Program

Monday May 14
Drill String Modeling

12:00	*Lunch*
13:00	Opening
13:10	*Keynote: Is it time to start using open source models to solve drill string dynamics issues?* Paul PASTUSEK and Greg PAYETTE
13:50	*Coffee break*
14:10	*Drill-string Dynamics in Deviated Wells in the Presence of Heave* Eric CAYEUX
14:50	*The importance of Physics in Drill String modelling* Bernt Sigve AADNØY and Dan SUI
15:30	*Coffee break*
15:50	*Semi-analytical models of the oil-well drillstring* Sigve HOVDA
16:30	*High frequency torsional oscillations in BHAs: Examples and Theory* Benjamin JEFFRYES, Zhengxin ZHANG, Yuelin SHEN, Wei CHEN, Jibin SHI, Wesley BONSTAFF, Kien TANK, David L. SMITH and Yezid AREVALO
19:00	*Dinner*

Tuesday May 15

Self excited vibrations

8:00	*Breakfast*
9:00	*State-Dependent Delay Effect in Drilling* Xie ZHENG, Vipin AGARWAL and Balakumar BALACHANDRAN
9:40	*Effect of compression and torsion on the stability of drilling processes* Bence BERI and Gabor STEPAN
10:20	*Coffee break*
10:40	*Improving stability of steady drilling using a non-uniform distribution of cutters on the drill-bit* Sunit Kumar GUPTA and Pankaj WAHI
11:20	*Influence of Bit Design on the Stick-slip Vibrations of a Rotary Drilling System* Kaixiao TIAN and Emmanuel DETOURNAY
12:00	*Lunch*
13:00	*Effectiveness Analysis of Anti Stick-Slip Tools* Dapeng ZHAO
13:40	*Drilling experiment to determine the efficiency of a second generation downhole drilling regulator* Nils REIMERS
14:20	*Excursion to Pulpit Rock: 7,6km with 330m altitude gain (4-5 hours) walk.*
20:00	*Dinner*

Wednesday May 16

Control of drilling systems

8:00	*Breakfast*
9:00	*Drilling Automation – Some Industrial Challenges and Solutions* John-Morten GODHAVN and Espen Hauge
9:40	*Control-Oriented Modeling and Model Order Reduction for Managed Pressure Drilling Systems* Sajad NADERI LORDEJANI, Bart BESSELINK, Momhammad H. ABBASI, Glenn-Ole KAASA, Wil H. A. SCHILDERS and Nathan van de WOUW
10:20	*Coffee break*
10:40	*Performance and stability limits of distributed pressure control due to resonance caused by wave propagation* Glenn-Ole KAASA
11:20	*Nonlinear Modeling of Directional Drilling* Fahim SHAKIB, Emmanuel DETOURNAY and Nathan van de WOUW
12:00	*Lunch*
13:00	*Effects of latency, motor inertia and filtering on stick-slip mitigation control* Roman J. SHOR, Ulf Jakob F. AARSNES and Florent DI MEGLIO
13:40	*Advances in control of Hyperbolic Partial Differential Equations: opportunities for drilling* Florent DI MEGLIO, Ulf Jakob F. AARSNES and Roman J. SHOR
14:20	*Closing*

Contents

Is it time to start using open source models to solve drill string dynamics issues?

Paul Pastusek[1] and Greg Payette[2]

[1]ExxonMobil Development Co., [2]ExxonMobil Upstream Research Co.

1 Objective

The objective of modeling and measuring drilling dynamics and control systems is to enable the industry to drill a round, ledge free hole, without patterns, with minimum vibration, minimum unplanned dog legs, that reaches all directional and geological targets in one run per section at the fastest penetration rate possible.

2 Background

Starting in 1960 and before there have been hundreds of technical papers, models, and experiments on drilling dynamics. The detailed equations of many of these models have been published, but few have been re-used or extended except by the original investigator or group. A few of the notable historical model papers are: [4, 8, 9, 11, 16, 21, 22, 26, 27, 30, 31, 34, 35, 38, 47]. A brief literature review found more than 160 highly relevant references. Several recent model papers that are very well documented are: [1, 3, 5, 7, 12, 13, 14, 17, 20, 23, 24, 25, 29, 32, 33, 36, 37, 40, 41, 42, 43, 44, 45, 46, 50, 52, 54, 55, 56, 58, 59, 60].

While the industrys understanding of dynamics has significantly improved based in large part on the prior art, the models describing the system have often been recreated from scratch by each researcher and often focus on just one element of the system.

Compare this to the electronics industry, which created the open source program SPICE (Simulation Program with Integrated Circuit Emphasis) in 1973 [48]. SPICE has allowed each research organization and commercial vendor to add verifiable elements to SPICE that are usable by the entire industry to model the complete system.

The proposal is to create a Simulation Program for Understanding and solving Drilling Dynamics problems (SPUDD), or some other suitable acronym. It should be open source containing reusable open source elements defined by research organizations, tool vendors, and service companies. If each researcher and user do not have to start from a blank sheet to recreate their own models this will significantly speed up the industrys ability to create and maintain knowledge on the system dynamics.

It is not enough to react to vibrations and hole quality issues once drilling has started, but to design, model, and verify that the system will achieve these objectives before the first bit goes through the rotary table. [10, 50]

3 Model Requirements

At highest level there are three things needed to make a model reusable:

- The model itself: open source code shared in a publicly available repository.
- A users guide: how to run the core software, how to extend software capabilities (i.e., plug in new features, add new elements).
- A theory manual: to explain how the system works, its assumptions, and known limitations.

Below are more detailed criteria that should be considered in development of the general framework:

- **Modeling Scope/Complexity:** The development community will need to determine appropriate scope for the numerical formulation. The formulation(s) should be able to handle various levels of complexity. Below are listed some basic categories that ought to be considered and expanded upon by the development community:
  - Soft-string without buckling:
    - Quasi-static/steady-state (with or without rotation but no vibration)
    - Dynamic frequency domain.
    - Dynamic time domain.
  - Soft-string with buckling based on buckling formulas:
    - Quasi-static/steady-state (with or without rotation but no vibration).
    - Dynamic frequency domain.

    * Dynamic time domain.
  - Stiff-string:
    * Quasi-static/steady-state (with or without rotation but no vibration).
    * Dynamic frequency domain with linearization about a baseline stiff-string solution.
    * Dynamic time domain. Full non-linear solution at every time step or linearization about some baseline stiff-string solution and solved for dynamic perturbations (i.e., solve for the baseline solution once or infrequently).

- **Input Files:** These define what data is required as input to the framework and how to generate the input file(s). Text based input files with data inputs arranged in a standardized readable format are probably the most straight-forward means of providing the necessary inputs to the computational engine of the framework. The input files will likely include the following information:
  - Wellbore parameterization.
  - Drill string discretization.
  - Material and geometric properties for drill string components.
  - Drilling fluid properties.
  - Bit-rock interaction inputs.
  - Drill string environment interaction inputs.
  - Boundary conditions at the surface and the bit.

- **Output Files:** Like the input files, it will be important to prescribe a standardized format. Ideally, the format would be readable by a number of visualization programs or could easily be reprocessed to be compatible with such software (e.g., Matlab, Python, Tecplot, ParaView, EnSight, etc.). It is expected that the output file will include the following information:
  - Computed generalized displacements: displacements axial and lateral; rotations bending and twist.
  - Computed generalized internal forces: forces tension, shear; moments bending, torque; contact forces; friction forces.
  - Velocities and accelerations.
  - Stresses.

The (discrete) output contained in the output files should be sufficient to compute the state of the system at any point along the drill string at any given time. This should further allow a user of the software to place virtual sensors along the drill string.

- **Post Processing / KPIs:** It would be helpful for the development community to establish useful KPIs (key performance metrics) for interpreting time-based simulation results. A general suite of signal processing tools (spectral analysis, etc.) and energy approaches may prove to be useful for such an effort.

- **Stability:** The computational framework should be numerically stable. Sources of potential numerical instability may arise in: (a) the implementation of the contact problem when modeling bending effects (i.e., stiff-string analysis) and/or (b) the time integration procedure adopted for modeling dynamics.

- **Accuracy:** The framework should produce numerical results that accurately approximate the governing equations of the system. The user should be able to adjust the resolution of the spatial and temporal discretization procedures, but in general the system framework should guide the user to use the most appropriate discretization.

- **Computational Efficiency:** The framework should be computationally efficient. Advanced modern computational procedures and open source libraries should be adopted whenever possible. For example if the discretization procedure for the numerical framework leads to a sparse system of linear algebraic equations, open source linear solvers should be used, see for example Davis 1997 which describes the UMFPACK linear sparse equation solver (`http://faculty.cse.tamu.edu/davis/suitesparse.html`). Parallel computing capabilities should be considered in all aspects of the computational framework. The development community should seek to find the most efficient algorithms for solving the stiff-string contact problem that is both stable and computationally efficient.

- **Flexibility/Customization:** The framework should be flexible enough to be able to easily accommodate modifications. In particular, it should be relatively straightforward to model custom elements or tools within the drill string such as mud motors, axial oscillation systems, shock subs and torsional-axial spring devices.

- **Boundary Conditions:** The framework should allow for the implementation of simple as well as complicated boundary conditions. A user of

the software should be able to very easily implement custom boundary conditions at the bit and BHA (bit-rock interaction, reamer tools) and at the surface (rig compliance, auto-driller, active torsional damping, wave motion and heave compensation systems).

- **Along String Interactions with Environment:** It should be easy to implement interactions with the borehole (contact, different friction models), cuttings beds (friction) and drilling fluid effects. The framework should be able to accommodate these interactions with the drilling system in in the time domain or the frequency domain. For frequency domain implementations, the along string interactions with the environment may depend on prescribed excitation frequencies and potentially have a phase angle offset relative to the excitation frequencies.

4 Contributions to Open Source Code

Who would contribute their core modules? Based on other open source initiatives there are three common sources of main code, universities, national laboratories, and private companies. Universities get the benefit of citation rights, industry recognition, graduates with highly desirable skills. National labs already make a fair amount of their source code open source. Companies who donate code to open source often find it too expensive to support their private code and/or that the code itself is not their key market advantage. A number of open source software examples exist in the oil industry, just not yet in drilling [6, 15, 19, 39, 51, 53].

Theoretical extensions would come from a variety of sources. Universities and students could validate and extend the base code. Some areas of study might be: different stiff string methods of implementation, work on stability improvements, and contact problems. Also, there are a host of friction laws that have been proposed. Can these be measured and verified? Are any of these significantly better than others?

New components and refinements of existing component models could be published by vendors wanting to demonstrate the benefit of a particular tool to get it more rapidly adopted into the industry and to understand its limitations.

The boundary conditions can be modeled by vendors for these systems and these elements can be used and reused others. In addition, theoretical models of ideal components can be tested to evaluate the effect of a proposed component improvement.

A number of parameter studies could be completed by anyone in the user group. These would increase the understanding of potential operational limits of

tools and the system, identify best practices, as well as uncover potential model limitations.

Modeling expertise would be distributed throughout the industry to universities, consultants, service companies, and operators.

5 Proprietary Models

Does this compete with or enhance proprietary models? Proprietary models can and will always exists. Open source code and open source elements allow individual users to run their proprietary tools and models and compare the results to show the benefit of the extra fidelity. It is up to each company and researcher to keep their individual intellectual property and to publish only what they want to share.

However, with access to open source elements for the rest of the drill string and boundary conditions, complex elements that currently have to be constructed from scratch by every researcher can be included in the models evaluated to improve the fidelity of the results. These elements will have the benefit of industry input and review.

Service companies can model the system to show how their tool affects the entire system performance. When a product or service is commercialized it will reduce the risks to operators, contractors, and service companies if the tools have been run in a qualified simulation before running in the well. Once considered, it seems unforgivable to run a tool in the ground without knowing its effects on the entire system. To go back to the SPICE analogy, it would be as if a new component were substituted in an electronic circuit, plugged in, and turned on to see what will happen. In many cases it seems that this is what we do today with new tool trials in the oilfield.

6 Third Party Experts

It is estimated that less than 10% of drill strings that are put into the ground are modeled for dynamic stability. Making the code and elements open source would make models that are easier to use and understand. The number of drill stings evaluated will get significantly larger and there will be a growing need for third party modeling services.

This framework provides the inputs, outputs and engine but still allows others to wrap a user interface around it that is easy to use and best accommodates the workflows of whoever the user is. An example of this from the software industry is what Red Hat has done with Linux. They provide a product with support

that leverages an open source operating system i.e., Linux. In short, operators pay for the modeling expertise, the output and understanding, not the model itself.

7 Challenges / Barriers

There are two barriers that are often cited: Intellectual Property and Liability. The open source community has resolved the Intellectual Property issue by making the original code the property of the original contributor with public use rights given to everyone. GitHub is one sharing site where modifications and improvements are tracked and credit is given to those who contribute to the code improvements.

For drilling dynamics models there are many examples where all of the equations used in the code are published, just not the code itself. There is no IP held back in these examples, publishing the code will just make it easier to extend the original work rather than reproduce it. There are a number of ways to limit the liability of publishing code. An example is the GNU General Public License. It includes a long standing disclaimer of warranty and a limitations of liability. The original version of this license dates to 1989 and the current version was issued in 2007 [28].

8 The Next Steps

One study of open source initiatives evaluated those that succeeded vs those that failed [57]. One of the keys to success was the industry standing and social network of those proposing the effort. It is suggested that a guiding coalition be formed from industry leaders in dynamics. Those willing to support this effort could;

- propose joint papers for journals promoting this open source concept
- encourage use and reuse of the models
- review code
- review and critique published results
- provide mentorship to those getting started

Remaining steps are to:

- Publish this effort in SPE, IEEE, ASME, Journal of Acoustics and Vibration, or other journals to ask for donations of code and attract talent the cause.
- Set up a repository for code and documentation. GitHub is currently in use for many open source initiatives and has a large existing user community. Are there better options?
- Start using, reviewing, and improving the code submitted [2].

If you agree with this effort please add your name to a guiding coalition. The coalition can help to determine where to go from here [49]. This effort could include any of the following and more:

- Formal technical reviews of code options
- Annual user group meetings
- SPE Technical Sections
- Colloquium meetings
- Joint Industry Program

9 Conclusions

- The industry has been studying and trying to solve drill string vibration issues for 60 years. One of the key impediments to major improvements is the difficulty in building on the models of prior research.
- As a group we can challenge the industry to create an open source, sharable, expandable model of drilling systems.
- It is not enough to react to vibrations and hole quality issues once drilling has started, but to design, model, and verify that the system will achieve these objectives before drilling starts.

References

[1] Aarsnes, U., van de Wouw, N., *Dynamics of a distributed drill string system: Characteristic parameters and stability maps*, Journal of Sound and Vibration, Volume 417, 2018, Pages 376-412.

[2] Adewumi, A., Misra, S., Omoregbe, N., *A Review of Models for Evaluating Quality in Open Source Software*, IERI Procedia 4 (2013) 88-92, 2013 International Conference on Electronic Engineering and Computer Science

[3] Al-Hiddabi, S.A., Samanta, B., Seibi, A., *Non-linear control of torsional and bending vibrations of oilwell drillstrings*, Journal of Sound and Vibration, Volume 265, Issue 2, 2003, Pages 401-415.

[4] Angona, F.A., *Drill String Vibration Attenuation and Its Effect on a Surface Oscillator Drilling System*, Journal of Engineering for Industry Trans. ASME No. 64-Pet-5, May 1965

[5] Aslaksen, H., Annand, M., Duncan, R., Fjaere, A., Paez, L., & Tran, U. *Integrated FEA Modeling Offers System Approach to Drillstring Optimization*, Society of Petroleum Engineers. doi:10.2118/99018-MS (2006, January 1)

[6] Babaei, H., Baker, S., Cornett, A., *Validation of an Open-source CFD Tool to Support Efficient Design of Offshore Gravity-based Structures Exposed to Extreme Waves*, ISOPE-1-17-641, Proceedings of the Twenty-seventh (2017) International Ocean and Polar Engineering Conference, San Francisco, CA, June 25-30, 2017, 662-669

[7] Bailey, J. R., Elsborg, C. C., James, R. W., Pastusek, P., Prim, M. T., & Watson, W. W. *Design Evolution of Drilling Tools To Mitigate Vibrations*, Society of Petroleum Engineers, doi:10.2118/163503-PA, 2013, December 1

[8] Bailey, J.J., Finnie, I., *An Analytical Study of Drill-String Vibration*, Journal of Engineering for Industry, Tran. ASME, Vol. 82, Series B, No. 2, May 1960

[9] Baird, J. A., Caskey, B. C., Tinianow, M. A., & Stone, C. M. . *GEODYN: A Geological Formation/Drillstring Dynamics Computer Program*, Society of Petroleum Engineers. doi:10.2118/13023-MS (1984, January 1)

[10] Bhardwaj, V.K., Bello, O., Aragall, R., Oppelt, J., *Drilling Process Simulation: Status, Outlooks and Comparisons to Other Industries*, SPE-181040-MS, presented at the SPE Intelligent Energy International Conference and Exhibition, in Aberdeen, UK, 6-8 September 2016

[11] Birades, M. *Static and Dynamic Three-Dimensional Bottomhole Assembly Computer Models*, Society of Petroleum Engineers. doi:10.2118/15466-PA (1988, June 1)

[12] Butlin, T., Langley, R.S., *An efficient model of drillstring dynamics*, Journal of Sound and Vibration, Volume 356, 2015, Pages 100-123.

[13] Cayeux, E. . *Reconstruction of Pipe Displacement Based on High-Frequency Triaxial Accelerometer Measurements*, Society of Petroleum Engineers. doi:10.2118/189618-MS (2018, March 6)

[14] Chen, D. C.-K. *Developing and Field Implementation of a State-of-the-Art BHA Program*, Society of Petroleum Engineers. doi:10.2118/107238-MS (2007, January 1)

[15] Chubak, G., Morozov, I., *Open-source system for geophysical data processing and visualization*, SEG-2007-2060, San Antonio 2007 Meeting, 2060-2063

[16] Daering, D.W., Livesay, B.J., *Longitudinal and Angular Drill-String Vibrations With Damping*, Journal of Engineering for Industry, Trans ASME, November 1968, 671-679

[17] Dakel, M., Baguet, S., Dufour, R., *Nonlinear dynamics of a support-excited flexible rotor with hydrodynamic journal bearings*, Journal of Sound and Vibration, Volume 333, Issue 10, 2014, Pages 2774-2799.

[18] Davis, T.A., Duff, I.S., *An unsymmetric-pattern multifrontal method for sparse LU factorization*, SIAM J. Matrix Anal. Appl., vol. 18, pp. 140158, 1997.

[19] De Groot, P., Bril, B., *The Open Source model in GeoSciences and OpenTect in particular*, SEG-2005-0802, Houston 2005 Annual Meeting, 802-805

[20] Downton, G. C., *Systems Modeling and Design of Automated Directional Drilling Systems*, Society of Petroleum Engineers. doi:10.2118/170644-MS (2014, October 27)

[21] Dunayevsky, V. A., Abbassian, F., & Judzis, A., *Dynamic Stability of Drillstrings Under Fluctuating Weight on Bit*, Society of Petroleum Engineers. doi:10.2118/14329-PA (1993, June 1)

[22] Dykstra, M.W., *Nonlinear Drill String Dynamics*, Thesis (Ph.D.) University of Tulsa1996, 260 pages

[23] Dykstra, M. W., Neubert, M., Hanson, J. M., & Meiners, M. J., *Improving Drilling Performance by Applying Advanced Dynamics Models*, Society of Petroleum Engineers. doi:10.2118/67697-MS (2001, January 1)

[24] Elliott, A. S., & Hutchinson, M., *Fully-Coupled Nonlinear 3-D Time-Domain Simulation of Drilling Dysfunctions Using a Multi-Body Dynamics Approach*, Society of Petroleum Engineers. doi:10.2118/173154-MS (2015, March 17)

[25] Ertas, D., Bailey, J. R., Wang, L., & Pastusek, P. E., *Drillstring Mechanics Model for Surveillance, Root Cause Analysis, and Mitigation of Torsional and Axial Vibrations*, Society of Petroleum Engineers. doi:10.2118/163420-MS (2013, March 5)

[26] Fischer, F. J., *Analysis of Drillstrings in Curved Boreholes*, Society of Petroleum Engineers. doi:10.2118/5071-MS (1974, January 1)

[27] Fox, F. K., & Nasir, N., *Drill Collar String Design And Its Effect On Drilling M.E.R*, Society of Petroleum Engineers. doi:10.2118/501-MS, (1963, January 1)

[28] GNU General Public License, [Online Wikipedia] GNU General Public License is a free software license originally written by Richard Stallman, Available at: `https://en.wikipedia.org/wiki/GNU_General_Public_License` [Accessed 04-09-2018] (2018)

[29] Gupta, S.K., Wahi, P., *Global axialtorsional dynamics during rotary drilling*, Journal of Sound and Vibration, Volume 375, 2016, Pages 332-352.

[30] Halsey, G. W., Kyllingstad, A., Aarrestad, T. V., & Lysne, D., *Drillstring Torsional Vibrations: Comparison Between Theory and Experiment on a Full-Scale Research Drilling Rig*, Society of Petroleum Engineers. doi:10.2118/15564-MS (1986, January 1)

[31] Ho, H.-S., *General Formulation of Drillstring Under Large Deformation and Its Use in BHA Analysis*, Society of Petroleum Engineers. doi:10.2118/15562-MS (1986, January 1)

[32] Hohl, A., Herbig, C., Arevalo, P., Reckmann, H., & Macpherson, J., *Measurement of Dynamics Phenomena in Downhole Tools - Requirements, Theory and Interpretation*, Society of Petroleum Engineers. doi:10.2118/189710-MS (2018, March 6)

[33] Hovda, S., *Semi-analytical model of the axial movements of an oil-well drillstring in vertical wellbores*, Journal of Sound and Vibration, Volume 417, 2018, Pages 227-244.

[34] Jogi, P. N., Burgess, T. M., & Bowling, J. P., *Predicting the Build/Drop Tendency of Rotary Drilling Assemblies*, Society of Petroleum Engineers. doi:10.2118/14768-PA (1988, June 1)

[35] Kalsi, M. S., Wang, J. K., & Chandra, U. (1987, March 1), *Transient Dynamic Analysis of the Drillstring Under Jarring Operations by the FEM*, Society of Petroleum Engineers. doi:10.2118/13446-PA

[36] Kamel, J.M., Yigit, A.S. *Modeling and analysis of stick-slip and bit bounce in oil well drillstrings equipped with drag bits*, Journal of Sound and Vibration, Volume 333, Issue 25, 2014, Pages 6885-6899.

[37] Khulief, Y. A. Al-Naser, H., 2005. *Finite element dynamic analysis of drillstrings*, Finite Elem. Anal. Des. 41, 13 (July 2005), 1270-1288.

[38] Kreisle, L. F., & Vance, J. M., *Mathematical Analysis of the Effect of a Shock Sub on the Longitudinal Vibrations of an Oilwell Drill String.* Society of Petroleum Engineers. doi:10.2118/2778-PA (1970, December 1)

[39] Krogstad, S., Lie, K., Moyner, O., Nilsen, H.M., Raynaud, X., Skaflestad, B., *MRST-AD an Open-Source Framework for Rapid Prototyping and Evaluation of Reservoir Simulation Problems*, SPE 173317-MS, presented at the SPE Reservoir Simulation Symposium in Houston, TX 23-25 February 2015

[40] Liu, Y., Gao, D., *A nonlinear dynamic model for characterizing downhole motions of drill-string in a deviated well*, Journal of Natural Gas Science and Engineering, Volume 38, 2017, Pages 466-474.

[41] Ma, X., Vakakis, A.F., Bergman, L.A., *KarhunenLoeve analysis and order reduction of the transient dynamics of linear coupled oscillators with strongly nonlinear end attachments*, Journal of Sound and Vibration, Volume 309, Issues 35, 2008, Pages 569-587.

[42] Menand, S., Sellami, H., Tijani, M., Stab, O., Dupuis, D. C., & Simon, C., *Advancements in 3D Drillstring mechanics: From the Bit to the Topdrive*, Society of Petroleum Engineers. doi:10.2118/98965-MS (2006, January 1)

[43] Mirhaj, S. A., Kaarstad, E., & Aadnoy, B. S., *Torque and Drag Modeling; Soft-string versus Stiff-string Models*, Society of Petroleum Engineers. doi:10.2118/178197-MS (2016, January 26)

[44] Nandakumar, K., Wiercigroch, M., *Stability analysis of a state dependent delayed, coupled two DOF model of drill string vibration*, Journal of Sound and Vibration 332 (2013) 2575-2592

[45] Richard, T., Germay, C., Detournay, E., *A simplified model to explore the root cause of stickslip vibrations in drilling systems with drag bits*, Journal of Sound and Vibration, Volume 305, Issue 3, 2007, Pages 432-456.

[46] Shor, R. J., Dykstra, M. W., Hoffmann, O. J., & Coming, M., *For Better or Worse: Applications of the Transfer Matrix Approach for Analyzing Axial and Torsional Vibration*, Society of Petroleum Engineers. doi:10.2118/173121-MS (2015, March 17)

[47] Skeem, M. R., Friedman, M. B., & Walker, B. H., *Drillstring Dynamics During Jar Operation. Society of Petroleum Engineers*, doi:10.2118/7521-PA (1979, November 1)

[48] SPICE, (2018), [Online Wikipedia], SPICE (Simulation Program with Integrated Circuit Emphasis) is a general-purpose, open source analog electronic circuit simulator. It is used to predict circuit behavior. Available at: `https://en.wikipedia.org/wiki/SPICE`, [Accessed 04-09-2018]

[49] Spinellis, D., Giannikas, V., *Organizational adoption of open source software*, The Journal of Systems and Software 85 (2012) 666-682

[50] Sugiura, J., Samuel, R., Oppelt, J., Ostermeyer, G. P., Hedengren, J., & Pastusek, P., *Drilling Modeling and Simulation: Current State and Future Goals*, Society of Petroleum Engineers. doi:10.2118/173045-MS (2015, March 17)

[51] Taron J., Hickman, S, Ingbritsen, S.E., and Williams, C., *Using a fully coupled, open-source THM simulator to examine the role of thermal stresses in shear stimulation of enhance geothermal systems, ARMA 14-7525*, presented at the 48th US Rock Mechanics / Geomechanics Symposium in Minneapolis, MN, 1-4 June 2014

[52] Tikhonov, V., Valiullin, K., Nurgaleev, A., Ring, L., Gandikota, R., Chaguine, P., & Cheatham, C., *Dynamic Model for Stiff-String Torque and Drag (see associated supplementary discussion)*, Society of Petroleum Engineers. doi:10.2118/163566-PA. (2014, September 1)

[53] Tom, N., Lawson, M., Yu, Y., *Recent Additional in the Modeling Capabilities of an Open-Source Wave Energy Converter Design Tool*, ISOPE, Proceedings of the Twenty-fifth (2015) International Ocean and Polar Engineering Conference, Kona, Big Island, HI June 21-26, 2015

[54] Tucker, R.W., Wang, C., *An integrated mode for drill-string dynamics*, Journal of Sounds and Vibration, Volume 224(1), 1999, Pages 123-165.

[55] Vromen, T., Dai, C.-H., van de Wouw, N., Oomen, T., Astrid, P., Nijmeijer, H., *Robust output-feedback control to eliminate stick-slip oscillations in drill-string systems*, IFAC-PapersOnLine, Volume 48, Issue 6, 2015, Pages 266-271.

[56] Vromen, TGM 2015, *Control of stick-slip vibrations in drilling systems*, Doctor of Philosophy, TUE: Department of Mechanical Engineering, Eindhoven.

[57] Wang, L., Huang, M., Liu, M., *How the founders social capital affects the success of open-source projects: A resource-based view of project teams*, Electronic Commerce Research and Applications 28 (2018) 114-126

[58] Wierecigroch, M., Nandakumar, K., Pei, L., Kapitaniak, M. Vaziri, V., *State dependent delayed drill-string vibration – Theory, experiments and a new model*, Procedia IUTAM 22 (2017) 39-50

[59] Wilson, J. K., & Heisig, G., *Investigating the Benefits of Induced Vibrations in Unconventional Horizontals via Nonlinear Drill String Dynamics Modeling*, Society of Petroleum Engineers. doi:10.2118/173049-MS (2015, March 17)

[60] Wilson, J. K., & Noynaert, S. F., *A New Damping Model for Nonlinear Drillstring Dynamics: Understanding the Effects of Rotation, Eccentricity, and Confined Fluid Flow and Their Impact on Unconventional Drillstring Design*, Society of Petroleum Engineers. doi:10.2118/178817-MS (2016, March 1)

Drill-string dynamics in deviated wells in the presence of heave

Eric Cayeux

IRIS, Stavanger, Norway

1 Introduction

Drilling operations executed from floaters are subject to some vertical movements of the top of the drill-string, because of heave effects. Heave compensators may attenuate these oscillations, but especially when passive heave compensation is used, the residual displacement of the top of the drill-string may still be sufficient to cause large variations of hook-loads when the bit is on bottom. Pastusek et al. (2016) [11] pointed out that dynamic drill-string estimation under heave condition is a challenging problem that requires particular attention.

Axial displacements of the drill-string result in annulus pressure fluctuations, i.e. swab and surge, which in turn influence the hydraulically generated forces applying to the drill-string. There is therefore a tight connection between the elastic deformations of the drill-string and pressure waves propagating inside the wellbore.

To address those problems, a hydro-mechanical transient model has been developed. This model considers the coupling of the axial and torsional movements of the drill-string together with the associated hydraulic effects. The boundary conditions of the hydro-mechanical system are of great importance for the response of the system, and detailed models of the hoisting, top-drive and bit/rock interaction are integral parts of the model.

We will now describe the principles of the model and provide examples while drilling and when picking up off bottom.

2 Degrees of Freedom and Accounted Forces

A drill-string is an assembly of tubulars screwed together. Contacts between the drill-string and the borehole are in most cases not continuous as was the assumption made in pioneering torque and drag models like the one described

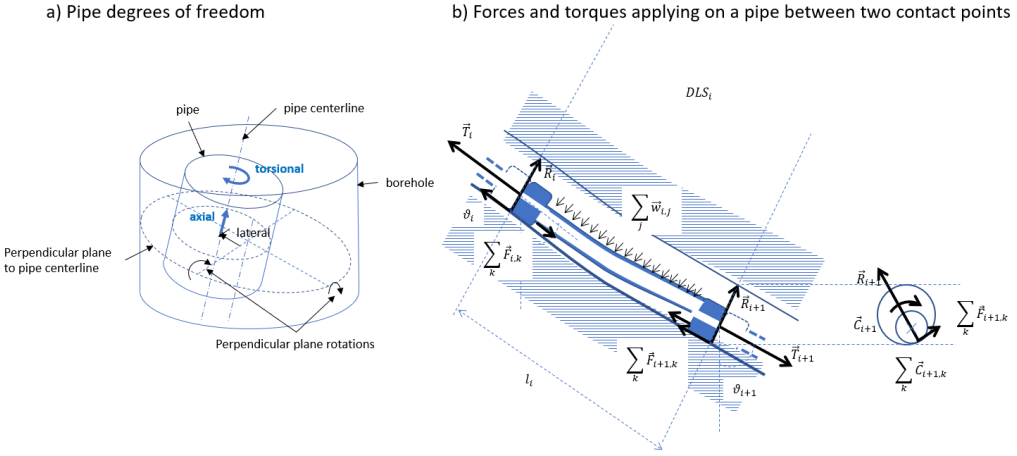

Figure 1: a) A pipe has six degrees of freedom inside a borehole. Those which are accounted for in the model are marked in blue. b) Illustration of the punctual and distributed forces and torques applied to a pipe element between two consecutive contact points i and $i+1$.

by Johancsik et al. (1984) [9], but localized at specific contact points, typically the tool-joints of drill-pipes or stabilizers in the bottom hole assembly (BHA). However, at this stage of the model development, we do not attempt to estimate the exact location of the contact points between the drill-string and the borehole, instead we assume that the contact points are located at any positions along the drill-string where the diameter is larger than the one of the pipe body, i.e. the tool-joints, the stabilizers and the bit.

The displacement of a pipe is subject to six degrees of freedom (DOF): one axial displacement, one angular rotation, a two-dimensional lateral translation and an angular tilting characterized by two angles (see fig. 1a). However, to simplify the mathematical modelling, we only consider the axial and torsional movements, i.e. two degrees of freedom.

If we denote a pipe element as the section of drill-string between two contact points corresponding to indices i and $i+1$ with a change of angle from θ_i to θ_{i+1} according to a wellbore curvature DLS_i, a pipe element is subject to punctual forces and torques at the contact points and distributed forces and moments along the element (see fig. 1b). Distributed forces are denoted $\vec{w}_{i,j}$ where j is an index representing the origin of the distributed force. There are both external and internal forces and torques. The external forces and torques considered by the model are: gravitational forces, pressure related forces, forces generated by the acceleration of fluid displaced in bends, forces and torques produced

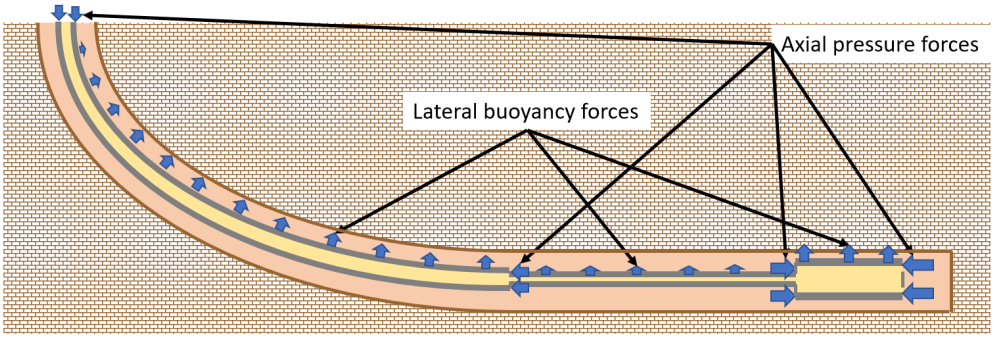

Figure 2: The vertical and axial pressure gradients generate distributed lateral forces on the drill-string and localized axial forces at any position where there is a change of diameter.

by viscous friction, mechanical friction between the element and the borehole, reaction forces between the element and the borehole $\vec{R}_i$. The internal forces and torques acting on an element are: the tensions at both ends of the element $\vec{T}_i$ and torques applied at the ends of the element $\vec{C}_i$.

3 Coupling With Transient Hydraulic Model

It may look surprising that buoyancy forces are not listed here. The reason is simply that buoyancy forces are a special type of pressure-induced forces where the gravitational field generates a vertical pressure gradient in a liquid which in turn results in local net forces along the length of drill-string elements. Pressure drops due to the relative movement of the drill-string and the drilling fluid also engender pressure gradients, this time oriented along the string, that cause additional net forces on the drill-string. The combined effect of these pressure gradients along the drill-string results in distributed perpendicular forces and also localized axial forces at any locations where there is a change of pipe diameter, e.g. when there is a change of pipe size and also at every tool-joint (see fig.2).

To correctly estimate the pressure-induced forces, it is therefore necessary to account simultaneously for the different sources of pressure gradients that apply along an element. A description of the calculation method for these forces can be found in [5] and [3]. But because of the dynamic nature of the drill-string movement, it is necessary to use a hydraulic model that is capable of modelling not only the effect of flow accelerations on pressure, but also swab and surge induced-pressure waves. Since pressure losses along the drill-string

directly influence local net forces on the pipe element, the drilling hydraulic calculations shall also account for the effect of local rotational speed along the drill-string as it increases pressure losses when the fluid moves axially.

We can note that pressure waves in drilling fluid propagate much slower than strain waves in metal like steel. It is therefore not necessary to solve the hydraulic partial differential equations, i.e. mass conservation and Navier-Stokes, together with the force and moment balance equations [1]. Futhermore, the hydraulic partial differential equations, mass and momentum balance, can be expressed as a mass transfer problem instead of a pressure wave propagation problem, therefore allowing for utilizing relatively long time steps [4]. Typically, the transient hydraulic model can be run with time steps that are five to ten times longer than those of the transient torque and drag model. Yet, as the mechanical model is stepped more often than the hydraulic one, it is necessary to perform some extrapolations of the pressure variations during the intermediate steps and to apply necessary corrections when the results of a new hydraulic time step are available. Such a method is described in [3].

4 Mechanical Friction

Kinetic friction always acts in the opposite direction to the relative velocity of the sliding surfaces. In our case, the sliding surfaces are typically the tool-joints. If there is both a rotational velocity and an axial movement, the kinetic friction generates both a drag force, i.e. a force oriented in the axial direction, and a torque because of the tangential force between the surfaces (see fig. 3a). In the general case, torsional and axial waves propagate along the drill-string, not necessarily at the same velocity, and therefore the local kinetic friction at any contact point varies with time.

If the sliding velocity at the contact point becomes zero, then static friction applies. The static friction force balances exactly all the other forces such that the surfaces stay without sliding as long as the static friction force does not exceed the static friction force magnitude limit:

$$\left\|\vec{F}_s\right\| \leq \mu_s \left\|\vec{F}_n\right\| \tag{1}$$

where $\vec{F}_s$ is the static friction force, μ_s is the static friction factor, $\vec{F}_n$ is the normal force.

The management of static friction requires a special treatment for any contact point that has entered such a condition, as it should be evaluated when static friction shall not be applied anymore. To respect the time continuity condition,

a) Friction between a tool-joint and the borehole

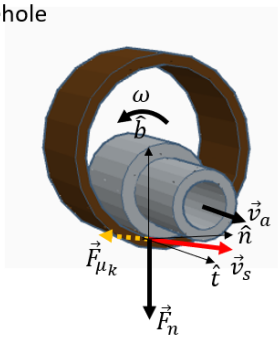

b) Depth of cut of a PDC bit as a function of normalized axial force

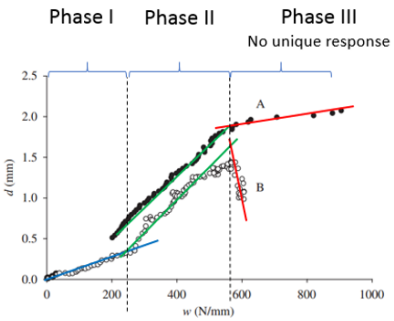

Figure 3: a) Schematic representation of contact between a tool-joint and the borehole. b) Illustration of the three performance phases achieved by a PDC bit as a function of the axial load (courtesy of Detournay et al. 2008 [7]).

it is not possible to utilize a simple Coulomb friction formulation, instead it is necessary to apply a Stribeck friction of the form:

$$\vec{F}_k = (\mu_k + (\mu_s - \mu_k)e^{-\frac{\|\vec{v}\|}{v_s}}) \left\|\vec{F}_n\right\| \frac{\vec{v}}{\|\vec{v}\|} \tag{2}$$

where v_s is the critical Stribeck velocity and μ_k is the kinetic friction factor with $\mu_k \leq \mu_s$

When kinetic friction applies, the unknowns of the problem are the axial displacement $x_{i,j}$ and the rotation angle $\theta_{i,j}$ where i is the index of the element and j is the time step index. In static conditions, i.e. $\vec{v}_{i,j} = 0$, we shall determine the static friction force $\vec{F}_{s_{i,j}}$ that is characterized by an axial and tangential component, the latter causing a torque at the contact point. In practice, the balance of forces and moments on an element i depends on forces and moments from elements $i-1$ and $i+1$, essentially because of the elastic deformations in the axial and torsional directions. There are therefore eight different possibilities: the element and its closest neighbours are all in kinetic displacement, the element and its closest neighbours are all static, the element is in kinetic movement and one of the neighbours is in static condition, the element is in kinetic movement and both neighbours are in static condition, the element is static and one of the neighbours is in kinetic movement, the element is static and the two neighbours are in kinetic displacement. Note that Aarsnes and Shor (2018) [2] have compared model predictions and observations in cases where transitions between static and kinetic friction apply, in a one-DOF context, namely when considering torsional

movement.

5 Bottom-side Boundary Conditions

When the bit is off bottom, it is subject to the same forces and torques that have been mentioned earlier. The unknowns are therefore the bit axial and angular positions that are imposed by the element immediately above the bit and the local forces and torques applied to the bit. However, when the bit is in contact with the formation, its axial position is constrained by the current bottom hole depth. The bit rotational speed and the depth of cut (DOC) per revolution define how fast the formation gets drilled. Detournay et al. (2008) [7] describe a PDC bit steady state rate of penetration (ROP) model that reproduces nicely results that are observed during drill-off tests [8]. In a much simplified view of the model, one can consider that the behaviour of the PDC bit can be decomposed in three phases. In phase I, the DOC is linearly proportional to the weight on bit (WOB) and passes through zero at zero WOB. During phase II, the DOC is also linear but with a steeper slope than in phase I while in phase III, the slope of the DOC as a function of the WOB is smaller than in phase II and even possibly negative (see fig. 3b). It is therefore possible to express the ROP as:

$$v_{bit} = \omega_{bit}(d_x + A_x \frac{F_{bit}}{d_{bit} g}) \tag{3}$$

where v_{bit} is the ROP, ω_{bit} is the bit angular velocity, F_{bit} is the force on bit, d_{bit} is the bit diameter, g is the gravitational acceleration, d_x and A_x are respectively the DOC at zero WOB and the slope of DOC relative to WOB normalized relatively to the bit diameter, x being the phase representing the working condition, i.e. either I, II or III.

The torque on bit (τ_{bit}) can be estimated from the WOB using the relationship from Pessier and Fear (1992) [12]:

$$\tau_{bit} = \mu_{k_{bit}} d_{bit} F_{bit} \tag{4}$$

where $\mu_{k_{bit}}$ is equivalent to a kinetic friction factor. Therefore when it is on-bottom, the unknown variables at the bit are the weight on bit and the bit angular position.

6 Top-drive Boundary Conditions

The rotational speed of the drill-string is controlled by the top-drive. The effective response of the top-drive depends on the motor capabilities and how it is

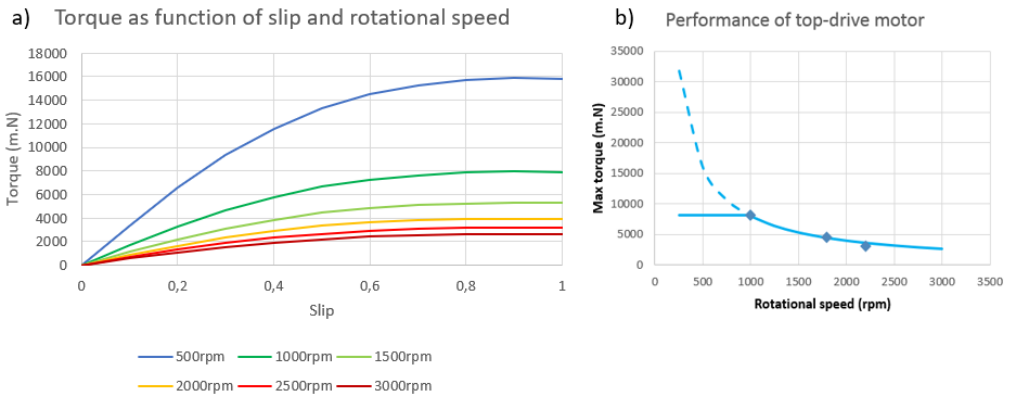

Figure 4: Rotor torque as a function of slip for various rotational speeds. Value derived for a typical AC motor used in modern top-drives.

controlled. In the simplest configuration and for a top-drive driven by AC (alternating current) motors, the control of the top-drive is performed by the PID (proportional-integral-derivative) controller included in the variable frequence drive (VFD) associated to the top-drive motor. However, more sophisticated control methods can be applied to mitigate stick-slip. An overview of such control methods can be found in Kyllingstad (2017) [10]. The capabilities of AC asynchronous motors are related to the slip of the rotor speed compared to the rotating magnetic field generated by the stator: $s = 1 - \frac{\dot{\alpha}_r}{\dot{\alpha}_s}$ where $\dot{\alpha}_r$ and $\dot{\alpha}_s$ are respectively the angular velocities of the rotor and the magnetic field generated by the stator.

The maximum torque is inversely proportional to the rotational speed (see fig. 4). However, at low rotational velocity, the electrical current in the windings would be very high and therefore much heat would be generated due to the non-negligible electrical resistance of the conductive materials. For that reason, the VFD limits the amount of electrical current that flows through the motor for rotational speeds lower than a given threshold (on fig. 4b this limit is 1000rpm) and therefore the maximum torque at low rotational speed is practically constant.

7 Hoisting System Boundary Conditions

The axial displacement of the top-drive, and consequently of the top of string, is performed by the hoisting system. There are essentially three types of hoisting principles: draw-works, ram-rig or rack and pinion. We will here focus on the most common one, i.e. the draw-works, that is based on a block and tackle

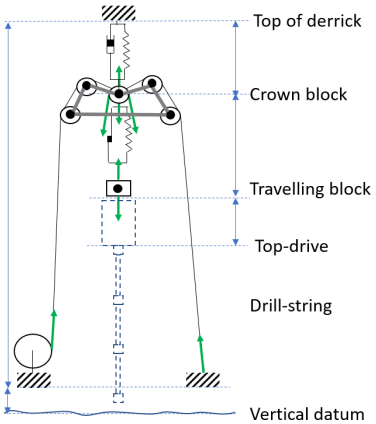

Figure 5: Schematic representation of a draw-works system with crown-mounted heave compensation.

system driven by electrical motors. On a floater, there is in addition a heave compensation system that can either be based on displacing the crown-block by means of hydraulic cylinders or utilizing actively the draw-works to control the position of the travelling equipment. The heave compensation can either be passive in which case an elasto-viscous damping system minimizes the vertical movement of the top of string with regards to a vertical datum (see fig. 5) or active when a controller actively maintains the position of the travelling equipment relative to a fixed elevation.

As for the top-drive, the response of the draw-works motors depends on the speed and load, and therefore a similar modelling approach is necessary to account for the torque response of the draw-work motors, yet one shall consider that the motor torque is also influenced by the number of layers of drill-line spooled on the draw-works drum. Also, the drill-line itself has some elasticity and there is mechanical friction at the level of the sheave bearings [6]. A direct consequence is that the apparent elasticity of the hoisting system depends on the position of the travelling equipment in the derrick.

8 Example from a Deviated Well with Passive Heave Compensation

As an example, we will take try to reproduce two sequences recorded from a drilling operation in the North Sea from a semi-submersible equipped with crown-

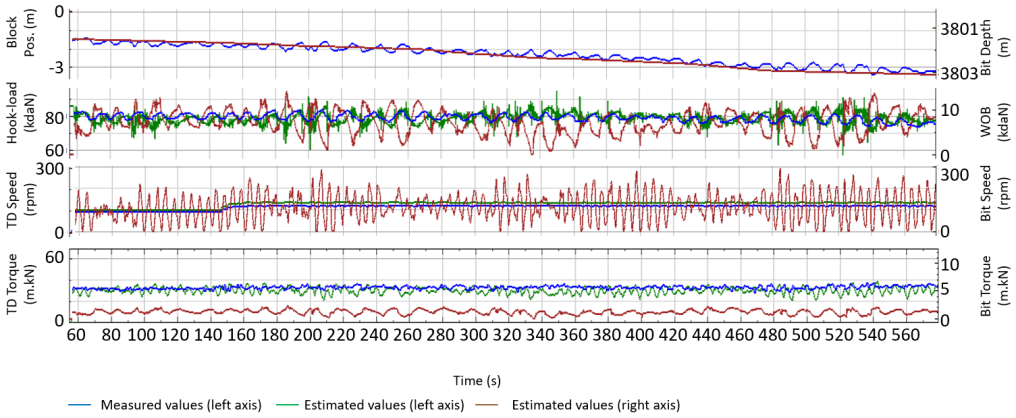

Figure 6: Estimation of the WOB, bit rotational velocity and bit torque while drilling from a floater with passive heave compensation.

mounted heave compensation system. The well is horizontal and the bit depth is 3800mMD.

Fig. 6 shows a first sequence corresponding to drilling the last meters of a stand. When utilizing calibrated parameters for the bit-rock interaction, i.e. A_x and $\mu_{k_{bit}}$, we obtain very comparable values for the calculated hook-load and top-drive torque to those measured. As it can be seen on the figure, there are large WOB oscillations induced by the residual top of string movement when utilizing passive heave compensation. These oscillations cause in turn substantial variations of the bit rotational velocity.

In the second sequence shown on Fig. 7, we estimate the evolution of the top of string force and top-drive torque while picking off bottom. The model predicts that the bit gets off bottom at time 84s and then returns on bottom for six seconds at time 89s. During that period, the top-drive torque is impacted by both the friction along the drill-string and the bit torque. Past time 100s, the top-drive speed is reduced to zero, yet there is a torque on the top-drive. The transient torque and drag model and the observations agree that the remaining top-drive torque decreases slowly as the drill-string is lifted. The predicted and observed top of string force oscillation during the pick-up are similar in period and amplitude, yet with a small phase shift.

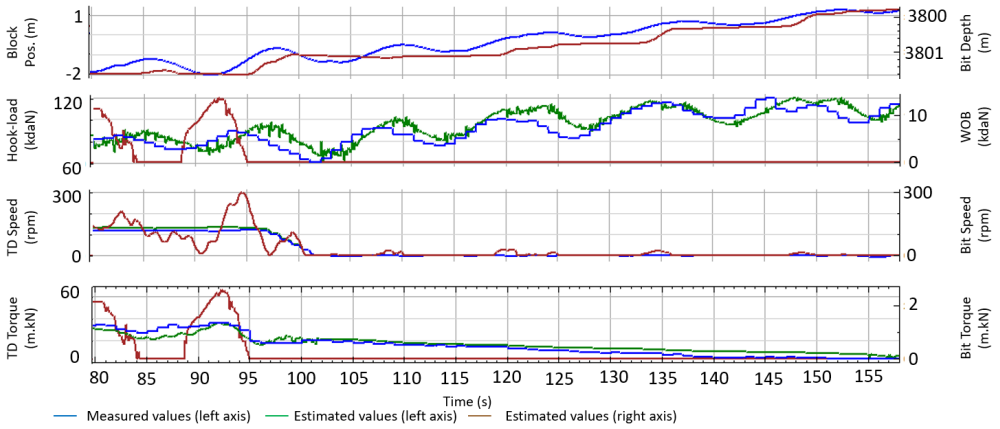

Figure 7: Comparison of the observed and predicted values for top of string force and top-drive torque while picking off bottom from a rig subject to heave.

9 Conclusion

Mechanical friction and pressure-generated forces influence the axial and torsional displacement of the drill-string. These forces are distributed along the drill-string and vary as a function of time. There is a coupling between hydraulic pressure waves and mechanical strain waves which necessitates the treatment of mechanical and hydraulic modelling simultaneously. However, the time step used for hydraulic modelling can be longer than the one utilized for mechanical estimations. Furthermore, there is a tight interaction between the response of the drilling machines such as the top-drive and the hoisting system, the drill-string displacements and forces. With a finite difference scheme to model the dynamic behavior of the drill-string, it is necessary to apply some special treatment for the discretized length of the pipes facing the bushing in order to model a smooth transition when getting in-slips and off-slips. The boundary conditions at the bit are important to estimate the bottom hole position and the ROP, especially in cases with substantial residual heave movement at the top of the string.

Acknowledgment

The author acknowledges the Research Council of Norway, ConocoPhillips, AkerBP, Statoil and Wintershall for financing the work through the research centre DrillWell - Drilling and Well Centre for Improved Recovery, a research cooperation between IRIS, NTNU, SINTEF and UiS.

References

[1] U.J. Aarsnes. *Modeling of Two-Phase Flow for Estimation and Control of Drilling Operations*. PhD thesis, NTNU, 2016.

[2] U.J. Aarsnes and R. Shor. Torsional vibrations with bit off bottom: Modeling, characterization and field data validation. *Journal of Petroleum Science and Engineering*, 163:712–721, April 2018.

[3] E. Cayeux. On the importance of boundary conditions for real-time transient drill-string mechanical estimations. In *IADC/SPE Drilling Conference*, Fort Worth, Texas, USA, 68 March 2018. SPE-189642-MS.

[4] E. Cayeux, B. Daireaux, E.W. Dvergsnes, H. Siahaan, and J.E. Gravdal. Principles and sensitivity analysis of automatic calibration of mpd methods based on dual-gradient drilling solutions. In *SPE Deepwater Drilling and Completions Conference*, Galveston, Texas, USA, 10-11 September 2014. SPE-170330-MS.

[5] E. Cayeux, H.J. Skadsem, B. Daireaux, and R. Holand. Challenges and solutions to the correct interpretation of drilling friction tests. In *IADC/SPE Drilling Conference*, The Hague, The Netherlands, 14-16 March 2017. SPE-184657-MS.

[6] E. Cayeux, H.J. Skadsem, and R. Kluge. Accuracy and correction of hook load measurements during drilling operations. In *SPE/IADC Drilling Conference*, London, England, UK, 17-19 March 2015. SPE-173035-MS.

[7] E. Detournay, T. Richard, and M. Shepherd. Drilling response of drag bits: Theory and experiment. *International Journal of Rock Mechanics and Mining Science*, 45:1347–1360, 2008.

[8] F.E. Dupriest and W.L. Koederitz. Maximizing drill rates with real-time surveillance of mechanical specific energy. In *SPE/IADC Drilling Conference*, Amsterdam,The Netherlands, 23-25 February 2005. SPE-92194-MS.

[9] C.A. Johancsik, D.B. Friesen, and R. Dawson. Torque and drag in directional wells-prediction and measurement. *Journal of Petroleum Technology*, 36(06):987 – 992, June 1984. SPE-11380-PA.

[10] . Kyllingstad. A comparison of stick-slip mitigation tools. In *SPE Drilling Conference*, The Hague, The Netherlands, 14-16 March 2017. SPE-184658-MS.

[11] P. Pastusek, M. Owens, D. Barrette, V. Wilkins, A. Bolzan, J. Ryan, K. Akyabi, M. Reichle, and D. Pais. Drill rig control systems: Debugging, tuning, and long term needs. In *SPE Annual Technical Conference*, Dubai, UAE, 26-28 September 2016. SPE-181415-MS.

[12] R.C. Pessier and M.C. Fear. Quantifying common drilling problems with mechanical specific energy and a bit-specific coefficient of sliding friction. In *SPE Annual Technical Conference*, Washington, D.C., USA, 4-7 October 1992. SPE-24584-MS.

The importance of Physics in Drill String modelling

Bernt S. Aadnøy and Dan Sui

University of Stavanger

Abstract

A drillstring is situated in a very complex environment subjected to large differences in pressures, forces and temperatures. The quality of a simulator depends on the correctness of the physical models chosen. This presentation will present some of the critical elements which are needed both for static calculations and for dynamic scenaria such as vibration analysis.

The drillstring is submerged into a fluid, leading to a buoyant force. We will show how this can be implemented for various cases, such as varying fluid densities and shut-in wellhead pressure. In particular we will show the projected height principle where the static axial pipe load can be simply determined for any wellbore inclination.

Wellbore friction is another critical issue. We will split the entire wellbore into two types of segments, straight and curved, the latter giving capstan effect. We will show how combined axial/rotational motion affect the frictional picture and we will show how drilling motors lead to reduced bit torque. Advanced trajectory models such a catenary profiles will be shown. A newly developed DLS filter will be presented for wellbore tortuosity. Using drillstring compliance functions we show the application of establishing a bottom reference instead of the drillfloor.

For drillstring dynamics we will show the geometric coupling between torsional, axial and transversal type vibrations. We will show the effect of axial load on transversal vibrations and also show the difficulty of modelling drillstring vibrations because of ill-defined string support.

Semi-analytical models of the oil-well drillstring

Sigve Hovda

Department of Geoscience and Petroleum, Norwegian University of Science and Technology
sigve.hovda@ntnu.no

1 Introduction

The models that we discuss in this paper can address various problems in drilling operations. For instance the effect of ocean waves on floating structures causes significant heave motions on the rig. During drilling operations, the drillstring is therefore excited with axial vibrations that can have different frequency content, dependent on the sea state and the transfer function of the floating structure [2]. When motions have large amplitude and high frequency, large pressure variations will happen downhole, see [8], [9] and [1]. Moreover, the drill bit is designed to work under constant axial load and in the case of heave vibrations, inefficient drilling and damaging vibrations can occur. In this paper we will describe the results of [7], where axial vibrations in a vertical well is given. Moreover, we will discuss the result of [6], where a deviated wellbore while reaming is assumed.

Another important issue while drilling deviated wellbores is the efficiency of hole cleaning. In an operation the crew can ream and wash the wellbore to remove cuttings at the cost of keeping the wellbore in gauge. If the hole diameter is enlarged, the level of hole cleaning issues will increase over time. In this paper we will also present some conclusions regarding a model for torsional vibrations that is described in [5].

The outline of the mathematical models are given in section 2. Focus on models that discuss heave motions are discussed in section 3, while models discussing detection of torque and drag are given in section 4. The paper is concluded in section 5.

2 Outline of mathematical framework in models

In this section, we outline the models only roughly and readers that are excited about a rigorous description are advised to address the respective papers. As

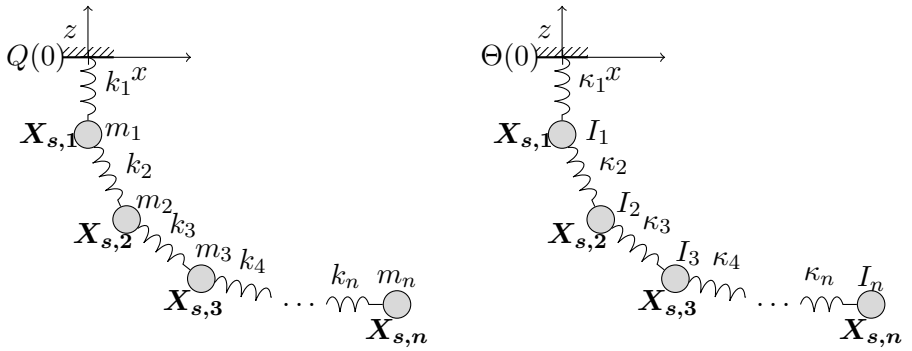

Figure 1: Schematic view of the model of the drillstring. The drillstring is considered as a set of n blocks with masses and moment of inertias denoted by m_i and I_i, respectively. These masses are connected to n springs. The spring constants related to the axial tension and compression forces are denoted by k_i, while the spring constants that are related to the torques are denoted by κ_i.

said before the drillstring is modeled as a set of n blocks that are connected by n spring elements, see Fig. 1. The first block is hanging from the first spring which is attached to a point that is called the "block position". The position and rotation of the block position are denoted by $Q(t)$ and $\Theta(t)$. In a three dimensional coordinate system the position of the unstressed blocks are denoted $\boldsymbol{X}_{s,i}$. Based on this, generalized coordinated for position and rotation of blocks from their initial unstressed positions are denoted by $q_i(t)$ and $\theta_i(t)$.

Newtons second law on all blocks gives this set of equations

$$
\begin{aligned}
0 &= m_1\ddot{q}_1 - m_1 g BF_1 g_{1,1} + k_1(q_1 - Q) - k_2(q_2 - q_1) - R_1 \\
0 &= m_i\ddot{q}_i - m_i g BF_i g_{1,i} + k_i(q_i - q_{i-1}) - k_{i+1}(q_{i+1} - q_i) - R_i \quad 2 \le i \le n-1 \\
0 &= m_n\ddot{q}_n - m_n g BF_n g_{1,n} + k_n(q_n - q_{n-1}) - R_n \\
0 &= I_1\ddot{\theta}_1 + \kappa_1(\theta_1 - \Theta) - \kappa_2(\theta_2 - \theta_1) - S_1 \\
0 &= I_i\ddot{\theta}_i + \kappa_i(\theta_i - \theta_{i-1}) - \kappa_{i+1}(\theta_{i+1} - \theta_i) - S_i \qquad 2 \le i \le n-1 \\
0 &= I_n\ddot{\theta}_n + \kappa_n(\theta_n - \theta_{n-1}) - S_n,
\end{aligned}
\tag{1}
$$

where g is gravity constant, BF_i is buoyancy factors and the $g_{j,i}$ are some constants related to the geometry of the wellbore. Moreover, external axial forces are given by the R_is and the external torque are given by S_is.

In various operations (such as tripping or reaming in vertical or deviated wellbores), physical assumptions can be made and this defines the R_is and S_is for each operation. In the case of drilling the torsional and axial vibrations are coupled, while when the bit is off bottom the torsional and axial vibrations can be assumed to be uncoupled.

The next step is to write the equations on some matrix form, decouple the equations by eigenvalue decomposition and finally solve the one dimensional second order differential equations separately. In the next section we describe how this is done for axial vibrations in a vertical wellbore.

3 Models to describe heave motions

In [7], a lumped element model for axial vibrations in a vertical well is described. This paper builds on [4]. In this situation, the external forces come from the interaction with the drilling fluid. It is assumed that the drilling fluid is Newtonian and incompressible. When the drillstring is moving up and down, all the drilling fluid in the annulus is accelerated and decelerated. This results in three forces acting on the drillstring: the steady-state viscous forces, the additional viscous forces related to the time effect of building up the velocity profile in the wellbore(the Basset forces) and the added mass effect. Note that the added mass effect is independent of the viscosity.

In [7] this set of equations on matrix form becomes

$$-\mathbf{B}(t^{-\frac{1}{2}} *_t \ddot{\boldsymbol{q}}) + \mathbf{M}\ddot{\boldsymbol{q}} + \mathbf{C}\dot{\boldsymbol{q}} + \mathbf{K}\boldsymbol{q} - \boldsymbol{g} - \boldsymbol{v} = \boldsymbol{f}(t), \tag{2}$$

where $\mathbf{B}$ is a diagonal matrix related to the Basset forces, $\mathbf{M}$ is a diagonal matrix with m_i on the diagonal, where the last diagonal element has an addition of the added mass effect. Moreover. $\mathbf{C}$ is a diagonal matrix related to steady state viscous forces and $\mathbf{K}$ is a tridiagonal matrix of the form

$$\begin{bmatrix} k_1+k_2 & -k_2 & 0 & \dots & 0 & 0 & 0 \\ -k_2 & k_2+k_3 & -k_3 & \dots & 0 & 0 & 0 \\ 0 & -k_3 & k_3+k_4 & \dots & 0 & 0 & 0 \\ \vdots & \vdots & \vdots & \ddots & \vdots & \vdots & \vdots \\ 0 & 0 & 0 & \dots & k_{n-2}+k_{n-1} & -k_{n-1} & 0 \\ 0 & 0 & 0 & \dots & -k_{n-1} & k_{n-1}+k_n & -k_n \\ 0 & 0 & 0 & \dots & 0 & -k_n & k_n \end{bmatrix}. \tag{3}$$

Table 1: Characteristic information about the well

Section number	1	2	3	4	5	6
Hole size [in]	36	26	17 1/2	12 1/4	8 1/2	6
End depth [m]	200	650	1350	2275	3700	4370
Drill pipe OD [in]	5	5	5	5	5	5
Drill pipe area [m^2]	0.0034	0.0034	0.0034	0.0034	0.0034	0.0034
Drill collar length [m]	24	45	53	100	170	175
Drill collar OD [in]	11 1/4	11 1/4	11 1/4	10	6 1/2	3 3/4
Drill collar area [m^2]	0.0406	0.0406	0.0406	0.0375	0.0344	0.0188
Viscosity [Pa s^{-1}]	0.0011	0.0011	0.03	0.03	0.03	0.03
Mud density [kg/m^3]	1025	1025	1400	1600	1800	1100

The inverse of this matrix is also used and it is found analytically in [3]. The expression $t^{-\frac{1}{2}} *_t \ddot{\boldsymbol{q}}$ is a vector of time convolution of $t^{-\frac{1}{2}}$ with $\ddot{q}_i$. The elements of $\boldsymbol{v}$ and $\boldsymbol{g}$ are constants related to the stretching of the pipe due to flow speed (assumed constant) and gravitational forces. The first element of $\boldsymbol{f}(t)$ is equal to $k_1 Q(t)$, while the others are zero.

This set of equations are coupled trough $\mathbf{K}$, but it can be decoupled by a series of coordinate transformations, involving the eigenvalue decomposition. Moreover the decoupled equations can be solved semi-analytically even though they are not linear. We have also changed the time scale to $\tau = (c_s/L)t$, where c_s is the speed of sound in the drillpipe (typically steel). Finally, we obtain

$$q_j(\tau) = Q(\tau) *_\tau s_{1,j}(\tau) + s_{2,j}(\tau), \tag{4}$$

where $s_{1,j}$ and $s_{2,j}$ are analytic functions that can be pre-computed before the convolution in Eq. (4). The function $s_{2,j}$ is related to the initial conditions and is equal to zero if the movement start from rest.

3.1 Some properties of the model

In order to get some intuition about Eq. (4), we found it instructive to focus our discussion around a vertical well with parameters given in table 1.

In Fig. 2, we have shown the amplification as a function of frequency of harmonic oscillation at the top for the four last sections. Clearly, the resonant frequency is lowered as a function of depth. Moreover, we also see the effect of neglecting Basset forces and the added mass effect. It is clear that these effects are very important, in terms of lowering the resonant frequency and also

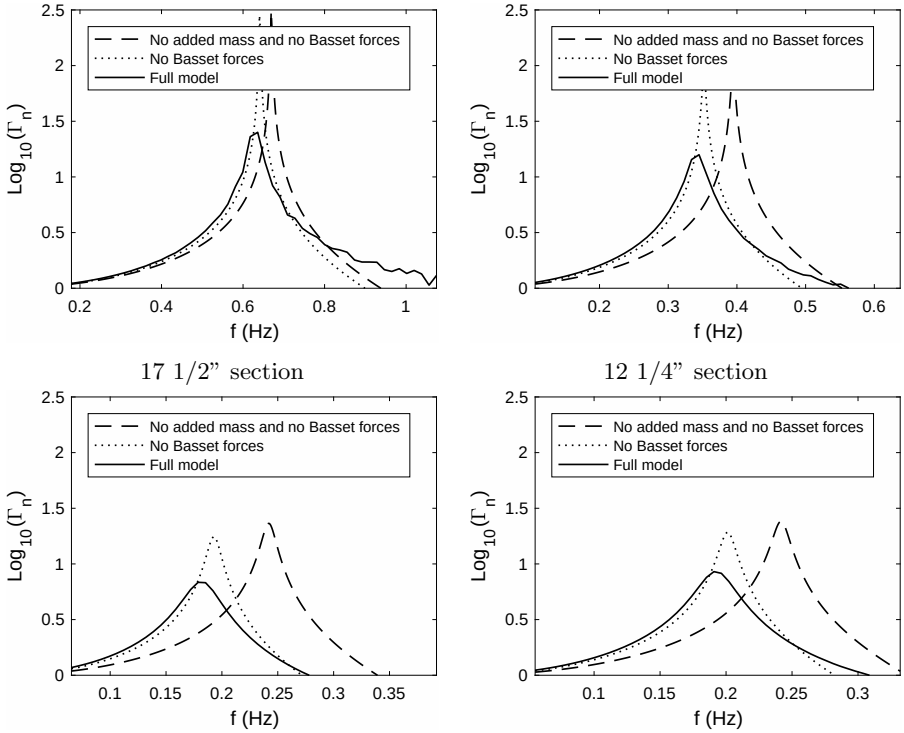

Figure 2: The amplification as a function of frequency in hertz on a log scale for the four last sections in the imaginary well. We see that the effect of added mass is lowering the resonant frequencies. It is important result that the Basset forces lowers the resonant frequencies and dampens the resonance on a factor of ten.

lowering the amplification. Heave motions are typically found at frequencies that are lower than the first eigenfrequency, meaning that the effect of the added mass can not be omitted. In the same paper, formulas for the pressure variations as a function of heave motions were also developed and it was clear that in the deepest section, where the surge and swab pressures are largest, the effect of added mass is almost dominating. This is an interesting result, since the added mass effect is independent of viscosity. This means that a simple model such as a model involving a Newtonian fluid can be sufficient to model downhole pressure in some cases.

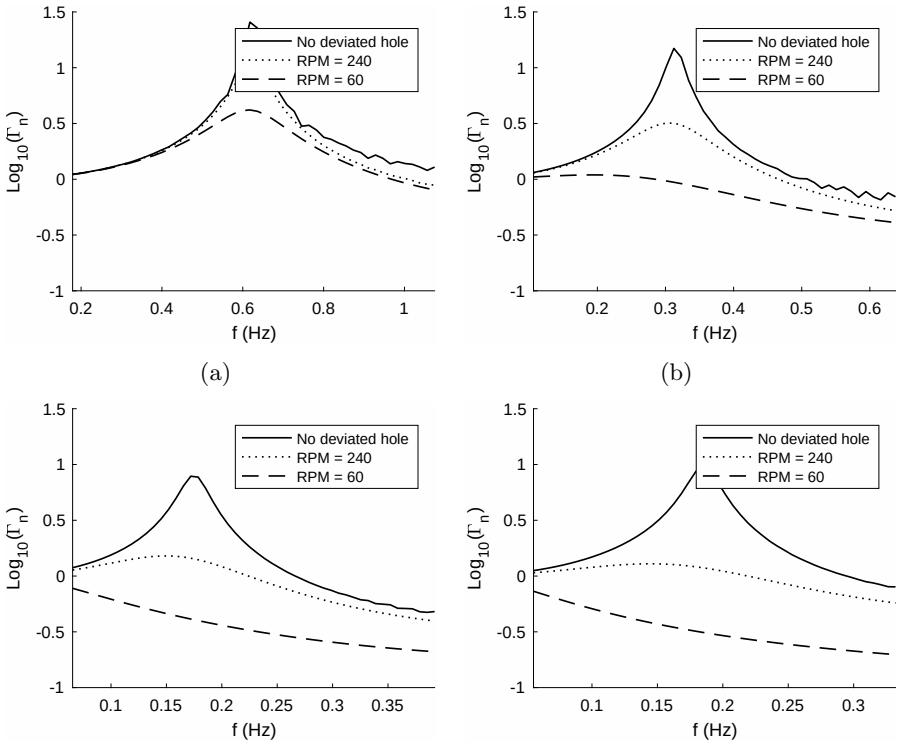

Figure 3: The amplification as a function of frequency on a log scale for section three (Fig. 3(a)) to section six (Fig. 3(d)). This shows that the Coloumb friction is an important damping factor in deviated holes, even when the rotation speed is high.

3.2 Deviated wellbores

In [6], the model in [7] was extended to axial vibrations while reaming in any three dimensional well geometry. Since constant rotation is assumed, the Coulomb friction is kinetic. It is shown that the Coulomb friction forces are approximately proportional with the $\dot{q}_i$s. The proportionality factor is inversely proportional to the rotation speed. We used a J-well with the same parameters as in table 1. In Fig. 3, we have plotted the effect of rotation speed on the amplification in the four last sections. It is interesting to see that a rotation speed of 240 RPM, the system is underdamped. This means that it is actually possible to build up energy in the drillstring in deviated wellbores.

4 Models to describe torque

In [5] we have developed the equations for torsional vibrations in deviated wellbores. We get the matrix form

$$-\mathbf{B}(t^{-\frac{1}{2}} *_t \ddot{\boldsymbol{\theta}}) + \mathbf{I_M}\ddot{\boldsymbol{\theta}} + \mathbf{C}\dot{\boldsymbol{\theta}} + \mathbf{K}\boldsymbol{\theta} + \boldsymbol{S_{co,ss}} = \boldsymbol{f}(t), \tag{5}$$

where $\mathbf{B}$ is a diagonal matrix with Basset forces due to acceleration or deceleration of rotation speed, $\mathbf{I_M}$ is a diagonal matrix with moments of inertia, $\mathbf{C}$ is a diagonal matrix with steady state viscous friction coefficients on the diagonal and $\mathbf{K}$ is a tridiagonal matrix with spring constants. Finally, $\boldsymbol{S_{co,ss}}$ is a vector of Coulomb friction forces that are perpendicular to the rotation. These forces are independent of the rotation speed. After the mathematical derivations, we end up with a solution that is analog to equation 4, i.e. a convolution of top side movement with some analytic functions.

In Fig. 4, we see the effect of starting rotation quickly in the four last sections. It is clear that the effect of Basset forces can not be neglected.

Moreover in [5], an algorithm for detecting the time-dependent Coulomb friction coefficient is outlined and discussed in terms of sensitivity. Mathematically, the algorithm seems robust and this motivates experimental studies in the future.

5 Conclusion

Various situations where the axial and torsional movement of the drillstring can be modeled semi-analytically are explained. For deeper understanding of the models the readers are advised to consult the original papers, but some important results are also given in this paper.

References

[1] F. Arvani, D. G. Rideout, and S. D. Butt. Dynamic model of a mobile offshore drilling unit in deep water environments for drilling simulation. In *ASME 2015 34th International Conference on Ocean, Offshore and Arctic Engineering*, volume 10, pages 1–7, St. John, Canada, 2015.

[2] O. M. Faltinsen. *Sea Loads on Ships and Offshore Structures.* Cambridge Ocean Technology Series, 1990.

[3] S. Hovda. Closed-form expression for the inverse of a class of tridiagonal matrices. *Numerical Algebra, Control and Optimization*, 6(4):437–445, 2016.

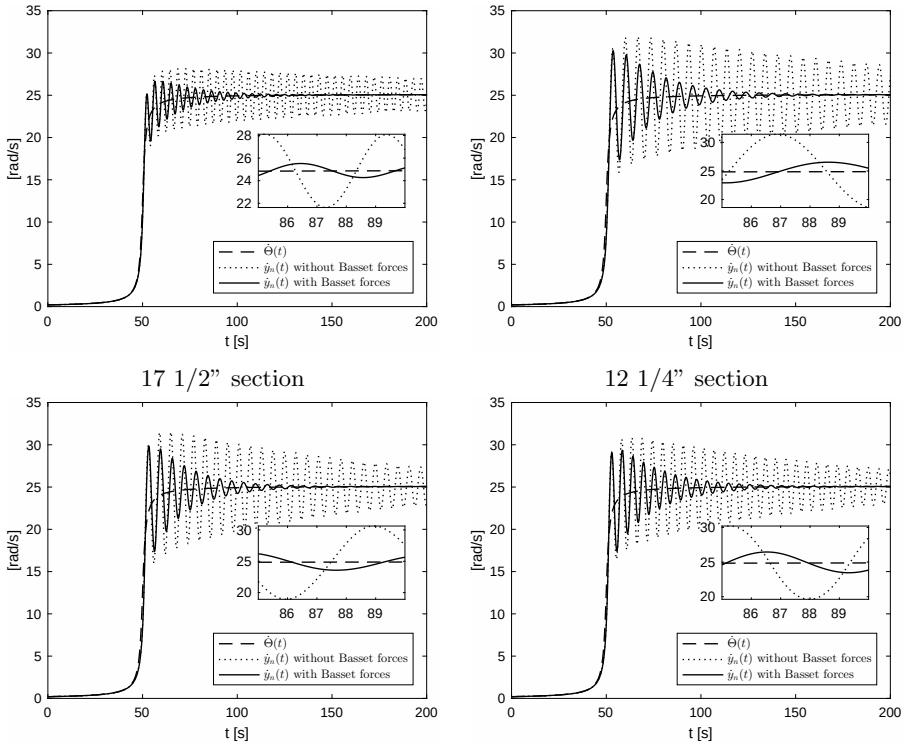

17 1/2" section | 12 1/4" section

8 1/2" section | 6" section

Figure 4: Downhole rotary speed in radians per second as a function of time in seconds. This is a realistic graph for turning on the rotary speed quickly.

[4] S. Hovda. Gibbs-like phenomenon inherent in a lumped element model of a rod. *Advances in Mechanical Engineering*, 9(8):1–12, 2017.

[5] S. Hovda. Automatic detection of abnormal torque while reaming. *Journal of Petroleum Science and Engineering*, 166:13–24, 2018.

[6] S. Hovda. Semi-analytical models on axial motions of an oil well drillstring in deviated wellbores. *Journal of Sound and Vibrations (submitted)*, 2018.

[7] S. Hovda. Semi-analytical models on axial motions of an oil-well drillstring in vertical wellbores. *Journal of Sound and Vibrations*, 417:227–244, 2018.

[8] L. Huang, G. V. Tahchiev, and Y. Cao. Investigation of drill bit heave response to drill rig heave excitation. In *International Society of Offshore and Polar Engineers*, pages 1–8, 2011.

[9] D. Zhao, S. Hovda, and S. Sangesland. Abnormal down hole pressure variation by axial stick-slip of drillstring. *Journal of Petroleum Science and Engineering*, 145:194–204, 2016.

High-frequency torsional oscillations – examples and theory

Benjamin Jeffryes, Zhengxin Zhang, Yuelin Shen, Wei Chen, Jibin Shi, Wesley Bonstaff, Kien Tang, David L. Smith and Yezid Arevalo

Schlumberger

It has long been known that the rotational dynamics of the drillstring are highly resonant, even in horizontal holes where much of the length of the drillstring is lying on the side of the borehole. This is because the torque required to rotate the drillstring against friction, and to cut the rock at the bit, only depends weakly on the rotation speed, so there is little vibrational damping present. It is well known that this can lead to stick-slip behaviour at low frequencies, normally at the fundamental resonance of the system. This can still create considerable problems in many drilling operations.

Small downhole sensors and large capacity memories have significantly increased our ability to observe what is happening near the bit, and these measurements are showing up some unexpected phenomena.

Even when the drillstring is not in stick-slip, the resonant nature of the system is easily seen in the dynamic measurements. Figure 1 shows the rotation speed, measured using a gyro close to the bit, while drilling a horizontal well with a rotary assembly (no downhole motor), for a period of 400 seconds with 1ms sampling.

The periodic nature of the variation in rotation speed is obvious, even at this resolution

Taking the Fourier transform of a longer section of data, including this, with a similar level of amplitude variation, gives the spectrum shown in figure 2, below 60 Hz and with a close-up below 10Hz.

The largest resonance here is at about 0.5 Hz, though this is not the fundamental (0.17 Hz), and many resonances of the full drillstring are visible. The drillstring is composed of sections with different sizes of pipe, and this results in increased resonant amplitudes at multiples of around 3.4Hz. Similarly, the local resonances of the BHA enhance amplitudes with a periodicity of 18Hz

However, looking only at these frequencies does not show the full picture. The data was acquired with a bandwidth of 512 Hz, though acquisition filters begin to attenuate the data from 230Hz. Figure 3 shows the full bandwidth

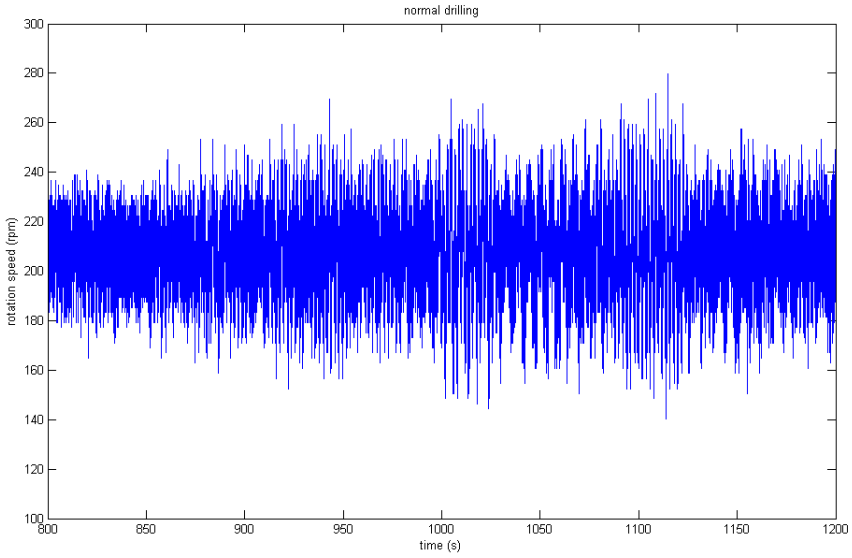

Figure 1: Sample of downhole rotation speed.

acquired. There is a very strong and narrow group of resonances between 140 and 175Hz, and also some narrow resonances possibly apparent near 300Hz.

If instead of taking the spectrum of the rotation speed (from a gyro) we use the signal from an accelerometer, oriented in a direction tangential to the rotational motion, a much richer picture emerges In addition to the group of resonances between 140 and 170Hz there is a further group between 280 and 350Hz, and others at just below 500Hz.

The cause of these resonances lies not with the structure of the BHA, but the long length of drillpipe above it. Each drillpipe consists of a narrow pipe section, terminated by a much thicker joint, containing the connection, so a long length of drillpipe is a periodic structure of short, high impedance sections (the joints), connected by long, low impedance sections. It is well known that such a structure cannot transmit rotational vibrations in certain frequency bands (known as stop bands), which centre around the frequencies at which 2 periods of the structure correspond to an integer number of wavelengths of oscillation. Although energy is not transmitted, it is not absorbed either, so in the stop bands all the energy is effectively confined near the bottom of, and below, the pipe.

Figure 5 shows a simple theoretical calculation of the absolute value of the reflection coefficient for a semi-infinite section tool joints, 10 m apart, on 4.5 inch continuous pipe. Total reflection, and low attenuation, can obviously combine to create high-Q resonances. If the sole consequence of this were changes in rotation

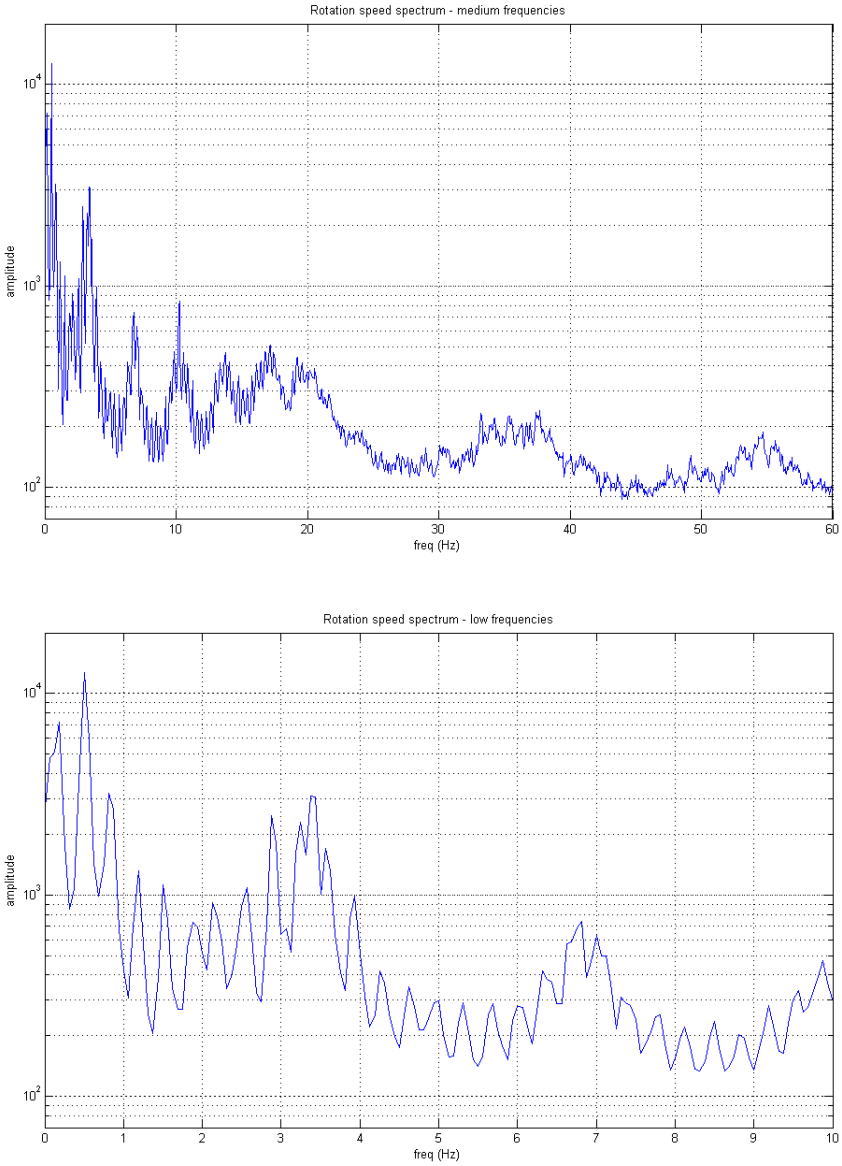

Figure 2: Fourier transform of downhole rotation speed.

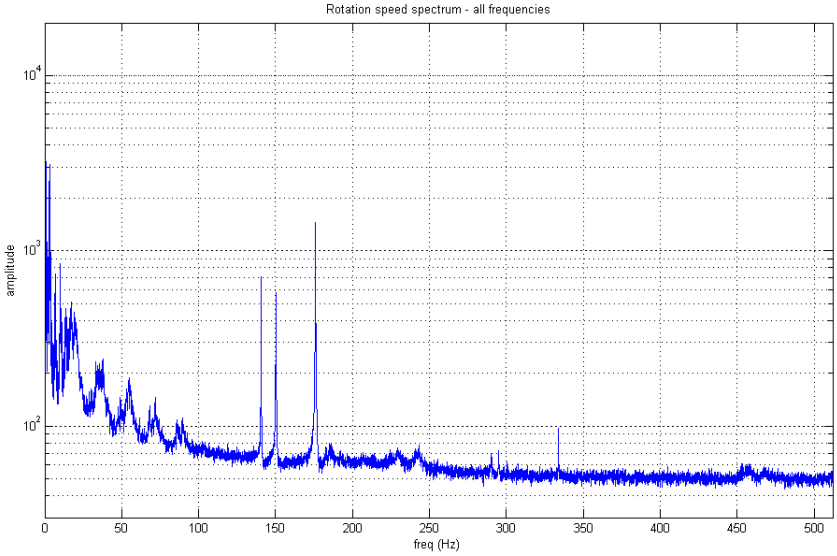

Figure 3: Full Fourier transform of downhole rotation speed.

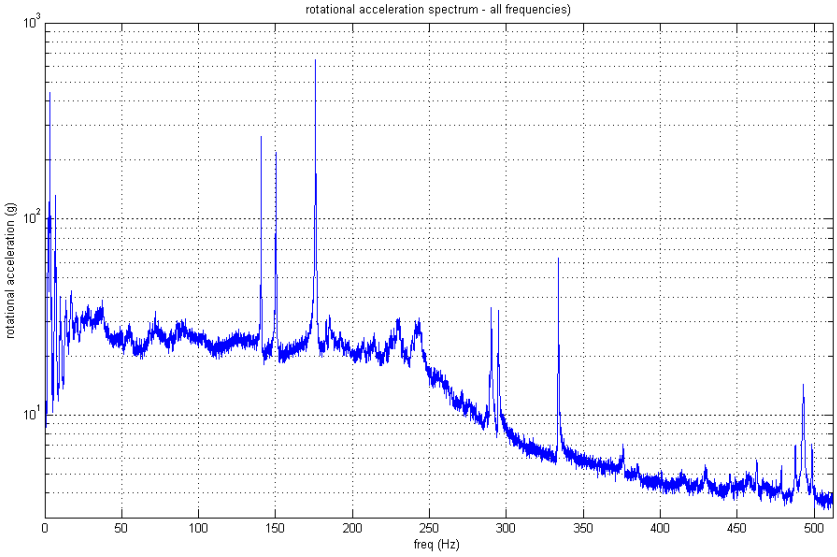

Figure 4: Full Fourier transform of rotational acceleration.

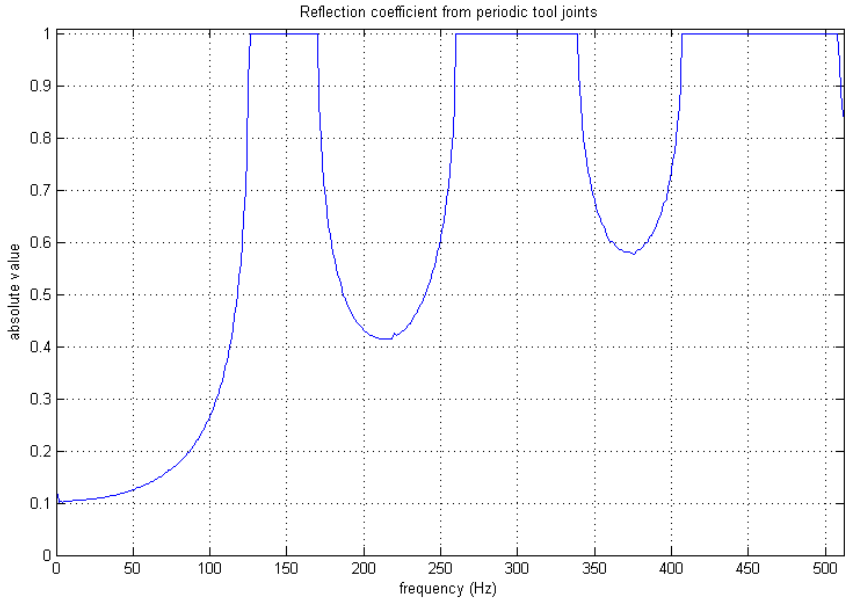

Figure 5: Theoretical reflection coefficient of periodic tool joints.

speed similar to those shown in figure 1 it would not be problematic, however figure 6 shows an hour of data from the same well. In blue is the signal from the gyro, red is the same signal low-pass filtered to below 6 Hz.

For some periods, the drillstring is in full stick-slip at low frequency, however, for the rest of the time there are high amplitude vibrations at higher frequencies.

In figure 7, the same low-pass filtered data is shown, together with the amplitude at two of the higher resonant frequencies, close to 142 and 177 Hz.

The drillstring vibration flips between low frequency stick slip and high-amplitude resonance at two high frequencies, 142 Hz and 177Hz. The amplitude at the other resonance in the first stop-band, 151 Hz, is always very low. Although this is not obviously stick-slip from the raw data in figure 6 (during periods of high-amplitude at high frequency, the minimum rotation speed is above zero), the phase difference at these frequencies between the bit and the sensor position means that when these high-amplitude resonances are at their highest amplitude, there is stick-slip at the bit. In this entire data set, stick-slip is only seen at two of the three resonances in the first stop band.

These high amplitude rotation speed variations also lead to high amplitude torque variations, with hundreds of thousands of torque cycles per hour of drilling. This torque variation would not cause excessive fatigue if the total cycles seen by the tubulars were in the thousands, but with millions of cycles,

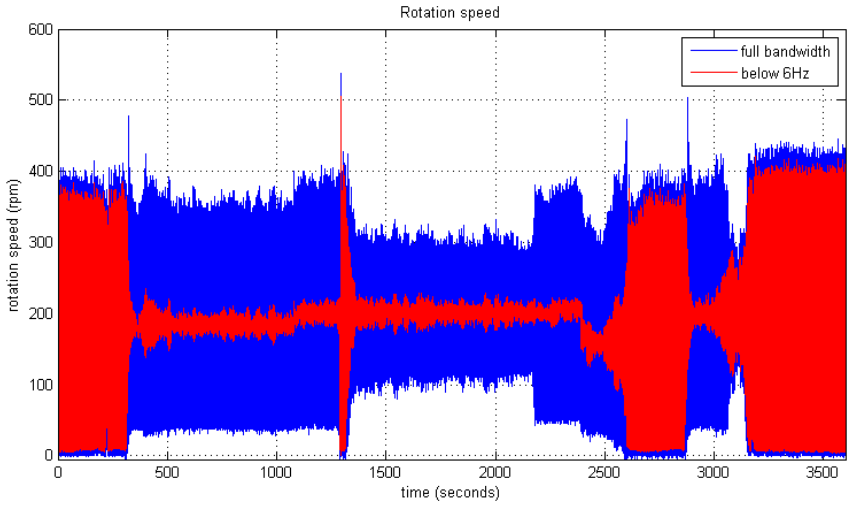

Figure 6: One hour of rotation speed data during high-amplitude oscillations.

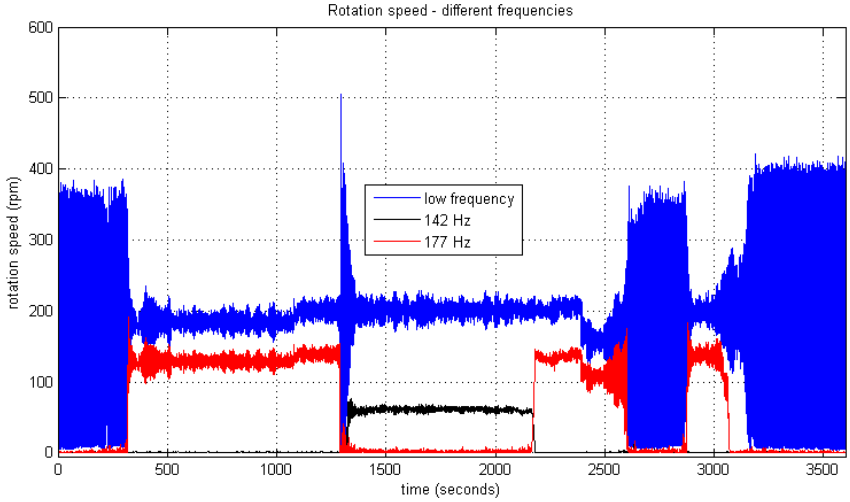

Figure 7: Rotation speed data in different frequency bands.

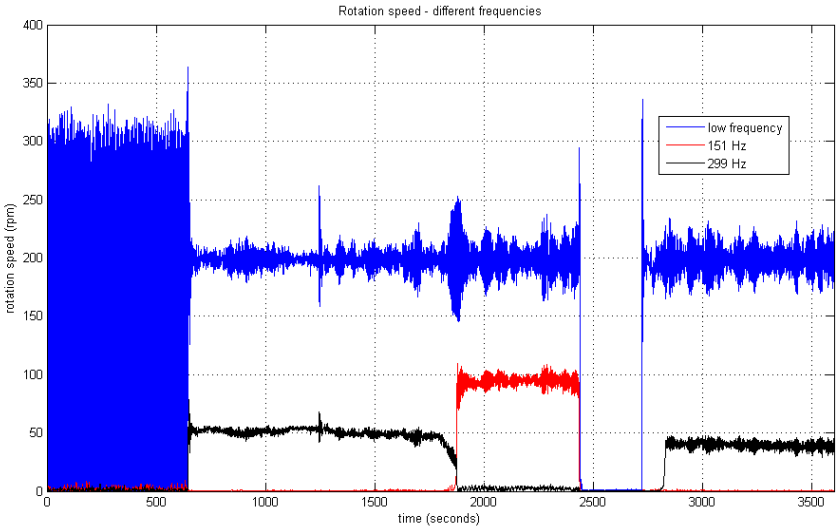

Figure 8: Decomposed rotation speed second BHA.

fatigue failure occurs at stress-concentrating features such as ports.

During this data acquisition campaign we recorded data for two very similar sections, with near identical drillstrings. The high frequency resonances for the two BHAs were within a fraction of a Hz for the two drillstrings. However, for the second drillstring, a different situation was seen with respect to high frequency stick-slip. The resonances at 142 Hz and 177 Hz were never seen at high-amplitude. In contrast the high amplitudes are seen at the other resonance in the first stop band (151 Hz) and at just one of the three resonances in the second stop band (299 Hz).

Figure 8 shows a section of data from the second section drilled, similarly decomposed Although the 299Hz is not obviously full amplitude, in addition to the phase effects, it has been attenuated by a factor of about 2.5 by the acquisition filters.

In contrast to low frequency stick-slip where one stick-slip cycle corresponds to multiple rotations of the drill bit, at these high frequencies the drill bit is only moving forward a few degrees each cycle. For the example above, with the mean rotation speed at 200rpm and 299Hz stick-slip, there are close to 100 cycles per rotation of the drill bit.

Motor drilling

Increasingly in modern drilling practice, positive displacement motors are used not just in conventional steering applications but also to provide additional rotation speed and power to the drill bit when drilling with rotary steerable

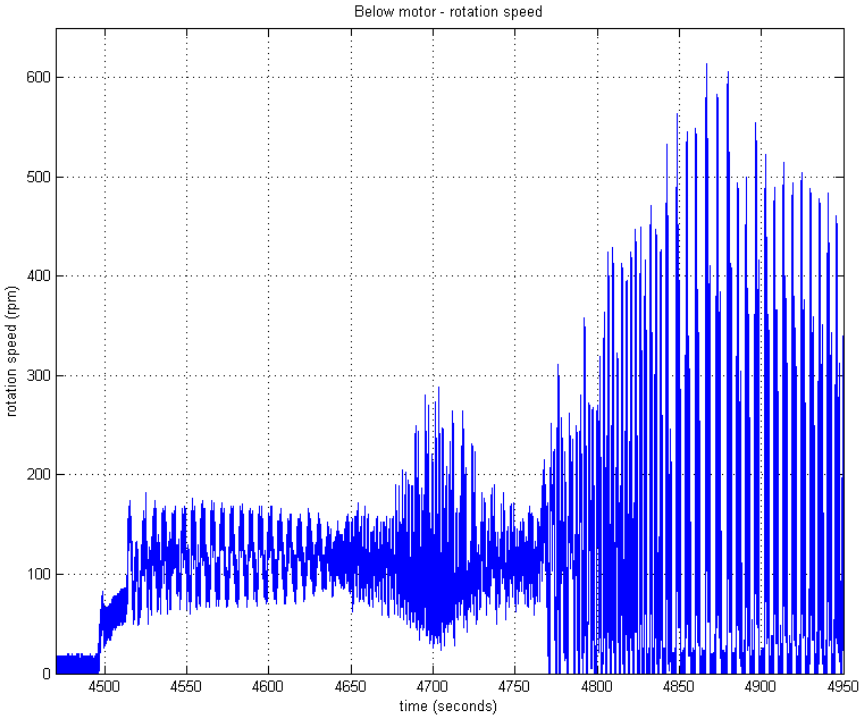

Figure 9: Rotation speed data from below a motor.

systems. In such applications, there is a length of tubular below the motor that can range from around 5m up to 50m.

We have known for some time that the impedance contrast between the sub-motor tubulars and the motor-rotor can lead to resonances trapped below the motor, but until recently the fact that these can lead to high-frequency stick-slip and other pathological vibrations had not been recognised. Figure 9 shows a snap-shot from a particularly extreme example. It shows about 500 seconds of gyro (rotation speed) data recorded below a motor, running with a rotary steerable system. This is near the end of the bit run, under very harsh conditions. Flow, and hence motor rotation, commences at about 4500 seconds, and the bit goes on bottom just before 4650 seconds. Figure 10 shows a decomposition into low frequency and high frequency resonant components.

After a short burst of high-frequency at 4700 seconds, the bit goes into full low-frequency stick-slip, combined with high-frequency resonance. Looking in more detail, figure 11 shows a close-up when the drill bit is still off bottom.

The drillstring above the motor is in high-amplitude oscillation, probably

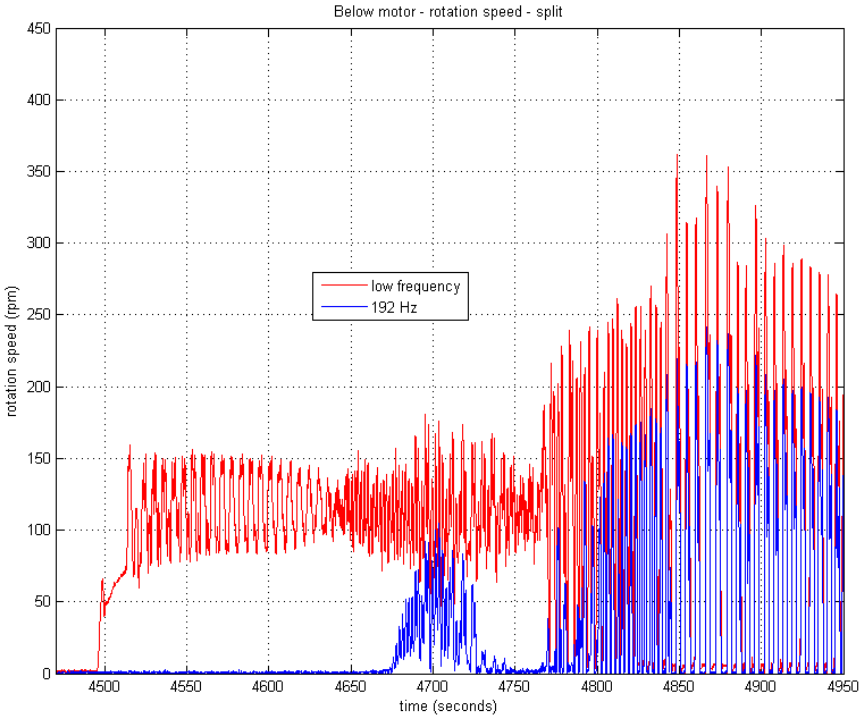

Figure 10: Below-motor rotation speed decomposed by frequency.

full stick-slip, at the resonant frequency of about 0.2Hz, but there is a significant component at the next resonance (0.6Hz). The motor though is rotating smoothly, giving a minimum bit rotation speed of about 80rpm. Figure 12 shows what happens after the bit goes on bottom. The bit stops rotating, implying that the motor is going into stall, and the system goes into a stall stick-slip cycle at close to the 0.6Hz resonance.

During each of the moving stages of the stall stick-slip cycle, the 192Hz resonance is also excited but not consistently. However, within less than a minute, the stall stick-slip cycle switches to 0.2 Hz as shown in figure 13.

Now, during each stick-slip cycle which lasts around 5 seconds, the motor stalls and then as the bits average speed accelerates, full amplitude 192Hz oscillations are excited at the same time, so at the peak of the cycle, the bit is oscillating between 0 and around 600 rpm.

In conclusion, high frequency rotational oscillations are proving to be a significant issue in drilling, especially as they cause fatigue failures in downhole tools. However, with the acquisition of extensive field data, our ability to model them

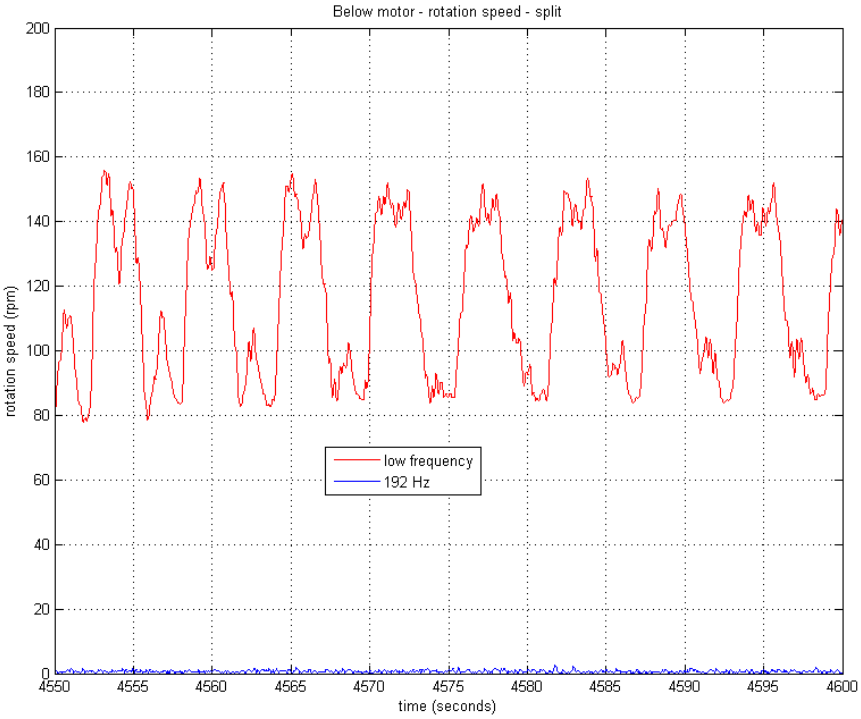

Figure 11: Off-bottom rotation speed.

and devise methods for their mitigation increase. We should however probably still expect surprises

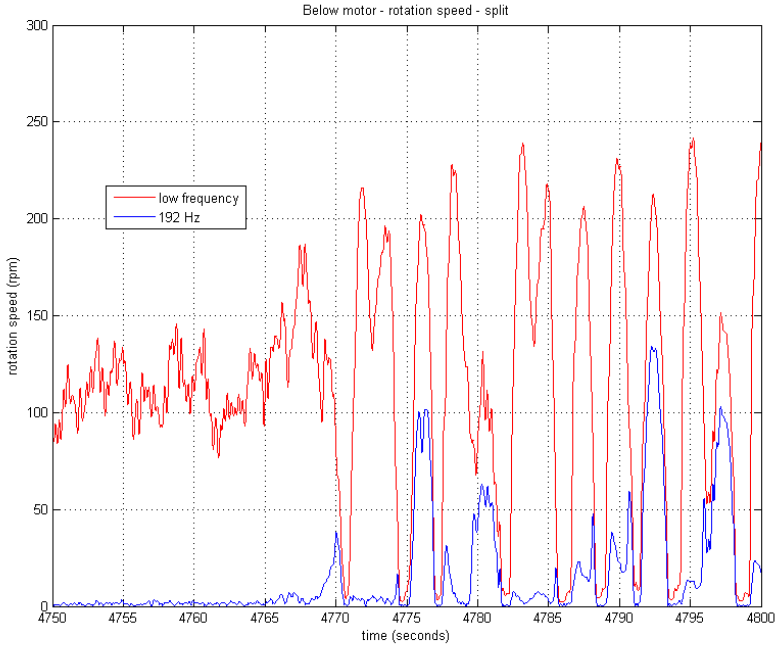

Figure 12: Stall stick-slip initiation.

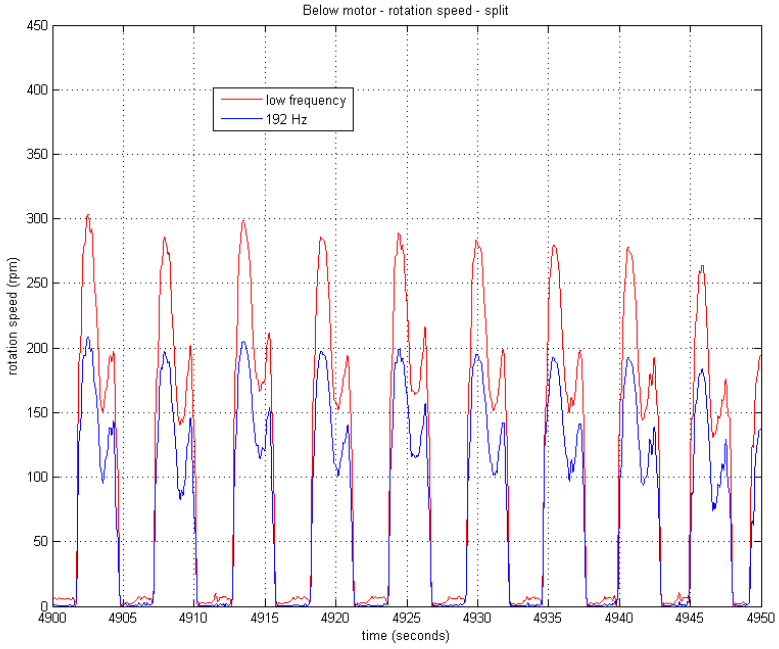

Figure 13: Full stall stick-slip cycling, with high-frequency resonance.

State-Dependent Delay Effect in Drilling

Xie Zheng, Vipin Agarwal and Balakumar Balachandran

Department of Mechanical Engineering, University of Maryland, College Park, USA

1 Introduction

Systems described by delay-differential equations arise in many science and engineering fields (i.e., networked systems, biological systems). One example in the engineering field is rotary drilling dynamics [1, 2, 3]. As shown in earlier work, the state-dependent delay can arise in the description of the cutting action of the drill bit blade on the rock interface. This delay can play an important role in determining stick-slip behavior of the system. In related previous work conducted in the authors' group, reduced-order models, finite-element based discretization, and the presence of the state-dependent delay have been discussed [3, 4]. In the current work, the authors carry out a nonlinear analysis and numerical studies with a reduced-order model to further our understanding of the state-dependent delay effect.

The remaining part of this paper is organized as follows. In Sections 2 and 3, the authors follow their earlier work reported in reference [5] and set the stage for the analyses to follow. A reduced-order model is presented to describe the axial-torsion dynamics of drilling. For the sake of analyses, a nondimensionalized form of the governing equations is provided. Later, linear stability analysis is conducted by using the D-subdivision scheme. In Section 4, the solutions of the nonlinear system are examined by using a continuation method. The implicit state-dependent delay is rewritten as an explicit function by using a Taylor expansion to facilitate the analysis. Hopf bifurcations of fixed points are determined and it is found that the nature of these bifurcations can be subcritical or supercritical depending on the parameter values. It is found that the state-dependent delay can have a destabilizing effect in certain cases. The axial damping ratio and torsion damping ratio are found to have a significant influence in determining the effect of the state-dependent delay on the system dynamics.

2 Modeling and nondimensionalization

In Figure 1(a), an illustrative model of a drill-string system is provided. The axial and torsion motions of interest are also shown. At the top end of the drill sting, a constant axial speed V_0 and a rotation speed Ω_0 are imposed on the system. The governing equations of motion take the form

$$\begin{array}{rcl} M\ddot{Z}(t) + C_a\dot{Z}(t) + K_a(Z(t) - V_0 t) & = & W_s - W_b(t) \\ I\ddot{\Phi}(t) + C_t\dot{\Phi}(t) + K_t(\Phi(t) - \Omega_0 t) & = & -T_b(t) \end{array} \tag{1}$$

Here, M and I are the respective translational and rotational inertias, K_a and K_t are the respective translational stiffness and torsion stiffness, and C_a and C_t represent the respective translational damping and torsion damping. Furthermore, W_s is the sum of the weight of both the drill pipe and drill collar. W_b and T_b respectively denote the weight and torque on the bit, and they are both determined by bit-rock interactions. Each of them can be decomposed in terms of cutting and friction components, as follows.

$$\begin{array}{rcl} W_b(t) & = & W_{bc}(t) + W_{bf}(t) \\ T_b(t) & = & T_{bc}(t) + T_{bf}(t) \end{array} \tag{2}$$

The subscripts bc denotes the cutting component of the drill bit and bf denotes the friction components on the drill bit, respectively. Following the earlier work of Detournay and Defourny[6], those components can be expressed as

$$W_{bc}(t) = \epsilon a \zeta R(d(t))H(\dot{\Phi}(t)) \qquad T_{bc}(t) = \frac{1}{2}\epsilon a^2 R(d(t))H(\dot{\Phi}(t)) \tag{3}$$

$$W_{bf}(t) = \sigma a l H(d(t))H(\dot{Z}(t)) \qquad T_{bf}(t) = \frac{1}{2}\mu\gamma a^2 \sigma l sgn(\dot{\Phi})H(d(t))H(\dot{Z}(t)) \tag{4}$$

where the $R(.)$ function is the unit ramp function and $H(.)$ is the Heaviside step function. In Figure 1, two successive blades of a polycrystalline diamond compact drill bit are shown along with the delayed states. For an individual blade, the instantaneous depth of cut can be determined as

$$d_n(t) = Z(t) - Z(t - \tau) \tag{5}$$

Assuming that the cutting action is uniform across the N blades, then, the cutting depth is

$$d(t) = N d_n(t) \tag{6}$$

where the delay τ is given by

$$\Phi(t) - \Phi(t - \tau) = \frac{2\pi}{N} \tag{7}$$

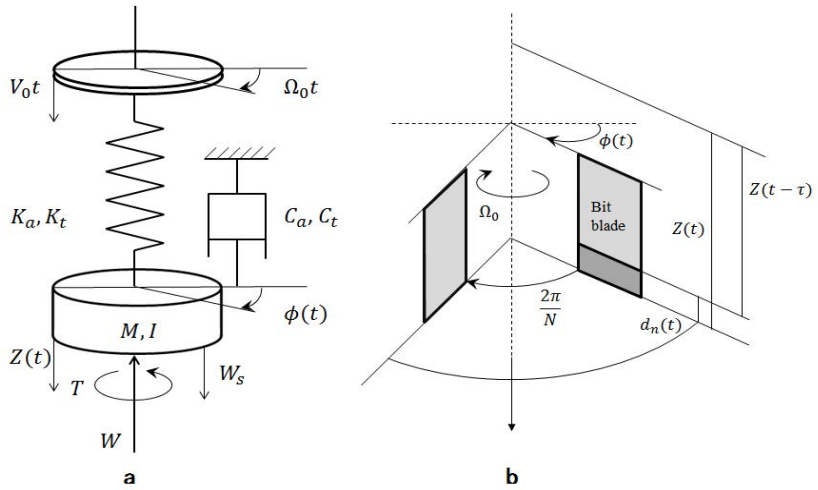

Figure 1: (a) Representative reduced-order model of drill-string system. (b) Two successive blades of a drill bit.

The state-dependent delay $\tau(\Phi(t))$ is the elapsed time for the drill bit to rotate over an angle of $\frac{2\pi}{N}$, and this delay depends only on the state Φ. Next, the equations of motion are cast into dimensionless form. Following earlier work [2], the characteristic time $t_* = \sqrt{I/K_t}$ and characteristic length $L_* = 2K_t/\epsilon a^2$ are introduced. Then, once can write the nondimensional variables as

$$z = \frac{Z - \bar{Z}}{L_*} \qquad \varphi = \Phi - \bar{\Phi} \qquad \hat{t} = t/t_* \qquad \hat{\tau} = \tau/t_* \tag{8}$$

Here, $\bar{Z}$, and $\bar{\Phi}$ correspond to the equilibrium solution of Eq.(1), which is a trivial solution in the absence of vibrations. The axial state z and angular state φ are functions of dimensionless time $\hat{t}$. With the nondimensional variables, the governing equations can be recast as

$$\begin{aligned} \ddot{z}(\hat{t}) + 2\xi\eta\dot{z} + \eta^2 x(\hat{t}) &= -\psi\delta(\hat{t}) \\ \ddot{\varphi}(\hat{t}) + 2\kappa\dot{\varphi}(\hat{t}) + \varphi(\hat{t}) &= -\delta(\hat{t}) \end{aligned} \tag{9}$$

The dimensionless parameters are defined as

$$\begin{aligned} \xi &= \frac{C_a}{2\sqrt{K_a M}} \qquad \kappa = \frac{C_t}{2\sqrt{K_t I}} \\ \psi &= \frac{\epsilon a \zeta I}{K_t M} \qquad \eta^2 = \frac{K_a}{M} t_*^2 = \frac{K_a I}{K_t M} \end{aligned} \tag{10}$$

Table 1: Parameters used for drilling operations (values adopted from references [1, 4])

Parameter	Symbol	Value	Unit
Mass	M	3.4×10^4	kg
Axial damping	C_a	1.56×10^4	N s/m
Axial stiffness	K_a	7.0×10^5	N/m
Moment of inertia	I	116	kg m^2
Torsion damping	C_t	32.9	N s m/rad
Torsion stiffness	K_t	938	N/m
Radius of drill bit	a	0.108	m
Wear flat length	l	0.0012	m
Intrinsic specific energy of rock	ϵ	$0 - 110$	MPa
Contact strength	σ	60	Mpa
Cutter face inclination	ζ	0.6	-
Friction coefficient	μ	0.6	-
Geometry parameter of drill bit	γ	1	-
Number of blades on drill bit	N	4	-

The parameters ξ and κ are the damping ratios associated with axial and torsional motions, respectively. η represent the ratio of axial natural frequency to torsional natural frequency. The quantity ψ is dependent upon the rock strength and drill-bit geometry.

δ is the dimensionless perturbation of cutting depth δ, and this can be written as

$$\delta(\hat{t}) = N[z(\hat{t}) - z(\hat{t} - \hat{\tau}) + (\hat{\tau} - \hat{\tau}_0)v_0] \tag{11}$$

where v_0 is the dimensionless penetration rate, ω_0 is the dimensionless angular speed, and $\hat{\tau}_0$ is the constant steady-state time delay. These quantities take the forms

$$\omega_0 = \Omega_0/t_* \qquad v_0 = \frac{V_0/L_*}{\Omega_0} = \frac{\epsilon a^2}{2K_t\Omega_0}V_0 \qquad \hat{\tau}_0 = \frac{2\pi}{N\omega_0} \tag{12}$$

The dimensionless state-dependent delay is given by

$$\hat{\tau} = \hat{\tau}_0 - \frac{1}{\omega_0}(\varphi(\hat{t}) - \varphi(\hat{t} - \hat{\tau})) \tag{13}$$

After substituting Eq.(11) and Eq.(13) into Eq.(9), the governing equations

can be rewritten as

$$\ddot{z}(\hat{t}) + 2\xi\eta\dot{z}(\hat{t}) + \eta^2 z(\hat{t}) = -N\psi(z(\hat{t}) - z(\hat{t}-\hat{\tau})) + N\psi v_0(\varphi(\hat{t}) - \varphi(\hat{t}-\hat{\tau}))$$
$$\ddot{\varphi}(\hat{t}) + 2\kappa\dot{\varphi}(\hat{t}) + \varphi(\hat{t}) = -N(z(\hat{t}) - z(\hat{t}-\hat{\tau})) + Nv_0(\varphi(\hat{t}) - \varphi(\hat{t}-\hat{\tau})) \quad (14)$$

3 Linear stability

According to the work of Hartung [7], a true linearization of the system with state-dependent delay is not possible due to the fact that the solution of the system is not differentiable with respect to state-dependent delay. Hence, one needs to find a constant delay model which has the same local stability properties as the original system. Making use of the method discussed by Insperger and Stepan [8],and letting $\hat{\tau} = \hat{\tau}_0$, the resulting linearized system is

$$\ddot{z}(\hat{t}) + 2\xi\eta\dot{z}(\hat{t}) + \eta^2 z(\hat{t}) = -N\psi(z(\hat{t}) - z(\hat{t}-\hat{\tau}_0)) + N\psi v_0(\varphi(\hat{t}) - \varphi(\hat{t}-\hat{\tau}_0))$$
$$\ddot{\varphi}(\hat{t}) + 2\kappa\dot{\varphi}(\hat{t}) + \varphi(\hat{t}) = -N(z(\hat{t}) - z(\hat{t}-\hat{\tau}_0)) + Nv_0(\varphi(\hat{t}) - \varphi(\hat{t}-\hat{\tau}_0)) \quad (15)$$

From these linearized equations, the characteristic equation is determined as

$$P_0(s) + P_1(s)(1 - e^{-\bar{\tau}s}) = 0 \quad (16)$$

where P_0 and P_1 are polynomials in the eigenvalue s. These polynomials can be determined as

$$P_0(s) = s^4 + (2\xi\eta + 2\kappa)s^3 + (\eta^2 + 4\kappa\xi\eta + 1)s^2 + (2\xi\eta + 2\kappa\eta^2)s + \eta^2$$
$$P_1(s) = (N\psi - Nv_0)s^2 + (2\kappa N\psi - 2\xi\eta N v_0)s + (N\psi - N\eta^2 v_0) \quad (17)$$

Following the procedure of the D-subdivision method, the authors substitute $s = i\omega$ and $\bar{\tau} = 2\pi/\omega_0$ into Eqs.(17) and separate the real and imaginary parts. After a rather lengthy calculation, one obtains the stability crossing set in the ω_0-v_0 domain as

$$v_{0SDD} = \frac{1}{N[\alpha(\omega^2 - \eta^2) + 2\beta\xi\eta\omega]}[\frac{\alpha^2 + \beta^2}{2} + (\alpha(1 - \omega^2) + 2\beta\kappa\omega)N\psi]$$
$$\omega_{0_SDD} = \frac{2\pi\omega}{N(\Theta_1 + (2k-1)\pi)}, \qquad k = 1, 2, ..., \quad (18)$$

Here,

$$\alpha = Real(P_0) \qquad \beta = Imag(P_0) \qquad \Theta_1 = \angle\frac{-P_1}{P_0 + P_1} \quad (19)$$

Results obtained on the basis of stability boundaries in the $\omega_0 - v_0$ parameter space is shown in Figure 2. From the plots, it is evident that the damping ratios play an important role in determining the stability boundaries. The results obtained agree well with the numerical findings reported in an earlier work by the authors' group [4].

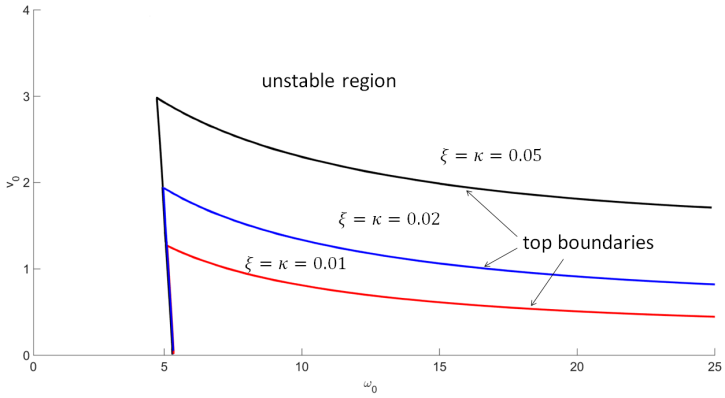

Figure 2: Stability charts in the plane of the drive speed ω_0 and the penetration speed v_0, for different values of ξ and κ.

4 Nonlinear analysis of the system with the state-dependent delay

In Eq.(14), the state-dependent delay term is the only source for nonlinearity of our nondimensionalized system and it is in term of implicit function. The software DDE-BIFTOOL [10] can be used to carry out continuation of solution branches of systems with delays. Here, this tool is used to study the bifurcations of solution of the nonlinear systems with constant delay and state-dependent delay. However, to use this tool, the state-dependent delay must be in an explicit form. To address this, the state-dependent delay in Eq.(13) is rewritten as a three level, nested constant delay in the form

$$\hat{\tau} = \hat{\tau}_0 - \frac{1}{\omega_0}(\varphi(\hat{t}) - \varphi(\hat{t} - (\hat{\tau}_0 - \frac{\varphi(\hat{t}) - \varphi(\hat{t} - \hat{\tau}_0)}{\omega_0}))) \tag{20}$$

By using a Taylor expansion and only keeping the first two orders, the explicit form of state dependent delay is determined as

$$\hat{\tau} = \hat{\tau}_0 - \frac{1}{\omega_0}(\varphi(\hat{t}) - \varphi(\hat{t} - \hat{\tau}_0)) - \frac{1}{\omega_0^2}(\varphi(\hat{t}) - \varphi(\hat{t} - \hat{\tau}_0))\dot{\varphi}(\hat{t} - \hat{\tau}_0) \tag{21}$$

After combining the nondimensionalized governing system Eqs. (14) together with the explicit state-dependent delay function Eq.(21) and using the DDE-BIFTOOL, the authors generate the bifurcation diagram with different dimensionless damping ratios as shown in Figure 3. The continuation of the periodic

orbits is stopped, when the state-dependent delay $\hat{\tau} < 0$. Along the y axis, the maximum value of the dimensionless φ of the orbit is shown.

Similarly to the turning case [9], when a subcritical Hof bifurcation of a fixed point occurs, an unstable limit cycle (periodic orbit) coexists with the stable equilibrium. When a supercritical Hopf bifurcation of a fixed point occurs, an stable limit cycle (periodic orbit) coexists with the unstable equilibrium. From the figures, it can be discerned that when the dimensionless axial and torsional damping ratios are small, branches of periodic motions bend to the left locally; this is a characteristic of a subcritical bifurcation. However, as the damping ratios are increased, the periodic solution branches start to bend to the right; this menas that the nature of the Hopf bifurcation has changed from subcritical to supercritical.

5 Concluding remarks

In this work, the effect of the state-dependent delay on drilling dynamics has been elucidated by considering a representative reduced-order model for coupled axial and torsion dynamics. The linear stability of the equilibrium solution of the system was analyzed by using the D-subdivision method, and the nonlinear stability analysis was conducted with the aid of a continuation scheme. From the results, it can be inferred that both the axial damping ratio and torsion damping ratio play a significant role in determining the linear stability of the equilibrium solution and the nature of the Hopf bifurcation of the equilibrium solution.

References

[1] Richard,T., Germay, C., and Detournay, E. (2007) A simplified model to explore the root cause of stickslip vibrations in drilling systems with drag bits. J. Sound Vib. 305(3),432-456.

[2] Besselink,B., van de Wouw, N., and Nijmeijer, H.(2011) A semi-analytical study of stick-slip oscillations in drilling systems. ASME J. Comput. Nonlinear Dyn. 6(2),p.021006.

[3] Liu X., Vlajic N., Long X., Meng G., and Balachandran B.(2014) State-dependent delay influenced drill-string oscillations and stability analysis ASME J. Vibration and Acoustics DOI: 10.11115/1.4027958.

[4] Liu X., Vlajic N., Long X., Meng G., and Balachandran B. (2014) Coupled axial-torsional dynamics in rotary drilling with state-dependent delay: stability and control J. Non-linear Dyn 78:1891-1906.

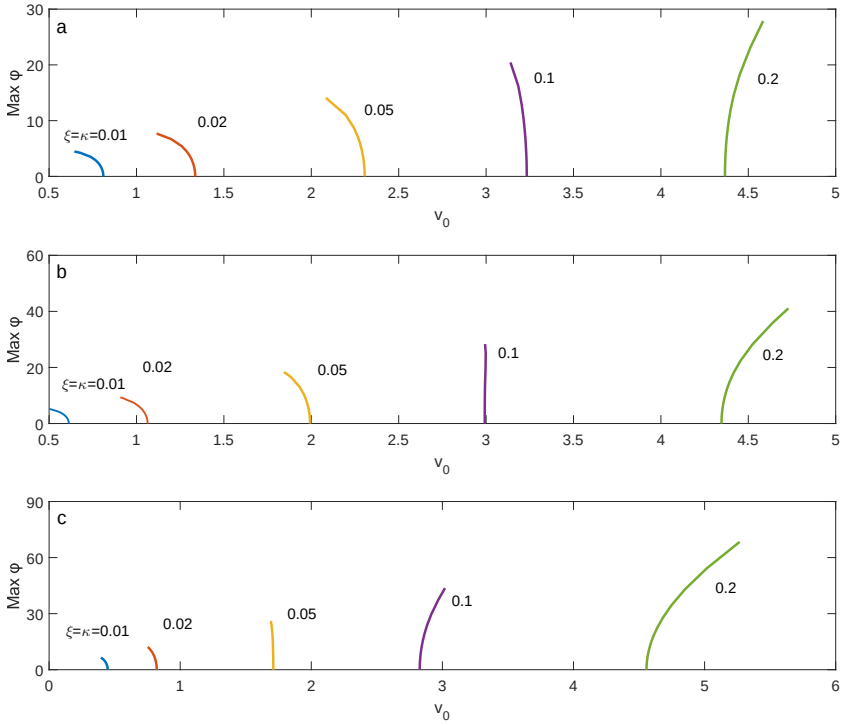

Figure 3: Stability charts in the plane of the drive speed ω_0 and the penetration speed v_0, for different values of the damping ratios ξ and κ: (a) $\omega_0 = 10$, (b) $\omega_0 = 15$, and (c) $\omega_0 = 25$.

[5] Zheng X. and Balachandran B. (2017) State-Dependent Delay and Drill-String Dynamics. Procedia IUTAM, Volume 22, 31-38.

[6] Detournay,E., and Defourny, P.(1992) A phenomenological model for the drilling action of drag bits. Int. J. Rock Mech. Min. Sci. Geomech. Abstr.,29(1):13-23.

[7] Hartung F. and Turi J. (2000) Linearized stability in functional-differential equations with stat-dependent delays. Proceeding of the conference Dynamical Systems and Differential Equations, added volume of Discrete and Continuous Dynamical Systems: 416-425.

[8] Insperger T., Stepan G., and Turi J.(2007) State-dependent delay in regenerative turning processes, Nonlinear Dyn. 47(1-3): 275-283.

[9] Insperger T., Barton D. A. W., and Stepan G. (2007) Criticality of Hopf bifurcation in state-dependent delay model of turning processes Int. J. Non-Linear Mechanics 43: 140-149.

[10] K. Engelborghs, T. Luzyanina, G. Samaey, DDE-BIFTOOL v.2.00: a Matlab package for bifurcation analysis of delay differential equations, Technical Report TW 330, Department of Computer Science, K.U.Leuven, Leuven, Belgium, 2001.

Effect of compression and torsion on the stability of drilling processes

Bence Beri* and Gabor Stepan

Budapest University of Technology and Economics, Department of Applied Mechanics, Muegyetem rkp. 5, Budapest 1111, Hungary
*Corresponding author. E-mail address: beri@mm.bme.hu

1 Motivation

Recent developments in deep drilling for the oil and gas industry require to take into account more and more dynamical effects that arise during the process. One of the problems in deep drilling is the occurance of unexpected self-excited vibrations that might appear due to several reasons like the stick-slip effect [1, 2, 3] primariliy related to the torsional oscillations of the drill string, the drill bit-rock interaction [4], and the high structural flexibility of the drilling system. This often results in expensive drill bit failures.

In this study, we focus on the dynamic loss of stability through the drill bit-rock interaction by investigating an equivalent model of milling. The manufacturing processes such as drilling and milling are both subjected to the so-called regenerative effect when either the rotating cutting tool or the workpiece or both are flexible and the chip thickness varies due to the relative vibrations of the tool and the workpiece. The general mechanical model where the regenerative effect first appeared was introduced by Tobias [5] and Tlusty [6]. The tool meets the surface that was formed in the previous cut, that is, the past state of the tool excites the system after a certain time.

The dynamics of the deep drilling process is greatly affected by both the drill dynamics and the high flexibility of the drill string. In the drill dynamics, the regenerative cutting force is introduced because of the hard earth crust removal that gives a regenerative delay in the same way as explained above for machining. However, the drill string is subjected to the combination of longitudinal, torsional and lateral vibrations that all affects the complex dynamics of the system.

This work investigates only the lateral vibrations and considers the system as a damped spring/lumped mass oscillator that models the drill bit and one

segment of the drill string. The goal is to show how the axial (compressive) component of the cutting force and the presence of torsional torque affect the linear stability of the process.

The drill bit/drill string system is modelled by a cantilever beam that is considered to be prismatic, homogeneous, linearly elastic and inextensible. Its mathematical model is based on the Euler-Bernoulli beam theory and the effect of compression and torsion appears through the lateral stiffness of the system. To provide a wider picture about the influence of the applied loads on the stability of the drilling process, different cases are investigated: constant and varying loads. The latter case is somewhat in connection with the regenerative effect. Since compression and torsion decrease the lateral stiffness and modifies the bending natural frequency of the system, it has a destabilizing effect, that is, it reduces the stable region of the drilling process. The changes of the standard stability charts are presented and the reduction of the stable parameter regions is shown.

2 Modelling and Analysis

In order to investigate the lateral vibrations of the drill bit/drill string system, we need to consider a 2 DoF mechanical model shown in Fig.1(a). The system is modelled as a cantilever beam and it is assumed to have symmetric parameters in the directions x and y, and diagonal modal matrices arise in the equation of motion. The governing equation of the system is given by

$$\mathbf{M}\ddot{\mathbf{q}}(t) + \mathbf{C}\dot{\mathbf{q}}(t) + \mathbf{K}\mathbf{q}(t) = \mathbf{F}(t)\,, \tag{1}$$

where

$$\mathbf{q}(t) = \begin{pmatrix} x(t) \\ y(t) \end{pmatrix}\,, \quad \mathbf{F}(t) = \begin{pmatrix} F_x(t) \\ F_y(t) \end{pmatrix}$$

are the position and the cutting force vectors, and $\mathbf{M}\,,\mathbf{C}$ and $\mathbf{K}$ are the modal mass, damping and stiffness matrices, respectively. Based on Fig.1(a), the x and y components of the cutting force acting on the edge j have the form

$$\begin{aligned} F_{j,x}(t) &= F_{j,r}(t)\sin\varphi_j(t) + F_{j,t}(t)\cos\varphi_j(t) \\ F_{j,y}(t) &= F_{j,r}(t)\cos\varphi_j(t) - F_{j,t}(t)\sin\varphi_j(t) \end{aligned} \tag{2}$$

where $\varphi_j(t) = 2\pi\Omega t/60 + 2\pi j/N$ is the angular position of the edge j, N is the number of cutting edges and Ω is the speed of rotation in rpm. The cutting force components $F_{j,r}$ and $F_{j,t}$ are expressed by

$$\begin{aligned} F_{j,r}(t) &= K_r b h_j^q(t)\,, \\ F_{j,t}(t) &= K_t b h_j^q(t)\,, \end{aligned} \tag{3}$$

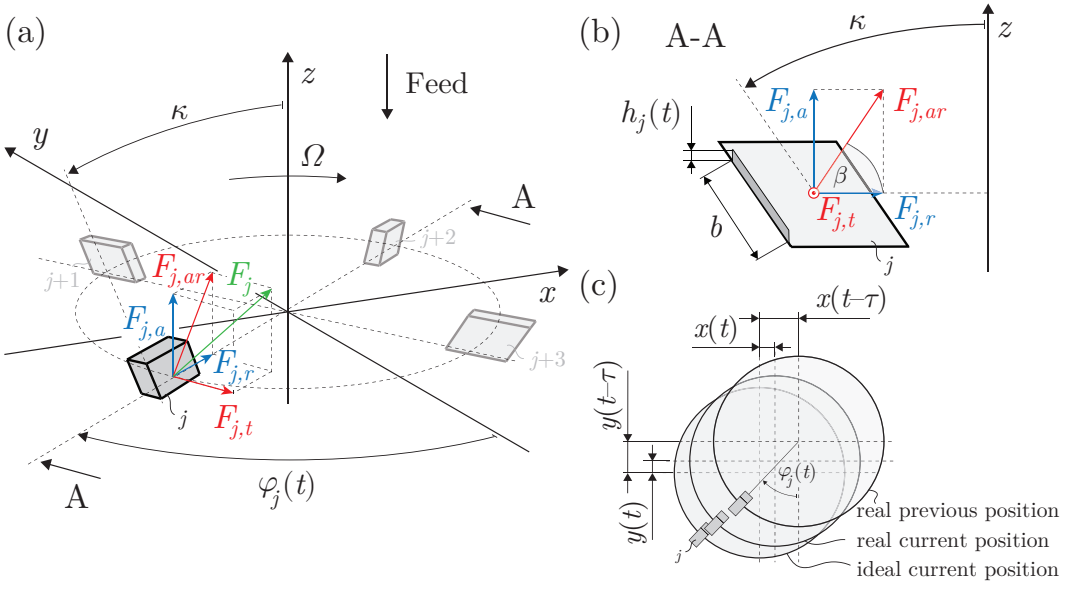

Figure 1: Mechanical model of the drill bit/drill string system. (a) The distribution of the cutting edges with the orientation of the cutting force components on the edge j. (b) The definition of the chip thickness h and the chip width b. (c) The introduction of the regenerative effect.

respectively where K_r and K_t are cutting force parameters, b is the chip width, h is the chip thickness and q is the cutting force exponent [9]. The exponent q represents a strong nonlinearity and plays significant role in determining the cutting conditions to reach the stable region of the process.

In the mechanical model (see Fig.1(a)), it is assumed that the tool never leaves the surface, thus the instantaneous chip thickness $h > 0$ during the process. The chip thickness h can be given as the combination of the feed and the present and delayed position of the drill bit in the form (see Fig.1(b) and (c))

$$h_j(t) = h_s + \frac{1}{\tan\kappa}\left[(x(t-\tau) - x(t))\sin\varphi_j(t) + (y(t-\tau) - y(t))\cos\varphi_j(t))\right] \quad (4)$$

where h_s is the feed per cutting edges and $\tau = 60/(N\Omega)$. After the substitution of Eqs.(3) and (4) into Eq.(2), the linearisation gives

$$\mathbf{F}(t) = K_r b h_s^q \begin{pmatrix} G_1(t) \\ G_2(t) \end{pmatrix} + \frac{q h_s^{q-1} K_r b}{\tan\kappa} \begin{pmatrix} G_{xx}(t) & G_{xy}(t) \\ G_{yx}(t) & G_{yy}(t) \end{pmatrix} (\mathbf{q}(t-\tau) - \mathbf{q}(t)) \quad (5)$$

where

$$G_1(t) = \sum_{j=1}^{N} \left(\sin \varphi_j(t) + \frac{K_t}{K_r} \cos \varphi_j(t) \right) \tag{6}$$

$$G_2(t) = \sum_{j=1}^{N} \left(\cos \varphi_j(t) - \frac{K_t}{K_r} \sin \varphi_j(t) \right) \tag{7}$$

$$G_{xx}(t) = \sum_{j=1}^{N} \left(\sin \varphi_j(t) + \frac{K_t}{K_r} \cos \varphi_j(t) \right) \sin \varphi_j(t) \tag{8}$$

$$G_{xy}(t) = \sum_{j=1}^{N} \left(\sin \varphi_j(t) + \frac{K_t}{K_r} \cos \varphi_j(t) \right) \cos \varphi_j(t) \tag{9}$$

$$G_{yx}(t) = \sum_{j=1}^{N} \left(\cos \varphi_j(t) - \frac{K_t}{K_r} \sin \varphi_j(t) \right) \sin \varphi_j(t) \tag{10}$$

and

$$G_{yy}(t) = \sum_{j=1}^{N} \left(\cos \varphi_j(t) - \frac{K_t}{K_r} \sin \varphi_j(t) \right) \sin \varphi_j(t) \tag{11}$$

are τ periodic functions.

2.1 Nature of the applied loads

Based on the resolution of the cutting force F_j shown in Fig.1(a), its compressive (axial) component $F_{j,a}$ and the presence of the torsional torque M_t affect the lateral stiffness of the system and thus modify its natural frequency. Two cases can be separated: when the applied load is assumed to be constant and when it varies.

According to the Euler-Bernoulli beam theory, the lateral stiffness of the system under compression $F_a = \sum_{j=1}^{N} F_{j,a}$ and torsion M_t is expressed by [7, 8] in the form

$$k = -\frac{\nu F_a^2}{\nu F_a L + \nu M_t \dfrac{\sin(\mu L)}{\cos(\nu L)} - (2\nu^2 IE - F_a)\tan(\nu L)}, \tag{12}$$

where

$$\mu = \frac{M_t}{2IE}, \quad \nu = \frac{1}{2}\sqrt{\left(\frac{M_t}{IE}\right)^2 + \frac{4F_a}{IE}}.$$

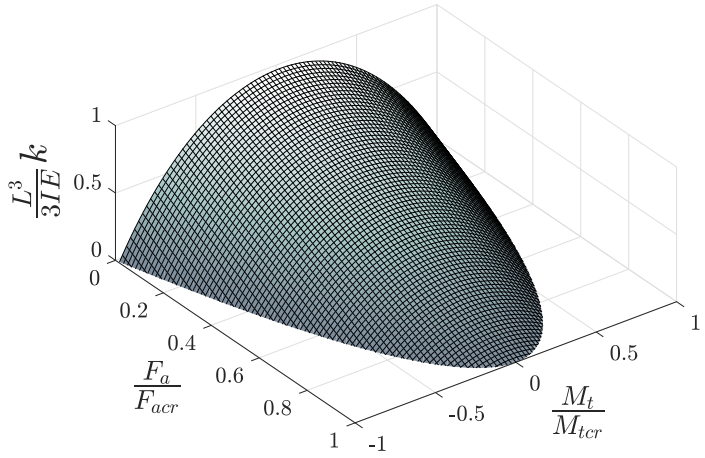

Figure 2: The dimensionless lateral stiffness of the system (see Eq. (12)) where $F_{acr} = \pi^2 IE/(4L^2)$ and $M_{tcr} = \pi IE/L$ (see Ref[8]).

Here, L is the length of the drill bit/drill string model and IE is the bending stiffness. Equation (12) can be approximated by the multi-variable power series [7]

$$k = k_0 - k_1 F_a - \mathcal{O}(F_a^2, M_t^2) \tag{13}$$

where $k_0 = 3IE/L^3$ and $k_1 = 6/(5L)$. It can be seen that the torsional torque M_t does not appear in the linear approximation of Eq.(12) and thus it has no effect on the change of the natural frequency of the system. Besides, in case of compression even the Euler buckling load $F_{cr} = \pi^2 IE/(4L^2)$ is satisfactory approximated by $k = 0$.

Corresponding to Eq.(3), the compressive (axial) force characteristic can be given by

$$F_{j,a}(t) = K_a b h_j^q(t)\,, \tag{14}$$

which is calculated as per cutting edges. By substituting Eq.(4) into Eq.(14), we obtain

$$F_a(t) = K_a b h_s^q + \frac{q h_s^{q-1} K_a b}{\tan\kappa} \begin{pmatrix} G_3(t) \\ G_4(t) \end{pmatrix} (\mathbf{q}(t-\tau) - \mathbf{q}(t)) \tag{15}$$

where

$$G_3(t) = \sum_{j=1}^{N} \sin\varphi_j(t) \tag{16}$$

and

$$G_4(t) = \sum_{j=1}^{N} \cos \varphi_j(t) \,. \tag{17}$$

According to Eqs.(13) and (15), we consider the stiffness matrix in Eq.(1) as

$$\mathbf{K} = \begin{pmatrix} k_0 - k_1 F_a(t) & 0 \\ 0 & k_0 - k_1 F_a(t) \end{pmatrix} . \tag{18}$$

2.2 Stability analysis

To perform the stability analysis of the drilling process, we use the small perturbation method where the solution can be decomposed as

$$\mathbf{q}(t) = \mathbf{q}_{\mathrm{P}}(t) + \boldsymbol{\epsilon}(t) \tag{19}$$

where $\mathbf{q}_{\mathrm{P}}(t)$ is a τ periodic stationary solution and

$$\boldsymbol{\epsilon}(t) = \begin{pmatrix} \xi(t) \\ \eta(t) \end{pmatrix} \tag{20}$$

is the perturbation around $\mathbf{q}_{\mathrm{P}}(t)$. The periodic component $\mathbf{q}_{\mathrm{P}}(t)$ of the drill bit motion can be calculated as the steady-state solution of

$$\mathbf{M}\ddot{\mathbf{q}}_{\mathrm{P}}(t) + \mathbf{C}\dot{\mathbf{q}}_{\mathrm{P}}(t) + \begin{pmatrix} k_0 - k_1 K_a b h_s^q & 0 \\ 0 & k_0 - k_1 K_a b h_s^q \end{pmatrix} \mathbf{q}_{\mathrm{P}}(t) = K_r b h_s^q \begin{pmatrix} G_1(t) \\ G_2(t) \end{pmatrix} . \tag{21}$$

Since the number of cutting edges N is larger than 1, the rhs of Eq.(21) is zero (see Eqs.(6) and (7)) and thus $\mathbf{q}_{\mathrm{P}}$ takes constant zero value as a stationary solution. Substitution of Eq.(19) into Eqs.(1), (5) and (15) and neglecting the higher order terms in $\boldsymbol{\epsilon}$, we get the variational system

$$\begin{aligned} \mathbf{M}\ddot{\boldsymbol{\epsilon}}(t) + \mathbf{C}\dot{\boldsymbol{\epsilon}}(t) + \begin{pmatrix} k_0 - k_1 K_a b h_s^q & 0 \\ 0 & k_0 - k_1 K_a b h_s^q \end{pmatrix} \boldsymbol{\epsilon}(t) \\ = \frac{q h_s^{q-1} K_r b}{\tan \kappa} \begin{pmatrix} G_{xx}(t) & G_{xy}(t) \\ G_{yx}(t) & G_{yy}(t) \end{pmatrix} (\boldsymbol{\epsilon}(t-\tau) - \boldsymbol{\epsilon}(t)) \end{aligned} \tag{22}$$

that is used to determine the stability of the drilling process.

3 Results

Since the system matrices are assumed to have symmetric parameters in both directions x and y and they are diagonal, the natural angular frequency ω_n of the system can be calculated directly in accordance with Eq.(13). When the value of the compressive force F_a is zero or constant then the natural angular frequency ω_n is also a constant number. In the stability charts, the dimensionless chip width $\bar{b} = qh_s^{q-1}K_r b/(mf_{n0}^2 \tan\kappa)$ is used where m is the modal mass and $f_{n0} = \sqrt{k_0/m}/(2\pi)$ is the basic natural frequency. There is a connection between the cutting force parameters K_t, K_r and K_a, that is, $K_r = \sigma K_t$ and $K_a = \sigma K_t \tan\beta$ where σ is an empirical number and β is assumed to be equal to κ (see Fig.1(b)).

The dimensionless stability lobes shown in Fig.2 can be constructed by using the so-called semi-discretization method [10]. $\bar{b}$ is proportional to the chip width b, thus only the practically relevant domain $\bar{b} > 0$ is depicted. It can be seen that the constant compressive force provides a shifted stability map. The map moves left and down because the lateral stiffness of the system decreases, which affects the natural angular frequency, too.

In contrast, in case of varying compression, the natural frequency f_n also depends on the chip width b, which leads us to the dimensionless stability diagram, which is depicted in Fig.3(c). Since the natural frequency decreases as $\bar{b}$ increases, the lobe structure is shifted a little down and deflected both to the left and also somewhat to the right compared to the non-compressed case. This means, for example, that the available maximum values of the chip width b are reduced in the stable pockets of the charts.

Vibrations arise when the system loses its stability and these vibration frequencies arising at the stability boundary of the drilling process is also shown in Fig.3(a) and (b). The continuous lines represents the so-called secondary Hopf (Neimark-Sacker) bifurcation and the dotted lines show the period doubling bifurcation. It can be seen that the period doubling bifurcation vanishes where the frequency lines of the Hopf bifurcation intersect each other.

4 Conclusion

This paper brings up the topic of the stability of the deep drilling process by investigating an equivalent model of the milling operation. The system is described by a 2 DoF dynamical model. The cutting force F_j can be resolved to a radial force $F_{j,r}$, a tangential force $F_{j,t}$ and an axial force $F_{j,a}$ that acts on the drill bit as compression. Besides, torsional torque M_t also appears. This study investigates two cases: when the applied load is considered to be either constant or varying.

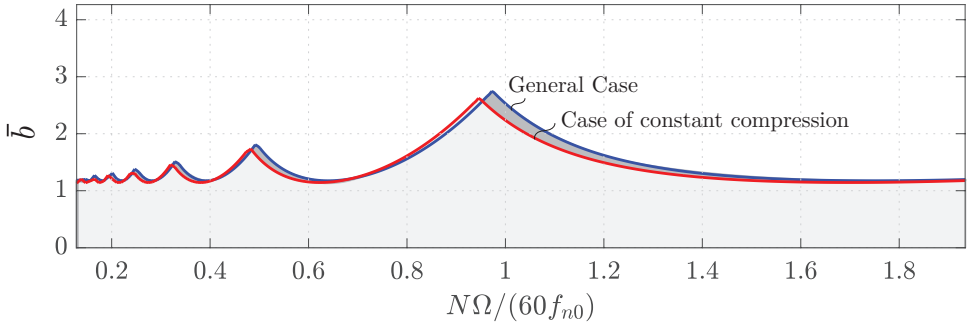

Figure 3: Comparison of the dimensionless stable regions of the drilling process where the general case means the system under no compression. The numerical values $\sigma = 0.3$, L =2.5 m, $\kappa = 80\,\text{deg}$, $q = 0.55$, $\zeta = 0.2$ and $F_a = 350$ kN are used.

Based on the Euler-Bernoulli beam theory, the lateral stiffness of the drill bit/drill string system can be calculated, which depends on compression F_a and torsion M_t, respectively. It also describes the variation of the natural frequency of the drill bit/drill string system. However, it can be shown that the torsional torque M_t has no effect in the linear approximation of the stiffness.

By using constant compression, the so-called lobe structure is slightly shifted to the left and down compared to the general case with no compression. In contrast, under varying compression, the stability map is shifted down and bent both to the left and slightly to the right compared to the general non-compressed case. The vibration frequencies arising at the stability boundary reveal how the period doubling bifurcation vanishes as the frequency lines of the secondary Hopf bifurcation intersect.

These phenomena may play a relevant role when the complex drill bit dynamics is considered including all the axial, torsional and lateral vibrations.

Acknowledgements

The research leading to these results has received funding from the European Research Council under the European Unions Seventh Framework Program (FP/2007-2013)/ERC Advanced Grant Agreement No. 340889.

References

[1] Baumgart A. Stick-slip and bit-bounce of deep-hole drill strings. Journal of Energy Resources Technology, 2000; Vol. 122, pp. 78-82.

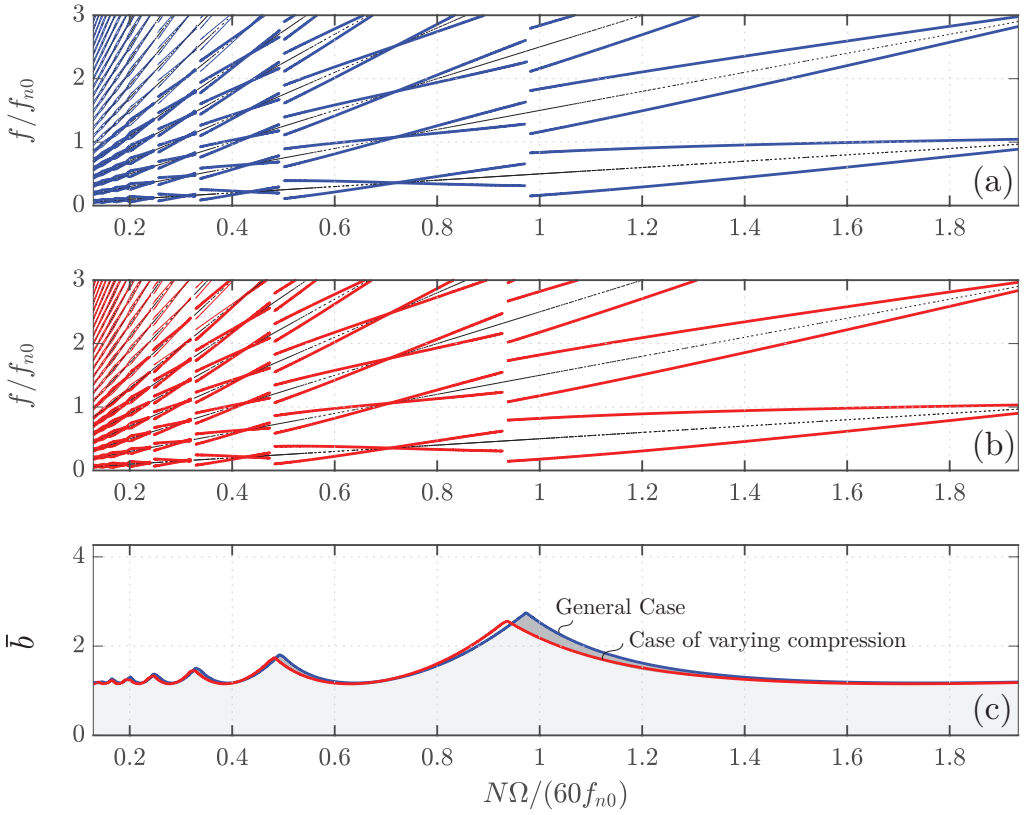

Figure 4: (a) Dimensionless frequency diagram in the absence of compression F_a. (b) Dimensionless frequency diagram in the presence of compression F_a. (c) Comparison of the stable regions of the drilling process where the general case means the system under no compression. The numerical values $\sigma = 0.3$, $K_t = 200 \times 10^6$ N/m^{q+1}, $h_s = 0.01$ m, L =2.5 m, $\kappa = 80\,\text{deg}$, $q = 0.55$ and $\zeta = 0.2$ are used.

[2] Kovalyshen Y. Understanding root cause of stickslip vibrations in deep drilling with drag bits. International Journal of Non-Linear Mechanics, 2014; Vol. 67, pp. 331-341.

[3] Aarsnes UJF, Shor RJ. Stick-slip and Torsional Friction Factors in Inclined Wellbores. MATEC Web of Conferences. 2018; Vol. 148. pp. 16002.

[4] Liu X, Vlajic N, Long X, Meng G, Balachandran B. Coupled axial-torsional dynamics in rotary drilling with state-dependent delay: stability and control. Nonlinear Dynamics. 2014; Vol. 78. pp. 1891-1906.

[5] Tobias SA. Machine tool vibration. Blackie, London (1965).

[6] Tlusty J, Polacek M. The stability of machine tools against self-excited vibrations in machining. International Research in Production Engineering, ASME, 1963; Vol. 1:465-474.

[7] Beri B, Stepan G, Hogan SJ. Effect of Potential Energy Variation on the Natural Frequency of an Euler-Bernoulli Cantilever Beam Under Lateral Force and Compression. Journal of Applied Mechanics. 2017; Vol. 84. pp. 051002.

[8] Beri B, Hogan SJ, Stepan G. Structural stability of a light rotating beam under combined loads. Acta Mechanica. 2017;Vol. 228. pp. 3735-3740.

[9] Altintas Y. Manufacturing Automation. UK, University Press Cambridge. 2012.

[10] Insperger T, Stepan G. Semi-Discretization for Time-Delay Systems. Springer-Verlag, New York. 2011.

Improving stability of steady drilling using a non-uniform distribution of cutters on the drill-bit

Sunit Kumar Gupta, Pankaj Wahi

Department of Mechanical Engineering, Indian Institute Of Technology Kanpur, Kanpur, Uttar Pradesh-208016, India, wahi@iitk.ac.in

1 Introduction

Drill-string plays an important role in rotary deep drilling systems. Drill-string, consisting of a series of drill-pipes, is used to transmit rotary power from the top to bottom hole assembly which further carries drill-collar and drill-bit. Hence, any failure in drill-string causes the shut down of the entire drilling operation and loss to drilling industry. Self-excited vibrations in axial, torsional and lateral directions, which manifest as bit-bounce, stick-slip and whirling motion, respectively are one of the major cause of drill-string failure. Therefore, it is necessary to understand their origin and explore methods to suppress these vibrations.

One of the major cause of these self-excited vibrations is attributed to the regenerative effect which is associated with a varying depth of cut per revolution due to axial vibrations. The depth of cut with the regenerative effect can be modeled using a delayed value of the axial displacement. However, the time-delay which is the time taken by one cutter to occupy the position of the previous cutter depends on the current and delayed value of the drill twist making it an implicit state-dependent delayed equation [1–4]. However, all of them employ drill-bits where the cutters are uniformly distributed. In this work, we explore the effect of a non-uniform distribution of the cutters along the drill-bit on the stability of steady drilling and hence, avoiding self-excited vibrations. We have found the state-dependent delay model to be rather cumbersome for this purpose. Instead we have modified the recently proposed alternate approach to model the axial-torsional dynamics of rotary drilling [5, 6] to accommodate the uneven distribution of the cutters.

There are several different approaches which have been employed in the literature to control/suppress self-excited vibrations in rotary drilling. They can be broadly classfied into three categories: proper design of drilling apparatus along

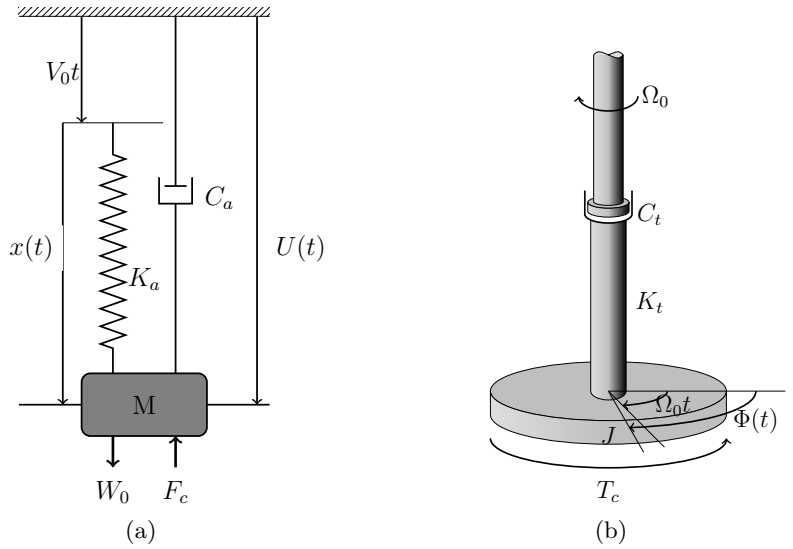

Figure 1: Schematics of (a) axial and (b) torsional dynamics of drill-string.

with proper choice of operating parameters [6–9]; by passive control through the use of additional devices like shock absorbers or shock subs which are essentially tuned vibration absorbers [10, 11]; and the use of active controllers wherein an actuator applies a force at the drill-bit depending on the measured vibration levels [12–15]. Our approach of distributing the cutters non-uniformly on the drill-bit fits into the first category and is motivated by its successful application in improving stability in multi-cutter machining processes, viz. in milling or drilling in metals [16–18]. In order to study the effect of non-uniform distribution of cutters on the drill-bit on the stability of the steady drilling state, we compute the stability of the system numerically using a modified version of the discretized equations developed in [5] instead of an exact analytical stability analysis as performed in [6, 19] for simplicity. We observe that this method is fairly effective in mitigating drill-string vibrations. We start with a brief description of a mathematical model for rotary drilling with such a drill-bit.

2 Mathematical model

In this section we briefly outline the simplified lumped parameter axial-torsional model of rotary drilling [1] which is being used in the current work. In the axial direction, the drill-string is modeled as a spring-mass-damper system with spring stiffness (K_a), viscous damping coefficient (C_a) and the combined mass (M) of the drill-pipes and the bottom hole assembly (BHA) lumped at the end

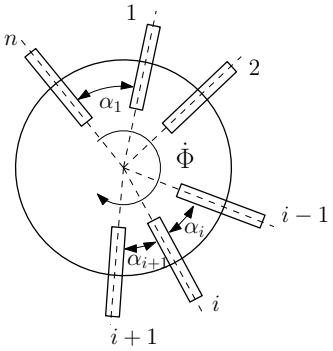

Figure 2: Schematic for the nonuniform angular distribution of cutters/blades on a drill-bit. The angle α_i is constant as the drill-bit is considered as a rigid body.

(Fig. 1a). For torsional oscillations, the drill-string is modeled as a system with torsional spring stiffness (K_t), torsional viscous damping coefficient (C_t) and the combined rotary inertia of the drill-pipes and the BHA (J) about the rotational axis (Fig. 1b). Equations of motion for this system in the axial and torsional directions are [1, 2]

$$M\ddot{U}(t) + C_a\dot{U}(t) + K_a\left\{U(t) - V_0 t\right\} = W_0 - \xi\epsilon a d(t) H(\dot{\Phi}) H(d(t))\,, \tag{1a}$$

$$J\ddot{\Phi}(t) + C_t\dot{\Phi}(t) + K_t\left\{\Phi(t) - \Omega_0 t\right\} = -\frac{\epsilon a^2 d(t)}{2} H(\dot{\Phi}) H(d(t))\,. \tag{1b}$$

For a drill-bit with n identical, uniformly distributed cutters the total depth of cut per revolution $d(t)$ will be $d(t) = nd_n(t)$ with $d_n(t)$, the depth of cut per cutter, is given by

$$d_n(t) = U(t) - U\left(t - t_n\right). \tag{2}$$

In the absence of the torsional oscillations t_n will be $\dfrac{2\pi}{n\Omega_0}$. However, in the presence of torsional oscillations, this definition of t_n does not hold any longer and t_n can be determined by

$$\Phi(t) - \Phi(t - t_n) = \frac{2\pi}{n}. \tag{3}$$

In the case of a drill-bit with a non-uniform distribution of cutters/blades as shown in Fig. 2, different cutters will experience different depths of cut. Note from Fig. 2 that we have identified the n^{th} cutter with the zeroth cutter and accordingly, α_i represents the angular separation between the $(i-1)^{th}$ and i^{th}

cutter. For a drill-bit with n cutters, the depth of cut for the i^{th} can be obtained as

$$d_i(t) = U(t) - U(t - t_i(t)) \,, \quad i = 1,\, 2,\, \cdots n \tag{4}$$

with different delays $t_1(t),\, t_2(t) \cdots t_i(t) \cdots t_n(t)$ associated with cutters $1,\, 2 \cdots i \cdots n$ computed through

$$\Phi(t) - \Phi(t - t_i(t)) = \alpha_{i+1} \,, \quad i = 1,\, 2,\, \cdots n \tag{5}$$

With the above definition of the depth of cut for each cutter and under the assumption of a homogeneous rock, we can get the depth of cut per revolution (which governs the resultant cutting forces and torques) as

$$d(t) = \sum_{i=1}^{n} d_i(t) \,. \tag{6}$$

The various state-dependent delays, $t_i(t)$'s, assoicated with different cutters are independent of each other, making it fairly complicated to compute the stability of the system analytically. Also, the above description of the depth of cut associated with each cutter is valid only when each cutter on the drill-bit is always in contact with the cut-surface. As soon as any cutter on the drill-bit loses contact with the surface being cut due to excessive axial vibrations (full or partial bit-bounce), some of the relations in Eqs. (5) governing the time delays $t_i(t)$ will not remain valid throughout. This shortcoming of the state-dependent delay differential equation model (SDDDE) model has already been highlighted in [5]. Since the computation of the time delay $t_i(t)$ and in turn the instantaneous depth of cut $d_i(t)$ per cutter becomes involved using Eqs. (4) and (5) in the event of bit-bounce, we adopt the global model [5] for the depth of cut. Following the procedure mentioned in [5], we non-dimensionlize the equations of motion which are reproduced below:

$$\begin{aligned} \ddot{x}(\tau) + 2\zeta\beta\dot{x}(\tau) + \beta^2 x(\tau) &= \psi\delta_0 - \psi \sum_{i=1}^{n} \delta_i(\tau) H(\omega + \dot{\theta}(\tau)) H(\delta_i(\tau)), \\ \ddot{\theta}(\tau) + 2\kappa\dot{\theta}(\tau) + \theta(\tau) &= \delta_0 - \sum_{i=1}^{n} \delta_i(\tau) H(\omega + \dot{\theta}(\tau)) H(\delta_i(\tau)) \,, \end{aligned} \tag{7}$$

where δ_0 is the nondimensional steady depth of cut per revolution while $\delta_i(\tau)$ represents the nondimensional instantaneous depth of cut for the i^{th} cutter. Since we are analyzing the stability characteristics of the steady drilling state which

will imply always cutting condition, Heaviside functions are dropped from the Eq. (7) along with tilde (for notational convenience) to get

$$\begin{aligned} \ddot{x}(\tau) + 2\zeta\beta\dot{x}(\tau) + \beta^2 x(\tau) &= \psi 2\pi v - \psi \sum_{i=1}^{n} \delta_i(\tau)\,, \\ \ddot{\theta}(\tau) + 2\kappa\dot{\theta}(\tau) + \theta(\tau) &= 2\pi v - \sum_{i=1}^{n} \delta_i(\tau)\,, \end{aligned} \tag{8}$$

where $v = \dfrac{v_0}{\omega_0} = \dfrac{n\,\delta_0}{2\pi}$ is the nondimensional velocity ratio. In what follows, we present the modifications in the alternate model for the depth of cut to account for this variable separation between the different cutters.

2.1 Modified model for the depth of cut

As mentioned earlier in the text, we will adopt the approach developed in [5] for seamlessly incorporating multiple delays due to the non-uniform distribution of cutters in the dynamics of rotary drilling. For the sake of completeness, we reproduce the salient details of the approach. We had defined the cut surface between two successive cutters by a function L which defines the perpendicular distance of the material point on the cut surface at a given angle ϕ and time τ from some reference (as shown in Fig. 3). Under the assumption that all cutters are identical and the drill-bit moves as a rigid body, the cut surface between any two successive cutters is the same for all sections and the domain of ϕ is $(0, 2\pi/n]$. For a non-uniform distribution of cutters, the domain of ϕ for each cutter will be different and it will be given by $\phi \in (0, \alpha_i]$ for the cut surface between the $(i-1)^{th}$ cutter and the i^{th} cutter. Hence, by considering the domain of ϕ to be $(0, \alpha_{max}]$ where $\alpha_{max} = \max(\alpha_i,\, i = 1,\, 2,\, \cdots n)$ and a single function L representing the cut surface seems like a good option. This option will work well till all the cutters are always in contact since the cut surface between any two cutters can be obtained by considering the appropriate portion of that sliced from the full-domain. This option is good enough for the current purpose of stability evaluation of the steady drilling state. However, we would like to present the model which can possibly take care of self-interruptions as well. Under such conditions, we can no longer represent the cut surface between any two successive cutters by the same function L. There is a possibility of partial bit bounce wherein some cutter has lost contact with the cut surface while the other cutters are still in engagement. Accordingly, the cut surface between some cutters will remain the same while the cut surface between two other pair of cutters will continue to be modified by the cutting action. Therefore, we introduce separate functions $L_i(\phi, \tau)$ to represent the cut surface between the cutters $i-1$ and i

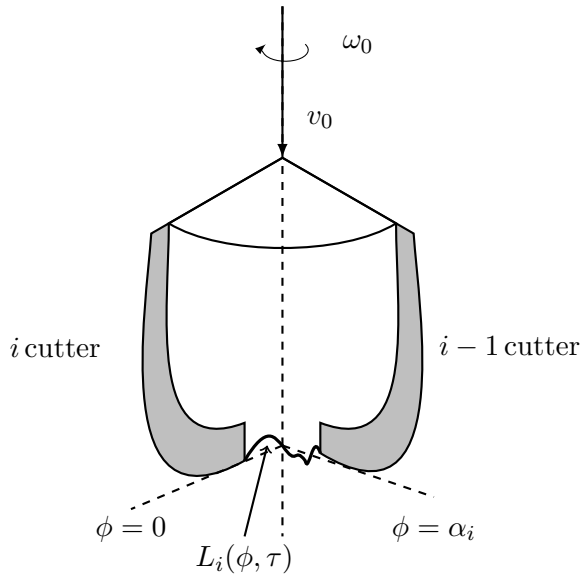

Figure 3: Schematic of the section between two successive cutters.

as shown in Fig. 3. We note that this increases the computational complexity as there will be separate equations governing the evolution of each function $L_i(\phi, \tau)$. However, this general formulation will take care of both partial and full axial self-interruption (bit-bounce) and we will be able to capture the full nonlinear behavior of the system which is part of future work. Following [5], we get the evolution of $L_i(\phi, \tau)$ for $\phi \in (0, \alpha_i]$ to be governed by the partial differential equation (PDE)

$$\frac{\partial L_i}{\partial \tau} + \left(\omega_0 + \frac{\mathrm{d}\theta}{\mathrm{d}\tau}\right) \frac{\partial L_i}{\partial \phi} = 0\,, \qquad i = 1, 2, \cdots, n\,. \tag{9}$$

To get the boundary condition for each PDE in Eq. (9), we note that the cut surface at the current cutter location (i^{th} cutter) $L_i(0, \tau)$ during the engaged position is its actual position, i.e.,

$$L_i(0, \tau) = L_i(0, 0) - v_0\tau - x(\tau) = -v_0\tau - x(\tau) \quad (\text{with } L_i(0, 0) = 0)\,. \tag{10}$$

During bit-bounce, the cut surface does not modify and we have $L_i(0, \tau) = L_{i+1}(\alpha_{i+1}, \tau)$ which leads to

$$L_i(0, \tau) = \min\left\{-v_0\tau - x(\tau), L_{i+1}\left(\alpha_{i+1}, \tau\right)\right\}\,, \qquad i = 1, 2, \cdots, n\,. \tag{11}$$

The instantaneous depth of cut for the i^{th} cutter can be obtained in terms of $L_i(0,\tau)$ and $L_{i+1}(\alpha_{i+1},\tau)$ as

$$\delta_i(\tau) = \max\left\{L_{i+1}\left(\alpha_{i+1},\tau\right) - L_i(0,\tau), 0\right\} = \max\left\{L_{i+1}\left(\alpha_{i+1},\tau\right) + v_0\tau + x(\tau)\,,\, 0\right\} \tag{12}$$

which includes the possibility of the cutter i on the drill-bit leaving the cut surface (bit-bounce) [5].

For the ease of further algebra, we introduce the function $\bar{L_i} = L_i + v_0\tau$ ([5, 20]) which modifies the governing PDE and the boundary condition (for $i = 1, 2, \cdots, n$) to

$$\frac{\partial \bar{L}_i}{\partial \tau} + \left(\omega_0 + \frac{\mathrm{d}\theta}{\mathrm{d}\tau}\right)\frac{\partial \bar{L}_i}{\partial \phi} - v_0 = 0\,, \tag{13}$$

$$\bar{L_i}(0,\tau) = \min\left\{-x(\tau), \bar{L}_{i+1}\left(\alpha_{i+1},\tau\right)\right\}\,. \tag{14}$$

The modified relation between the depth of cut for cutter i, $\delta_i(\tau)$ and $x(\tau)$ in terms of the new functions $\bar{L}_i$ is

$$\delta_i(\tau) = \max\left\{\bar{L}_{i+1}\left(\alpha_{i+1},\tau\right) + x(\tau), 0\right\}. \tag{15}$$

Equations (13), (14) and (15) together with Eq. (8) describe the complete global axial-torsional dynamics of rotary drilling with a non-uniform distribution of the cutters on the drill-bit. In the next section, we present a discretization of these coupled ODE-PDE system which will be further used for the stability analysis of steady drilling.

3 Reduced order system using Galerkin projection

For the discretization of Eq. (13), we follow the Galerkin projection approximation developed in [5] in which the function $\bar{L}_i(\phi,\tau)$ is approximated as

$$\bar{L}_i(\phi,\tau) = a_{0,i}(\tau)\left(1 - \frac{\phi}{\alpha_i}\right) + a_{1,i}(\tau)\frac{\phi}{\alpha_i} + \sum_{k=1}^{N-1} a_{k+1,i}(\tau)\sin\left(\frac{\phi k\pi}{\alpha_i}\right) \tag{16}$$

with N representing the number of terms in the approximation and $a_{j,i}(\tau)'s$ for $j = 0 \cdots N$ represent the undetermined functions of τ that define the cut surface between the cutters $i-1$ and i. From the above approximation for $\bar{L}_i(\phi,\tau)$, we have $\bar{L}_i(0,\tau) = a_{0,i}(\tau)$ and $\bar{L}_{i+1}(\alpha_{i+1},\tau) = a_{1,i+1}(\tau)$. Hence, the depth of cut, for cutter i, from Eq. (15) can be written as

$$\delta_i(\tau) = \max\{a_{1,i+1}(\tau) + x(\tau), 0\} \tag{17}$$

and the boundary condition from Eq. (14) becomes

$$a_{0,i}(\tau) = \min\{-x(\tau), a_{1,i+1}(\tau)\}. \tag{18}$$

Therefore, $a_{0,i}(\tau)$ for each cut surface section acts as a dummy variable with $a_{0,i}(\tau) = -x(\tau)$ during cutting and $a_{0,i}(\tau) = a_{1,i+1}(\tau)$ during cutter-bounce. For steady drilling, there will be no loss of contact and hence, $\delta_i(\tau) = a_{1,i+1}(\tau) + x(\tau)$ and $a_{0,i} = -x(\tau)$. In the remainder of this work, we will be using these relations only. On substituting $\bar{L}_i$ in Eq. (13), we get

$$\begin{aligned} -\dot{x}(\tau)\left(1 - \frac{\phi}{\alpha_i}\right) + \dot{a}_{1,i}(\tau)\frac{\phi}{\alpha_i} + \sum_{k=1}^{N-1} \dot{a}_{k+1,i}(\tau)\sin\left(\frac{\phi k\pi}{\alpha_i}\right) \\ + \left(\omega_0 + \frac{\mathrm{d}\theta}{\mathrm{d}\tau}\right)\left\{-x(\tau)\frac{1}{\alpha_i} + a_{1,i}(\tau)\frac{1}{\alpha_i} + \sum_{k=1}^{N-1} \frac{a_{k+1,i}(\tau)k\pi}{\alpha_i}\cos\left(\frac{\phi k\pi}{\alpha_i}\right)\right\} \\ - v_0 = 0\,, \end{aligned} \tag{19}$$

where dot represents derivative with respect to τ. Note that the above equation is not satisfied identically and the left hand side of the equation denotes the residue ($R_{e,i}$) as

$$\begin{aligned} R_{e,i} = -\dot{x}(\tau)\left(1 - \frac{\phi}{\alpha_i}\right) + \dot{a}_{1,i}(\tau)\frac{\phi}{\alpha_i} + \sum_{k=1}^{N-1} \dot{a}_{k+1,i}(\tau)\sin\left(\frac{\phi k\pi}{\alpha_i}\right) \\ + \left(\omega_0 + \frac{\mathrm{d}\theta}{\mathrm{d}\tau}\right)\left\{x(\tau)\frac{1}{\alpha_i} + a_{1,i}(\tau)\frac{1}{\alpha_i} + \sum_{k=1}^{N-1} \frac{a_{k+1,i}(\tau)k\pi}{\alpha_i}\cos\left(\frac{\phi k\pi}{\alpha_i}\right)\right\} - v_0\,. \end{aligned} \tag{20}$$

This residue $R_{e,i}$ is minimized in the Galerkin projection approach by making it orthogonal to the shape functions corresponding to the variables $a_{j,i}(t)$ for $j = 1, \cdots, N$. This results in the following N ODEs governing the evolution of the $a_{j,i}(\tau)$ for each i:

$$\int_0^{\alpha_i} R_e \frac{\phi}{\alpha_i}\mathrm{d}\phi = 0\,, \tag{21}$$

$$\int_0^{\alpha_i} R_e \sin\left(\frac{\phi k\pi}{\alpha_i}\right)\mathrm{d}\phi = 0\,, \qquad \text{for } k = 1, \cdots, N-1\,. \tag{22}$$

Note that the above set of equations explicitly involve $\dot{\theta}$ which provides direct coupling with Eq. (8) along with the indirect coupling with $x(t)$ which determines the depth of cut. Now, if there are n numbers of cutters on drill-bit, we will end up with $n \times N + 4$ first order ODEs defining the complete dynamics of the

drill-string during the continuous engagement condition. We will now use this reduced system of ODEs to obtain the stability properties of the steady drilling state. A study of the full nonlinear dynamic behavior of this case has been left for future work.

4 Steady drilling state and its stability

For the current analysis, we take $N = 25$ terms for the approximation of L_i. For the linear analysis, the system parameter values of $\beta = 1.5816$, $\psi = 13.8943$, $\zeta = 0.01$, and $\kappa = 0.01$ have been used. As noted earlier, steady drilling corresponds to $x(\tau) = \dot{x}(\tau) = \theta(\tau) = \dot{\theta}(\tau) = 0$ with the cut surface during steady drilling given by $\bar{L}_i(\phi, \tau) = v\phi \in (0, \alpha_i)$ which implies that $a_{1,i}(\tau) = v\alpha_i$ and $a_{j,i}(\tau) = 0$ for $j = 2, \cdots, N$. Writing this steady state drilling configuration in a compact form as $\mathbf{X_0}$ and linearizing Eqs. (8), (21), and (22) about it, we get the linearized equation in the state-space form

$$\dot{\mathbf{X}}(\tau) = \mathbf{A}\mathbf{X}(\tau)\,. \tag{23}$$

In the above, $\mathbf{X}(\tau) = \left\{a_{j,i}, x(\tau), \dot{x}(\tau), \theta(\tau), \dot{\theta}(\tau)\right\}$ with $j = 1,\ 2,\ \cdots N$ and $i = 1,\ 2,\ \cdots n$, (n being the number of cutters) is the state space vector and $\mathbf{A}$ is the Jacobian matrix of size $(n \times N + 4) \times (n \times N + 4)$ evaluated at the steady state $\mathbf{X_0}$ for the chosen system and operating parameters v and ω_0. The stability of the steady drilling state ($\mathbf{X_0}$) for different values of the operating parameters (v and ω_0) can be computed by calculating the spectrum of the Jacobian matrix $\mathbf{A}$. The boundary between stable and unstable drilling has been obtained as the set of parameters for which the dominant eigenvalue (the one with the largest real part) is purely imaginary. The linear stability charts thus produced in the space of operating parameters v and ω_0 have been compared for different distribution of the angles α_i for two and three cutters in Fig. 4. It can be noted from Fig. 4 that for both $n = 2$ and $n = 3$, the stable regime is much larger when the cutters are not equally spaced. An optimization study to obtain the distribution of the angular spacing between the various cutters leading to most stable configuration has been performed but not reported here for the sake of brevity. These results will be presented at the colloquium. For the case of $n = 3$, we have done further analysis with a certain specific relation between the angular spacing. In particular, we have considered a linear variation as well as the case when two angles are the same. These variations have been considered for milling operation [16–18] wherein it has been shown that the linear variation gives a larger stable region. These results for $n = 3$ are shown in Fig. 5. Also notice in Figs. 4 and 5 that there are multiple stable regimes when the angular spacing for the different

cutters is different. These preliminary results clearly point towards the efficacy of mitigating drill-string vibrations using non-uniform distribution of cutters on the drill-bit.

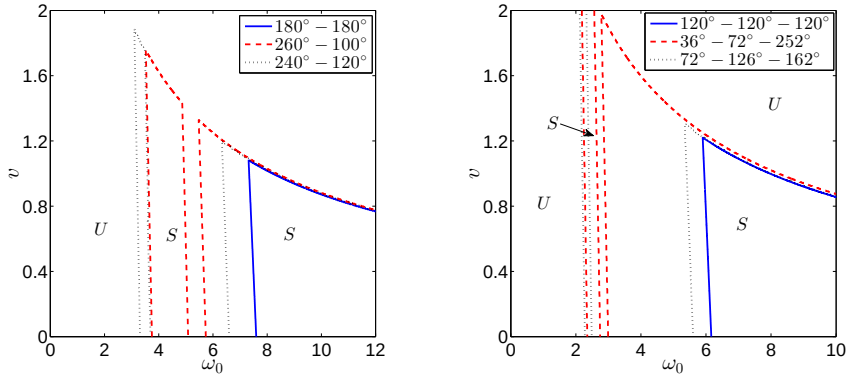

(a) (b)

Figure 4: Stability curves with random distribution for (i) $n = 2$ and (ii) $n = 3$ cutters on drill-bit with $\beta = 1.5816$, $\psi = 13.8943$, $\zeta = 0.01$, $\kappa = 0.01$.

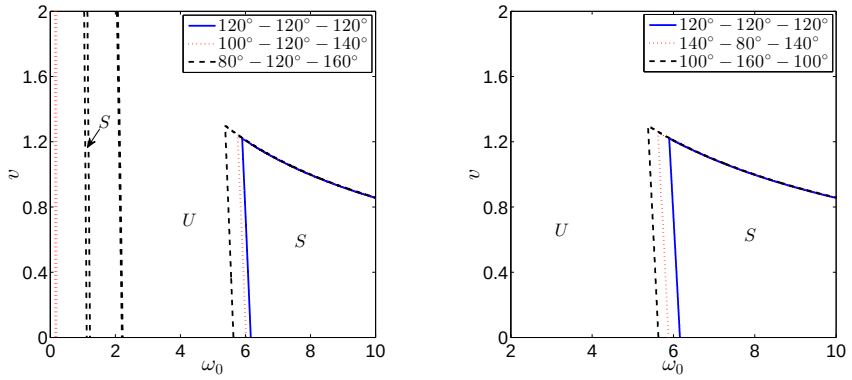

(a) (b)

Figure 5: Stability curves with (i) linear distribution and (ii) alternate variation of cutters with $n = 3$ in drill-bit with $\beta = 1.5816$, $\psi = 13.8943$, $\zeta = 0.01$, $\kappa = 0.01$.

5 Summary

From the results obtained in this work, we can observe that there is a significant improvement in the stability boundary with uneven distribution of the cutters as compared to a uniform distribution. It has to be noted that for the case of random distribution of cutters, the improvement is much larger than other variations which have been considered earlier in relation to milling[17]. This

observation further motivates us to find the optimum angles between the various cutters to enhance the stability of steady drilling which will be presented at the colloquium. A detailed nonlinear dynamic behavior of the system is currently being investigated and these results will also be presented at the collquium.

References

[1] T Richard, C Germay, and E Detournay. A simplified model to explain the root cause of stick-slip vibrations in drilling systems with drag bits. *Journal of Sound and Vibration*, 305(3):432–456, 2007.

[2] K Nandakumar and M Wiercigroch. Galerkin projections for state-dependent delay differential equations with applications to drilling. *Applied Mathematical Modelling*, 47(4):1705âĂŞ1722, 2013.

[3] S K Gupta and P Wahi. Criticality of bifurcation in the tuned axial–torsional rotary drilling model. *Nonlinear Dynamics*, pages 1–18, 2017.

[4] S K Gupta and P Wahi. Bifurcations in the axial-torsional state-dependent delay model of rotary drilling. *International Journal of Non-Linear Mechanics*, 2017.

[5] S K Gupta and P Wahi. Global axial–torsional dynamics during rotary drilling. *Journal of Sound and Vibration*, 375:332–352, 2016.

[6] S K Gupta and P Wahi. Tuned dynamics stabilizes an idealized regenerative axial-torsional model of rotary drilling. *Journal of Sound and Vibration*, 412:457 – 473, 2018.

[7] D W Dareing. Drill collar length is a major factor in vibration control. *Journal of petroleum technology*, 36(04):637–644, 1984.

[8] J J Bailey and I Finnie. An analytical study of drill-string vibration. *Journal of Manufacturing Science and Engineering*, 82(2):122–127, 1960.

[9] V I Gulyaev, P Z Lugovoi, V V Gaidaichuk, I L SolovâĂŹev, and I V Gorbunovich. Effect of the length of a rotating drill-string on the stability of its quasistatic equilibrium. *International Applied Mechanics*, 43(9):1017–1023, 2007.

[10] T W Warren, J H Oster, L A Sinor, and D C K Chen. Shock sub performance tests. In *IADC/SPE drilling conference*. Society of Petroleum Engineers, 1998.

[11] M A Elsayed and C Aissi. Analysis of shock absorber characteristics for drillstrings. In *ASME 8th Biennial Conference on Engineering Systems Design and Analysis*, pages 93–101. American Society of Mechanical Engineers, 2006.

[12] M Zamanian, S E Khadem, and M R Ghazavi. Stick-slip oscillations of drag bits by considering damping of drilling mud and active damping system. *Journal of Petroleum Science and Engineering*, 59(3):289–299, 2007.

[13] A P Christoforou and A S Yigit. Active control of stick-slip vibrations: The role of fully coupled dynamics. In *SPE middle east oil show*. Society of Petroleum Engineers, 2001.

[14] A S Yigit and A P Christoforou. Coupled torsional and bending vibrations of actively controlled drillstrings. *Journal of Sound and Vibration*, 234(1):67–83, 2000.

[15] S A Al-Hiddabi, B Samanta, and A Seibi. Non-linear control of torsional and bending vibrations of oilwell drillstrings. *Journal of sound and vibration*, 265(2):401–415, 2003.

[16] Y Altıntas, S Engin, and E Budak. Analytical stability prediction and design of variable pitch cutters. *Journal of Manufacturing Science and Engineering*, 121(2):173–178, 1999.

[17] E Budak. An analytical design method for milling cutters with nonconstant pitch to increase stability, part i: theory. *Transactions-American Society of Mechanical Engineers Journal of Manufacturing Science and Engineering*, 125(1):29–34, 2003.

[18] E Budak. An analytical design method for milling cutters with nonconstant pitch to increase stability, part 2: application. *Transactions-American Society of Mechanical Engineers Journal of Manufacturing Science and Engineering*, 125(1):35–38, 2003.

[19] K Nandakumar and M Wiercigroch. Stability analysis of a state dependent delayed, coupled two dof model of drill-string vibration. *Journal of Sound and Vibration*, 332(10):2575 – 2592, 2013.

[20] P Wahi and A Chatterjee. Self-interrupted regenerative metal cutting in turning. *International Journal of Non-linear Mechanics*, 43(2):111–123, 2008.

Influence of Bit Design on the Stick-slip Vibrations of a Rotary Drilling System

Kaixiao Tian and Emmanuel Detournay

Department of Civil, Environmental, and Geo- Engineering, University of Minnesota, USA

1 Introduction

When drilling a deep wellbore with a rotary drilling system, the drillstring often experiences self-excited vibrations, which can lead to dysfunctions such as bit bounce, stick-slip and whirling. Those dysfunctions will cause premature failure of drill bits and other components within the system.

The RGD model [11] analyzes the occurrence of stick-slip vibrations in rotary drilling systems equipped with PDC bits by reducing the drillstring into a two degrees-of-freedom coupled axial-torsional system, as sketched in Fig 1(a). The model also assumes a rate-independent bit-rock interaction law that accounts for both cutting by PDC inserts and frictional contact on the cutter wearflats [5] and further simplifies the bit geometry to n identical continuous blades evenly distributed around the bit axis of revolution. Given the rotary motion of the drill bit, the cutting process is subject to a "regenerative effect", as in metal machining processes [14, 13, 12, 9]. Indeed, the instantaneous depth of cut for any blade is $d_n(t) = U(t) - U(t - t_n)$, where $U(t)$ is the current axial position of the bit and the time delay t_n is the time required for the bit to rotate $2\pi/n$, see Fig 1(b). The regenerative effect thus introduces a single, discrete, and state-dependent delay t_n to the equations governing the bit dynamics. The delay is implicitly defined by $\Phi(t) - \Phi(t - t_n) = 2\pi/n$, where $\Phi(t)$ is the current angular position of the bit. The original RGD model has been extended to include axial stiffness, damping and multiple degrees of freedom [6, 7, 1, 10, 4, 8, 2].

Three time scales can be recognized in the RGD model: one related to the torsional oscillations $t_\omega = \sqrt{I/C}$, one related to the axial oscillations $t_v = \sqrt{M/K_r}$ ($K_r = \zeta \epsilon a$, where ζ quantifies the inclination of the cutting force, ϵ is the rock specific strength and a is the bit radius), and the time delay $t_n = 2\pi/n\Omega_o$. A parameter $\psi = (t_\omega/t_v)^2$ is defined to quantify the comparison between the two

time scales characterizing the drilling system. For deep well drilling $\psi \gg 1$, in line with field observations that axial vibrations are taking place on a much faster scale than the dominant torsional vibrations.

There are two major conclusions gained by analyzing the RGD model. First, there exist two regimes of instability: one evolving on a slow manifold (observed at higher rotation speed; dominated by marginally unstable torsional poles), and another evolving on a fast manifold (observed at lower rotation speed; dominated by unstable axial poles) [4]. Fast configurations rapidly degenerate into stick-slip or bit-bouncing dysfunction regimes, whereas slow configurations appear to be marginally unstable. From the partial dynamics with constant time delay, a critical rotation speed Ω_o^c can be recognized to separate these two regimes of instability. Scaled with the characteristic time of axial motion, this quantity reads $\tilde{\omega}_o^c = \Omega_o^c t_v = \sqrt{8/n}$, where n is the number of symmetric blades. This expression indicates that the stability of the system depends on bit geometry. A second conclusion is that given enough time there always exists a steady-state limit cycle, which corresponds to the fully developed stick-slip vibrations. By studying the average response of a limit cycle, the mean torque-on-bit $\langle T \rangle$ is found to increase with $K = W_{f,\max} - \langle W_f \rangle$, the averaged perturbation of the weight-on-bit due to frictional contact. Decreasing rotation speed will lead to a more unstable axial motion, more severe axial chattering (recurring loss of contact between wearflat and rock surface and/or axial stick-slips) and accordingly a larger K. Thus, an apparent velocity-weakening torque-on-bit law is achieved; it is a consequence rather than the root cause for the self-excited torsional vibrations.

In reality, PDC bits have a complex arrangement of cutters (Fig 2), which are responsible not only for multiple delays but also for a delay distribution that depends on the bit motion history. Since the delay distribution controls the stability of the bit, it is imperative to develop a model capable of capturing the exact design of PDC bits. This additional consideration, although greatly complicating the analysis, is expected to give more realistic insights into the mechanism of the stick-slip vibrations of a rotary drilling system.

2 Bit Characterization

A PDC bit is composed of fixed cutters mounted on a metal or matrix body. Fig 2(a) shows a typical layout of cutters. For this specific case, there are 32 cutters placed on 6 blades, 3 full and 3 partial. A full blade has 6 or 7 cutters mounted on it while a partial one has 4 cutters. Notice that the term "blade" here is different from the consideration in the RGD model, where each blade is seen as a continuous cutter. Single cutter experiments show that the cutting force exerted on a cutter is proportional to the cross-sectional area of the rock groove

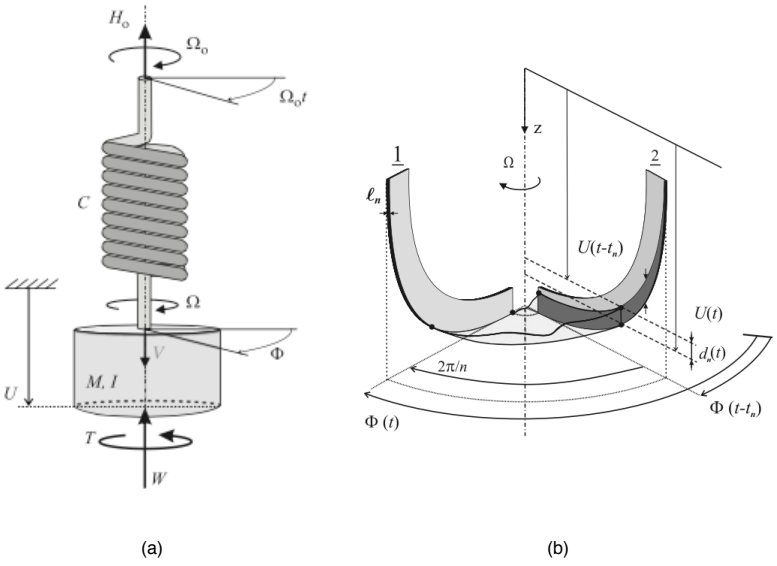

Figure 1: The RGD model [11]: (a) Quantities involved and sign conventions: the bottom hole assembly (BHA) is considered as a point mass M and moment of inertia I; the drillstring is considered torsionally as a spring with stiffness C, while axially as a string; due to the bit-rock interaction, there are reaction weight-on-bit W and torque-on-bit T; the drive system imposes a constant hook load H_o and a constant rotation speed Ω_o. (b) The regenerative cutting process considered in the model: local depth of cut for each blade is computed as the shift between the current and a past axial position.

traced by the cutter [3]. Thus to determine such area and compute the cutting force, it is necessary to project the cutter face onto a plane perpendicular to the cutter velocity $\mathbf{v}_i$. If one rotates the bit without axial advance, and projects each cutter face onto a plane corresponding to a fixed angular position Φ, the resulting picture is referred to as bit profile, as in Fig 2(b).

3 Linear Stability

For the linear stability analysis, a "stripping" method is applied to account for the real bit geometry. In the bit profile, define an array of radial positions $\{r_m\}$, with $r_m = m\Delta r$. When the projection of a cutter is intersecting with $r = r^*$ (r^* is a particular radial position), a rectangular strip is defined, with its height being the offset in z between the two intersections and its width the radial position

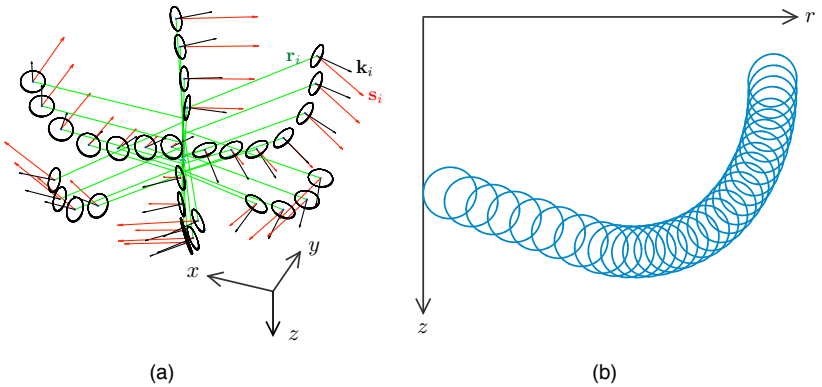

Figure 2: Subplot (a) gives a 3D representation of cutter faces mounted on a PDC bit. For cutter i, some unit vectors are defined: outward radial direction $\mathbf{r}_i$ (in $x-y$ plane), tangential direction $\mathbf{s}_i$ (in $x-y$ plane), and cutter face normal $\mathbf{k}_i$. The cutter velocity is given as $\mathbf{v}_i$ and it is approximately parallel to $\mathbf{s}_i$. Subplot (a) shows the bit profile that is achieved by rotating the bit without axial advance, and projecting each cutter face onto a plane at a fixed angular position Φ.

step Δr. This procedure is shown in Fig 3(a). As a result, at $r = r^*$, the real bit geometry is approximated by a "toy bit" with rectangular cutters (it looks like a core barrel). Fig 3(b) shows such a "toy bit". Particularly this one has 3 cutters, but for a real bit, the generated "toy bit" has different number of cutters at different r. Each "toy bit" reflects two geometric features not considered in the RGD model: multiple angular offsets (i.e. the bit is asymmetric) and axial offsets between cutters.

For the "toy bit" in Fig 3(b), we examine its local depth of cut for varying uniform motion as shown in Fig 3(c). First, we recognize D, the cutter diameter, as a characteristic length. In the plot $\delta = {}^{d}/_{D}$, and d represents the axial bit advance in one revolution, or equivalently, the instantaneous depth of cut of the bit for a uniform motion. It is observed that each local depth of cut $\delta_i = {}^{d_i}/_{D}$ varies linearly with δ, with $\sum_i \delta_i = \delta$. Each δ_i, similar to the local depth of cut d_n in the RGD model, corresponds to a particular delay. Here the term "delay" has a two-fold meaning: (i) an angular offset between cutters i and p, Φ_{pi} (how much cutter p is ahead of cutter i angularly) and (ii) the time delay corresponds to that angular offset, which, under uniform motion, is simply given by $t_{o,pi} = {}^{\Phi_{pi}}/_{\Omega_o}$. Thus, in Fig 3(c), any particular δ can be partitioned into contributions from each particular angular offset, or a particular delay. Note in the plot, for a small δ (region I), only the lowest cutter 1 is cutting rock, but

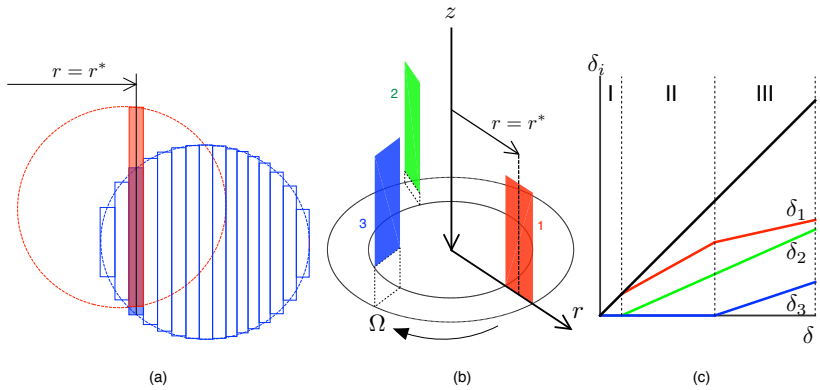

Figure 3: Subplot (a) illustrates the "stripping" method. Subplot (b) shows a an example of a "toy bit". Subplot (c) presents the relation between local depths of cut and bit penetration considering a toy bit with uniform motion. Note that such a relation is a function of the bit geometry.

with increasing δ (regions II and III), more cutters become active. Within a region, the slope of each line is a scaled angular offset. For instance, in region II, the slope of δ_1 reads $\Phi_{12}/2\pi$ and the slope of δ_2 reads $1 - \Phi_{12}/2\pi$. In summary, the $\delta_i - \delta$ plot in Fig 3(c) shows that various axial offsets between cutters result in a delay distribution that is a function of the depth of cut.

The above method can be extended to a full bit. For the stability analysis, the bit dynamics is linearized such that each time delay is frozen and the contact stress on the cutter wearflat is assumed constant. In order to account for the contribution of a specific delay (related to a unique angular offset Θ_j) to the cutting process, two arrays $\{\alpha_j\}$ and $\{\beta_j\}$ are defined. First introduce two characteristic quantities $\bar{W} = \zeta \epsilon a D$ and $\bar{T} = \epsilon a^2 D/2$. The dimensionless weight-on-bit due to cutting $\mathcal{W}_c = W_c/\bar{W}$, and the dimensionless torque-on-bit due to cutting $\mathcal{T}_c = T_c/\bar{T}$ can be related to the arrays $\{\alpha_j\}$ and $\{\beta_j\}$ by: $\mathcal{W}_c = \sum_j \alpha_j(\delta) \cdot \delta$ and $\mathcal{T}_c = \sum_j \beta_j(\delta) \cdot \delta$. For the cutter layout in Fig 5, the distributions of $\{\alpha_j\}$ and $\{\beta_j\}$, varying with δ, are shown in Fig 4, which are essential for computing the linear stability map, as in Fig 5. It is observed that critical rotation speed $\tilde{\omega}_o^c$ which separates two regimes of instability is a function of $\delta = d/D$; also for a certain δ, there may exist $\tilde{\omega}_o^c$ of different values.

4 Time Simulation

For the transient response of the model, a time simulation package is required. One challenge is to capture the complex regenerative effect introduced by the

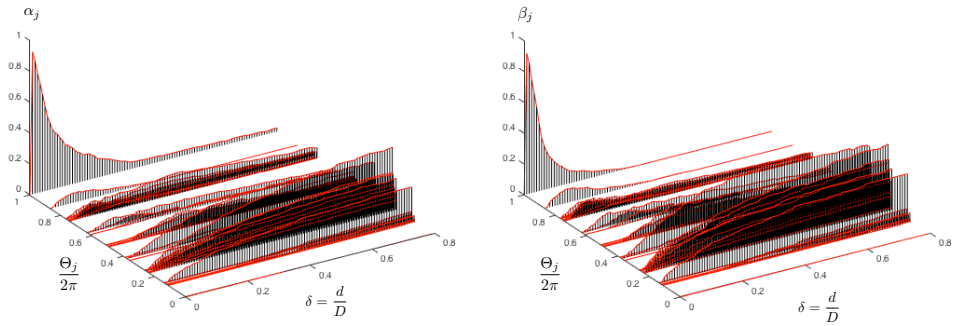

Figure 4: Distributions of $\{\alpha_j\}$ and$\{\beta_j\}$ for a real PDC bit: Θ_j is a unique angular offset and $\delta = d/D$ is a scaled depth of cut. The cutter diameter, D, is recognized as a characteristic length.

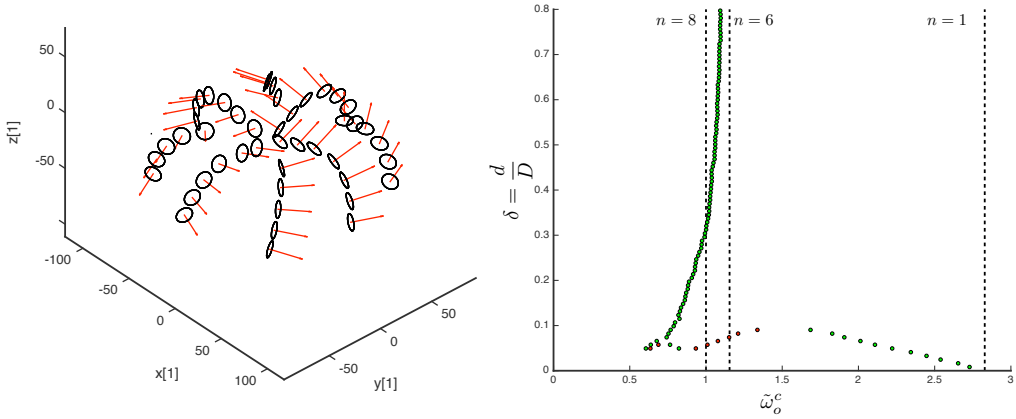

Figure 5: The stability map of a PDC bit under inspection (with 4 full blades, 3 partial blades): Each green dot represents a critical rotational speed corresponding to a left-crossing axial pole while each red dot represents a critical rotational speed corresponding to a right-crossing axial pole. In other words, for a given δ, the critical rotational speed(s) will segment the domain into regions of "slow" and "fast" axial instability. "Slow" axial instability, practically, can be seen as stable when damping exists in the model. The vertical dashed lines correspond to the critical rotational speeds in the RGD model: $\tilde{\omega}_o^c = \sqrt{8/n}$, where n is the number of symmetric and continuous blades. It is observed that for very small δ_o, the RGD solution is retrieved since the delay of 2π dominates.

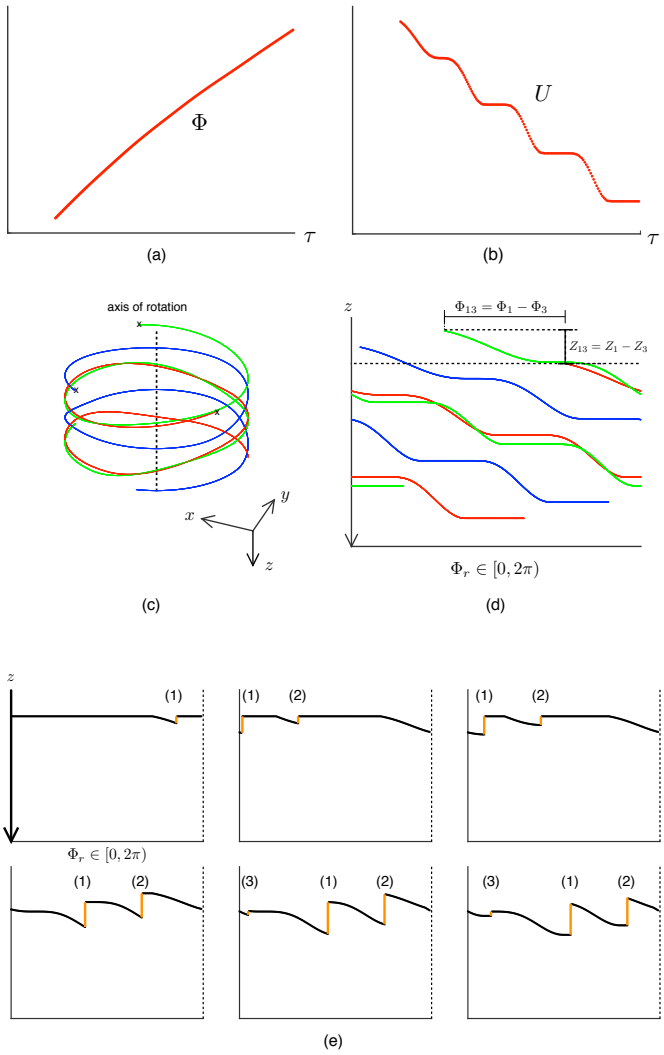

Figure 6: (a) Predefined torsional bit motion (b) Predefined axial bit motion (c) Motion trajectories of cutters (center points) in 3-D view: the crossings indicate the starting locations; the red, blue, and green curves correspond to cutter 1, 2 and 3, respectively (d) Motion trajectories of cutters in 2-D view: the angular position is converted to the range of $[0, 2\pi)$; the red, blue, and green curves correspond to cutter 1, 2 and 3, respectively (e) Some snapshots of the process of updating rock profile and finding local depth of cut: for each subplot, the x-axis depicts rock angular position Φ_r and the y-axis axial position z. Each jump in the rock surface, colored in tangerine, is related to a local depth of cut and number above denotes the corresponding cutter

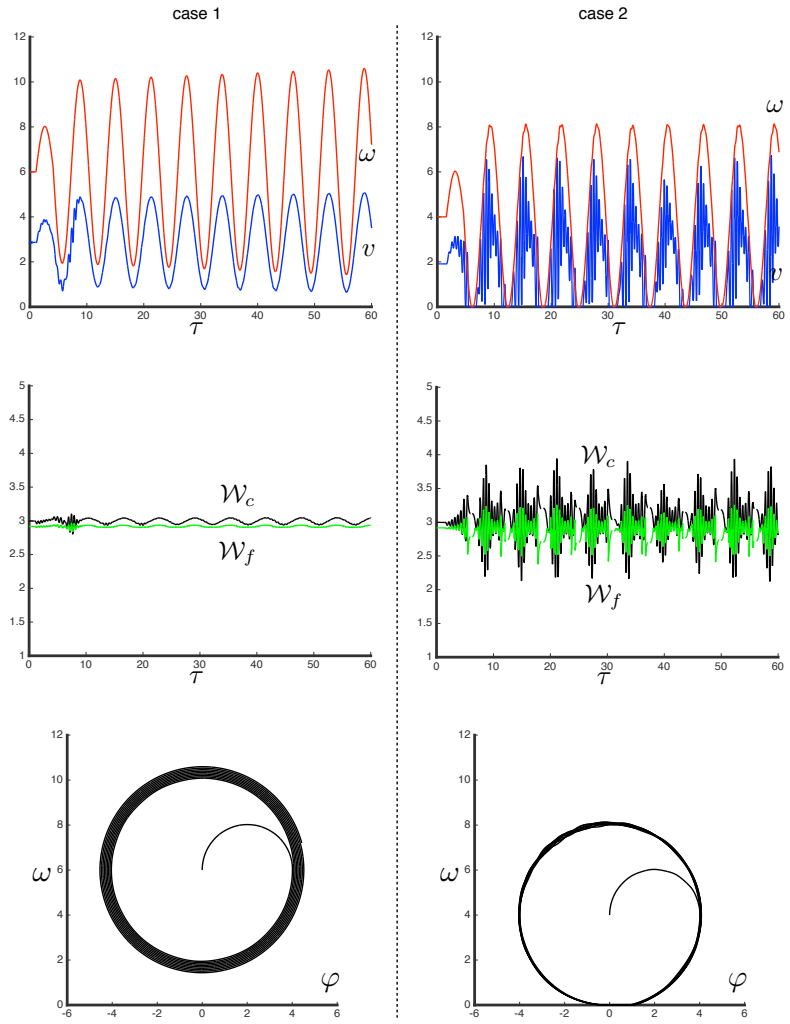

Figure 7: Verification of the stability map using time simulation: case 1 is of a slow configuration ($\delta_o = 3, \omega_o^c = 6$); case 2 is of a fast configuration ($\delta_o = 3, \omega_o^c = 4.5$). For each specific case, 3 subplots are shown: evolutions of angular and axial speed, evolutions of weight-on-bit due to cutting (dimensionless, plotted in black) and weight-on-bit due to frictional contact (dimensionless, plotted in green) and phase diagram of torsional motion

consideration of realistic cutter layouts.

The basic idea can be deduced from a "toy bit", like the one in Fig 3(b). Now consider a bit motion defined by evolutions of angular and axial positions with time, as shown in Fig 6(a)(b). As the bit can be treated as a rigid body, the bit motion can be readily translated to cutter motions, as shown in Fig 6(c). Note that all trajectories are identical in shape, but shifted angularly and axially by constant values corresponding to the angular/axial offsets between cutters. Introduce a new angular coordinate $\Phi_r \in [0, 2\pi)$ to depict rock surface at $r = r^*$. With this, the trajectories in Fig 6(c) can be converted into those in Fig 6(d). In this view, angular delays and relative heights can be readily recognized. Notice that while updating the rock profile at different angular positions, all cutters are advancing at the same "pace", i.e. sharing the same angular velocity. Accordingly, a given bit motion can be linked to the variations of rock profile with time, as in Fig 6(e). Each local depth of cut corresponds to a discontinuity in the rock profile.

Considering a full bit, this procedure in fact depicts the bit/rock interaction at a specific radial position r^*. If the result is integrated from 0 to a (radius of the bit), an extended bit/rock interaction law can be derived to compute transient weight-on-bit W and torque-on-bit T, which will enter the equations of motion at each time instance. Thus the time simulation can be conducted, which can be used to verify the linear stability map achieved previously in Fig 5. Such results are shown in Fig 7.

5 Conclusions

Under the framework of the RGD model, this work provides a methodology to bring the actual cutter layouts into the modeling of the self-excited stick-slip vibrations related to drilling with PDC bits. Linear stability analysis shows that critical rotation speed that separates two regimes of instability is a function of the depth of cut. The resulting linear stability map is verified using a time simulation code. This work provides tools to further explore the key factors of bit design, which may influence the torsional stability of a rotary drilling system.

References

[1] Besselink, B., N. van de Wouw, and H. Nijmeijer (2011). A semi-analytical study of stick-slip oscillations in drilling systems. *Journal of Computational and Nonlinear Dynamics 6*(2).

[2] Besselink, B., T. Vromen, N. A. H. Kremers, and N. van de Wouw (2016).

Analysis and control of stick-slip oscillations in drilling systems. *IEEE Transactions on Control Systems Technology 24*, 1582–1593.

[3] Coudyzer, C. and T. Richard (2005, April). Influence of the back and side rake angles in rock cutting. In *AADE National Technical Conference and Exhibition*, Number AADE-05-NTCE-75, Houston, Texas, U.S.A., pp. 1–12.

[4] Depouhon, A. and E. Detournay (2014). Instability regimes and self-excited vibrations in deep drilling systems. *Journal of Sound and Vibration 333*(7), 2019 – 2039.

[5] Detournay, E. and P. Defourny (1992). A phenomenological model for the drilling action of drag bits. *International Journal of Rock Mechanics and Mining Sciences and Geomechanics Abstracts 29*(1), 13–23.

[6] Germay, C., V. Denoel, and E. Detournay (2009). Multiple mode analysis of the self-excited vibrations of rotary drilling systems. *Journal of Sound and Vibration 325*, 362–381.

[7] Germay, C., N. van de Wouw, H. Nijmeijer, and R. Sepulchre (2009). Nonlinear drillstring dynamics analysis. *SIAM Journal On Applied Dynamical Systems 8*, 527–553.

[8] Gupta, S. K. and P. Wahi (2016). Global axial–torsional dynamics during rotary drilling. *Journal of Sound and Vibration 375*, 332 – 352.

[9] Insperger, T., G. Stepan, and J. Turi (2005, August). State-dependent delay model for regenerative cutting processes. In *Proceedings of Fifth EUROMECH Nonlinear Dynamics Conference, ENOC 2005*, Eindhoven, Netherlands, pp. 1124–1129.

[10] Nandakumar, K. and M. Wiercigroch (2013). Stability analysis of a state dependent delayed, coupled two DOF model of drill-string vibration. *Journal of Sound and Vibration 332*, 2575–2592.

[11] Richard, T., C. Germay, and E. Detournay (2007). A simplified model to explore the root cause of stick-slip vibrations in drilling systems with drag bits. *Journal of Sound and Vibration 305*(3), 432–456.

[12] Stepan, G. (1998). Delay-differential equation models for machine tool chatter. In F. C. Moon (Ed.), *Dynamics and Chaos in Manufacturing Processes*, Chapter 6, pp. 165–191. John Wiley and Sons.

[13] Tlusty, J. and M. Polacek (1963). The stability of machine tool against self-excited-vibrations in machining. In *Proceedings of the International Production Engineering Research Conference*, Pittsburgh, Pennsylvania, U.S.A., pp. 454–465. American Society of Mechanical Engineers.

[14] Tobias, S. A. (1965). *Machine-Tool Vibration*. New York: Blackey and Son Limited.

Drilling experiment to determine the efficiency of a second generation downhole drilling regulator

Nils Reimers

Tomax

Abstract

The economics in retrieving oil and gas resources from basement rock cant reach its peak potential without the use of Polycrystalline Diamond Compact (PDC) drill bit technology. The same goes for the development of distributed geothermal heat sources. The PDC significance comes from the sum of two important advantages: First is the mechanical specific efficiency (MSE) or energy to drill. This figure is close to half with PDC. Second is the potentially longer drilling distance with the PDC compared to the traditional alternative the insert bit. The insert bit has its crushing cones rolling on bearings with a fixed life. Because of the advantage, modern rigs are optimized to meet the PDC requirements. This includes high-torque pipe and derrick drilling machines. The PDC bias mean the same rigs are under-utilized if used with old technology. Furthermore, the wear on the rig and the workforce is increased from more bit trips. The reason the PDC advantage is not already being fully exploited in the basement is the high risk of impact damage that comes with the harder rock.

This paper presents the results from a project partly financed by the Norwegian government to investigate the potential of using the newly introduced counterforce assisted anti stick-slip tool to safeguards modern PDC technology and make it safe for basement drilling. The Anti Stick-slip Technology (AST) provides for autonomous controlled of the depth of cut based on the downhole torque on bit. Hence the regulator prevents the onset of such destructive vibrations that typically occurs if the cutters hangs up and releases in rock fractures.

The project used a modern drilling rig and drilling tests were done at 3000 feet in the South Scandinavian Basement that consists of gneiss and granite and has natural fractures. The budget for the project allowed new, premium bits to be used with the best available leeched cutter technology. The new counterforce assisted AST was used. This tool provides for an extended operational range

starting at zero foot-pounds of torque, meaning that the tool also regulates the first contact with the rock surface. The results are recorded and discussed using accurate downhole and surface data. Methods where applied to evaluate the bit condition while drilling.

The conclusions from the work where clear and is valuable for basement and hard rock drillers. Including what not to do with PDC bits in a basement drilling environment.

Drilling Automation – Some Industrial Challenges and Solutions

John-Morten Godhavn and Espen Hauge

Statoil Research Center, Norway

1 Introduction

Drilling automation has gained an increased interest the last few years boosted by the low oil price and last years focus on digitalization. Automation technology is a tool not only to drill faster and safer, but also to be able to do a better job while reducing the number of experts on-site. Terms such as digital twin are being used when a hydraulic model is running in parallel providing estimates of unmeasured states as well as detection of anomalies when the model outputs deviate from the rig measurements. The control of the drilling machines is moving from remote control to feedback control and even some autonomous solutions have been developed combining several machines. Some of the technologies recently piloted will be presented as well as work in progress and technology gaps and challenges to be solved towards our goal of automating the drilling operation further.

The drilling process can be divided into three main parts covering a wide range of topics for automatic control. The most mature part with respect to automation is the handling of the drill pipe and casing on the rig. The drill string consists of steel pipes that are screwed together. Each pipe is about 10 meters long. 3 such pipes are often racked together in what is called a stand. The driller must stop drilling every 30 meters or so, pull the bit off bottom, stop rotation, hang off the drill string in slips and stop the rig pumps circulation of drilling fluid (mud) into the drill string. The driller can then extend the drill string with another stand before drilling can continue. Special robots have been developed to move the pipes, unscrew/make up the stand by rotating the pipe, etc. These pipe handling robots are usually controlled by joysticks from the drillers chairs. Solutions exist where this is automated, and the different robots are coordinated including anti-collision functionality and fault handling.

The drilling fluid is complex and it is designed to serve several purposes. The process control for the drilling fluid is mostly manual, and offshore this is

usually handled by a service (mud) company. The process is like other chemical processes and will be discussed in some detail in the next section.

Maybe the most interesting part of the drilling process is what goes on downhole when we are making hole. This process integrates mechanical systems related to the drill string and bit (torque, drag, hook load, buckling, vibrations, directional drilling) with the fluid process (downhole flow, pressure, temperature and hole cleaning). A substantial effort is put into the planning phase which include selecting the downhole equipment (bit, sensors in bottom hole assembly), design the drilling fluid (density, viscosity, etc.), and to optimize the so-called drilling parameters (pump flow rate, weight on bit, drill string rotation). The goal is to stay within the constraints dictated by topside and downhole equipment as well as constraints given by the downhole formation (drilling window: pore pressure, collapse pressure and fracture pressure), and to clean the hole properly by transporting the cuttings out. Well control is an imperative part of drilling, and a project on early kick and loss detection is presented below

2 Control challenge: Drilling fluid mixing

This section addresses an open challenge for control. The mixing process for drilling fluids is a distributed, multivariable constrained control problem with severe nonlinearities, few online measurements, varying time delays and unmeasured disturbances. The drilling fluid (mud) serves several purposes in addition to being the primary well control barrier. Removal of cuttings from the bottom of the hole and to transport the particles to surface is of course very important. It is desirable that the mud can suspend cuttings (particles of the crushed rock) and weight material (typically barite added to make the mud denser), so that these particles do not sag when circulation is stopped. Another important function is to cool and lubricate the bit and the drill string due to the amount of energy which is generated when the bit is making hole. In the upper hole, water may be sufficient, but at greater depths more viscous and dense fluids are usually required. Deep wells, directional wells, high penetration rates, high mud weights, and high temperature gradients create conditions requiring close attention to the flow properties. The viscosity can be increased with polymers or clay material or decreased with chemical thinners or water. The mud density is selected according to the so-called drilling window, depicted in Figure 1.

Control of the subsurface pressures in the open hole is very important to avoid well control events. The lowest well pressure is the static pressure when the pumps are not circulating.

$$p = \rho g h, \tag{1}$$

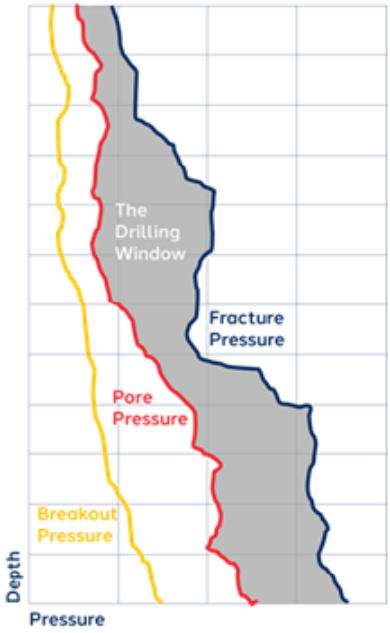

Figure 1: Drilling window.

Here p is the downhole pressure, ρ is the actual mud density including cuttings, g is gravity and h is the vertical depth. The mud density must be sufficiently high, so that the downhole pressure is greater than the pore pressure. If the pore pressure is greater than the well pressure, then one might experience an influx of formation fluids into the well. If this is gas, and the driller does not detect it, then it might end up as a blowout.

The downhole pressure p will increase with the friction in the annulus with the rig pumps running as well as the additional weight of the cuttings

$$p = \rho g h + p_{\text{fric}}(q_{\text{in}}) \tag{2}$$

Here ρ is the density of the mud including cuttings and p_{fric} is the annulus friction depending on the flow rate q_{in}. The downhole pressure must be lower than the tensile strength of the rock in the open hole, represented by the fracture pressure to avoid loss of mud to the formation.

It may be a challenge to select the mud properties and the flow rate. Good hole cleaning requires a combination of high enough flow rate and high enough viscosity. On the other hand, the flow rate and viscosity must often be kept low to ensure that the downhole pressure is kept below the fracture pressure.

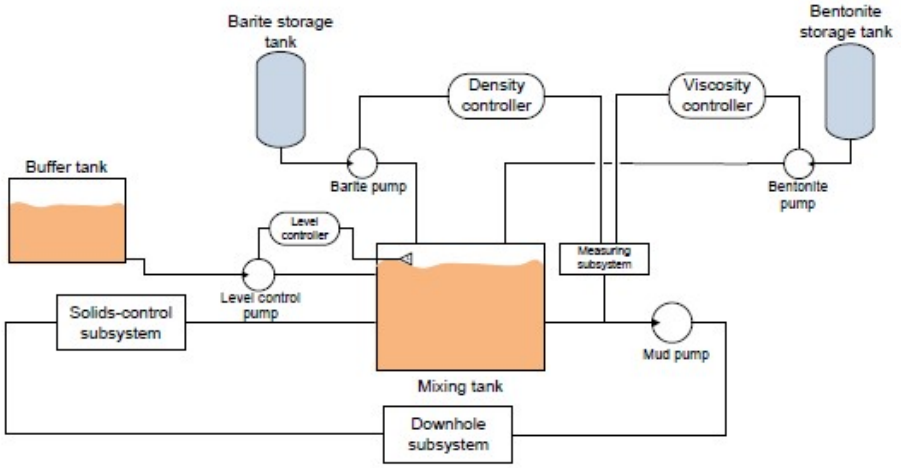

Figure 2: Mud mixing system.

The drilling fluid is designed in the planning phase and a premix of the mud is normally sent to the rig. The onsite mud engineer monitors the mud parameters and adjusts accordingly to maintain the desired specifications. The measurement of mud parameters is usually a manual process, where a sample is brought back to the lab. Consider the simplified process illustrated in Figure 2 where the objective is to control the two main mud parameters: density and viscosity.

The density of the mixed fluid is given by

$$\rho_{mix} = \frac{m_{\text{mud}} + m_{\text{barite}} + m_{\text{bentonite}}}{V_{mix}} \tag{3}$$

$$\approx \rho_{\text{mud}} + (\rho_{\text{barite}} - \rho_{\text{mud}}) \frac{V_{\text{barite}}}{V_{\text{mix}}} + (\rho_{\text{bentonite}} - \rho_{\text{mud}}) \frac{V_{\text{bentonite}}}{V_{\text{mix}}} \tag{4}$$

Here ρ_{mix} and V_{mix} are the density and the volume of the mixed fluid, ρ_{mud} mud is the density of the mud before the chemicals have been added, ρ_{barite} and V_{barite} are the density and the volume of the added barite and $\rho_{\text{bentonite}}$ and $V_{\text{bentonite}}$ are the density and the volume of the added bentonite. For viscosity it is more complicated. The nonlinear relation between the weight ratio r of the viscosifier, and the controlled variable, the viscosity μ_{mix} of the mixed fluid

$$\mu_{\text{mix}} = a\left(e^{br} - 1\right) \tag{5}$$

$$r = \frac{\rho_{\text{bentonite}} V_{\text{bentonite}}}{\rho_{\text{mud}} V_{\text{mud}}} \tag{6}$$

Figure 3 shows the nonlinearity. The process gain $\partial\mu_{\text{mix}}/\partial r$ increases with viscosity meaning that the viscosity is much more sensitive to added viscosifier, when the weight ratio is already high.

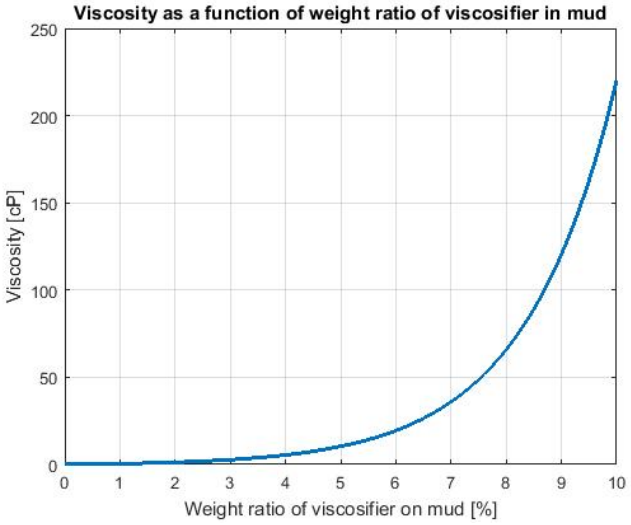

Figure 3: Viscosity as a function of weight ratio of viscosifier in mud.

There are several development projects ongoing in the industry to automate the mud mixing process. Online rheology (drilling fluid properties, viscosity etc.) measurements feeding measurements to a mud mixing control system, enabling the system to control the mud rheology using automatic sack cutters and remotely operated valves for chemical additives. This is a challenging multivariable constrained control problem, where in addition to the multivariable nonlinear mixing equations one must deal with constraints and a substantial transport delay, as one is primarily interested in the mud properties in the annulus. The time delay from when a new mud is mixed and pumped into well until it can be seen on the measurements coming out of the well is given by

$$t_{\text{delay}} = \frac{V_{\text{well}}}{Q_{\text{pump}}} = \frac{A_{\text{drillpipe}} L_{\text{drillpipe}} + \sum A_{\text{section-i}} L_{\text{section-i}}}{Q_{\text{pump}}} \tag{7}$$

Here V_{well} is the total well volume, which increases as the well is being drilled and Q_{pump} is the pump rate (time delay will increase when the pumps are off). Further, $A_{\text{drillpipe}}$ is the cross-section area in the drill pipe with length $L_{\text{drillpipe}}$, while $A_{\text{section-i}}$ is the cross-section area for annulus for a given section i of length $L_{\text{section-i}}$. Typically, the transport delay is one hour or more, and a controller must take this into consideration. Also, there are unmeasured disturbances, such as losses and contamination of the mud at the bottom of the well. Some fluids or particles from the mud might be left downhole to form a so-called mud cake, or filter cake, while cuttings and formation fluids, e.g. gas boiling out of the cuttings, might contaminate the mud and influence the mud properties that we want to compensate for. Lastly, the mud properties are highly sensitive to

temperature. The temperature at the mud rheology sensor must therefore be compensated for as well.

3 Estimation challenge: Early kick and loss detection

This section addresses a project the authors have been working on the last 2 years: estimation of influxes of formation fluids into the well, or losses of drilling fluids from a well during drilling.

Well control is a fundamental and prioritized task when drilling wells. Early detection of kicks (influxes of formation fluids to the wellbore) and losses (drilling fluid lost to the formation) is very important. Conventionally, influxes and losses are detected by the driller or the mud logger by monitoring trends. They mainly look at the active volume of drilling fluids on the rig, but also the flow out sensor (often a simple indicator, such as a paddle), the pump pressure, gas-in-mud sensors on the rig, and in some cases also the rate of penetration or hook load (drilling break). Detection then relies on the drill crews awareness and experience. During tripping they use a trip sheet with the expected volume changes based on steel volume in or out of the well. Kick and loss detection based on driller awareness often works well. However, it relies heavily on the drillers experience and work-load. An undetected event can escalate into a severe situation, blowout being the most severe, if not handled early. Kicks and losses during transient events such as when ramping the rig pumps down are particularly challenging to detect. Existing technologies for detecting kick and loss events include simple solutions based on active volume, with alerts to the operator being raised if the active volume exceeds or falls below threshold values. Often, these are not sufficiently accurate and they also raise false alarms. Other systems, such as services based on high accuracy flow meter monitoring can be used, but these are expensive, owing to the requirement to modify the rig, and to provide 24-hour monitoring with experts being onsite.

If a kick or loss event is detected, drilling is stopped and well control procedures are used to handle the situation. This can go on for several days. If the situation is more severe, the wellbore may need to be plugged and the on-going section must be re-drilled with a side track, resulting in up to a month of lost time. The earlier a kick or loss can be detected, the easier it is to handle the situation and ensuring that it does not develop into something more serious.

Kick and loss detection is more challenging on floating rigs in rough sea experiencing rig heave. The marine drilling riser has a flexible joint extending in length when rigs goes upwards with the waves and reducing in length when the rigs goes downwards. This means that the volume in the riser is changing quickly an this has a very large effect on the flow out rate from the well. The active

volume measurement is also directly influenced by the rig roll and pitch motion. Algorithms for kick and loss detection must consider these heave induced effects. Typically, some filtering is required, resulting in some delay in the detection of events.

3.1 Data- and test-driven development

Statoil has been working on internal development of kick and loss detection algorithms since 2014 following up previous projects in collaboration with others. The approach taken was inspired by recent developments using data driven methods. We started by collecting a library of field data from our operations in the order of 1000+ hours contained in 30+ data sets, each about 24 hours long and some of these containing a true loss/kick event. It is believed that these data sets cover most of the challenges related to field data, such as outliers, noise, hole in data, vendor specific variable naming, manual resets, sensor accuracy, etc. If our software gives good results on these data sets, then we should expect similar results in real time when deployed on a new rig or when drilling a new well. Automated tests were developed to test the algorithm on these data sets in one batch, and evaluation scripts calculated our main KPIs: false alarm rate, and probability of detection (true kick/loss events). In addition, the software development has been test-driven, i.e. we have developed unit tests, and other tests of the various software modules, as a part of the code development.

3.2 Modeling

We chose an approach using simple dynamic input-output models with a few model parameters. To avoid the need for configuration and model calibration, and to allow for changes in the model parameters, we decided to go for adaptive models, where the model parameters are adjusted in real time to fit the data observed. The challenge is then how and when to adjust the parameters. We need to balance the parameter updates by adjusting enough to track the data and avoid false alarms, but not too much hiding true kick and loss events.

3.2.1 Flow in

The most important input parameters for the driller that influence well control are the rig pump flow rate and the hook velocity. When the drill string is moved into or out of the well with a velocity v_{pipe}, then a compensated flow in rate including steel volume is given by:

$$q_{\text{comp}} = q_{\text{in}} + A_p v_p \tag{8}$$

Here the pipe velocity is the time derivative of the bit depth and A_p represents the cross-section area of steel pipe moving in or out of the well bore.

3.2.2 Flow out

The flow out rate q_{out} measurement is calibrated to track the true flow out with a bias (offset) k_{bias} and a scale factor k_{scale}:

$$q_{\text{out}} = k_{\text{scale}} q_{\text{meas}} + k_{\text{bias}} \tag{9}$$

The expected flow out rate q_{exp} is modeled as a lowpass filtered and delayed function of the compensated flow in rate:

$$q_{\text{exp}} = \frac{q_{\text{comp}}(t - \tau_d)}{1 + \tau_c s} \tag{10}$$

The parameter values time delay τ_d and time constant τ_c are found during pump stops and pump starts to best fit the calibrated measurement of calibrated flow out rate q_{out}.

3.2.3 Pump pressure

The expected pump pressure pexp is modeled as a stepwise linear function of the flow in rate:

$$p_{\text{exp}} = p_{0,\text{inj}} + \begin{cases} b_1 q_{\text{comp}} + p_{01}, & \text{for} \quad 0 < q_{\text{in}} < q_{\text{pivot},1} \\ \quad \vdots & \\ b_K q_{\text{comp}} + p_{0K}, & \text{for} \quad q_{\text{pivot},K-1} < q_{\text{in}} < q_{\text{pivot},K} \end{cases} \tag{11}$$

where $p_{0,\text{inj}}$ is an injection term. The function of the injection term is to compensate for slow variations in pressure due to, for example, the length of the well and the weight of cuttings in the annulus. The parameters b_i and p_{0i} are adjusted to best fit the measured pressure when the flow in rate is near constant.

3.2.4 Active volume

The expected active volume V_{exp} and the mud volume in flowline V_{fl} are modeled with a simple linear dynamic model driven by the compensated flow in rate:

$$q_{\text{fl}} = k_{\text{vol}} V_{fl}(t) - k_{\text{flow}} q_{\text{comp}}(t) \tag{12}$$

$$\frac{d}{dt} V_{fl} = q_{\text{comp}}(t - \tau_V) - q_{fl}(t) \tag{13}$$

$$\frac{d}{dt} V_{\text{exp}} = q_{fl}(t) - q_{\text{comp}}(t - \tau_V) + q_{\text{loss}}(t) \tag{14}$$

The time delay τ_V along with the parameters k_{vol} and k_{flow} are found to best match the measured active volume measured during a pumps off/on event. The variable q_{fl} is an estimate of the flow rate out of the flow line and into the active pit. The variable q_{loss} is an estimate of mud lost on the shakers.

3.2.5 Alarm logic by voting

Once the expected measurements have been calculated, a detection algorithm combines the information from the different measurements and the deviations from the corresponding models to determine whether an influx or loss event may have occurred. Estimated influx/loss volumes are calculated by accumulating deviated measurement values:

$$V_{\text{IOflow}} = \int q_{\text{IOflow}} = \int q_{\text{meas}} - q_{\text{exp}} \tag{15}$$

$$V_{\text{IOrpes}} = \int f(p_{IO}) = \int f(p_{\text{meas}} - p_{\text{exp}}) \tag{16}$$

$$V_{\text{IOvol}} = V_{\text{meas}} - V_{\text{exp}} \tag{17}$$

Here q_{IOflow} is the deviated flow out rate, the difference between the measured flow out rate and the expected flow out rate from the model. The q_{IOflow} value is accumulated into a corresponding gain/loss volume V_{IOflow}. Similarly, p_{IO} is the deviated pump pressure, determined as the difference between the measured pump pressure and the expected pump pressure. The deviation in pressure is calculated to an assumed representative gain/loss flow rate, which again is accumulated into a gain/loss volume V_{IOpres} comparable with the volume calculated from the deviated flow out. Lastly, V_{IOvol} is the deviated active volume determined as the difference between the measured active volume and the expected active volume. The 3 calculated gain/loss volumes V_{IOflow}, V_{IOpres} and V_{IOvol} are then assessed. The main mechanism of our voting algorithm is to generate a kick alarm if 2 out of 3 of these volumes are positive and above given thresholds, while a loss alarm is generated if 2 out of 3 of these volumes are negative and below given thresholds. In addition, we have custom-made alarms for large deviations on single gain/loss volumes and a separate module to generate alarms while tripping. The algorithm can either run locally at the rig, generating an alarm on the drillers screen, or alternatively remotely, generating an alarm in a real-time support center. When an alarm is raised, appropriate action should be taken, either to verify that everything is ok or to stop drilling and initiate the appropriate well control procedure.

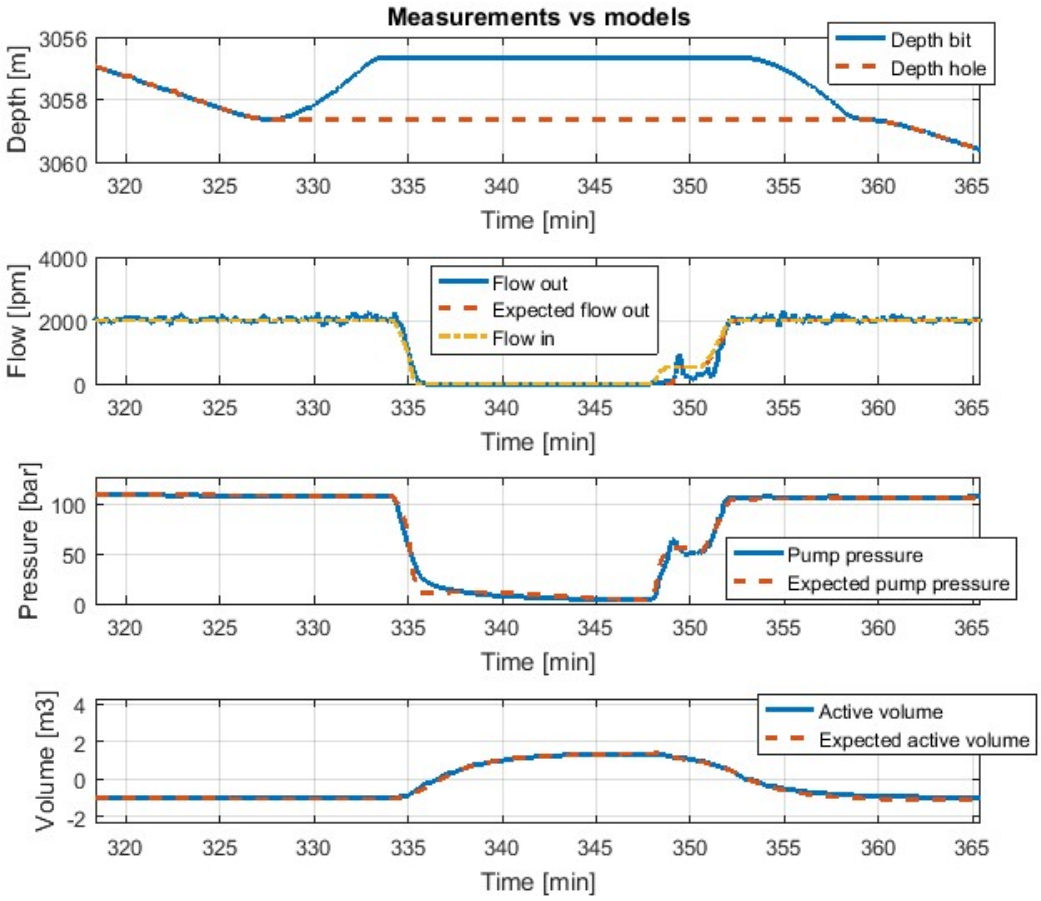

Figure 4: Performance of the models for expected flow out, pump pressure and active volume during a simulated connection.

3.3 Results

The algorithm presented above has been tested both on a library of field data and in real time operations, both offshore on a floating drilling rig with presentation on the drillers screen and remotely onshore streaming data in real time. The results are promising. Most of the true events have been detected and there has been a limited number of false alarms. Some of the false alarms can be explained by unmeasured disturbances, such as starting and stopping of a boost pump, pumping high viscosity pills, etc. The algorithm is still being improved. Results are displayed in Figure 4 and Figure 5.

In Figure 4, the upper plot shows the bit depth and the hole depth. It is seen how they pull off bottom about 5 meters before they stop the pumps and

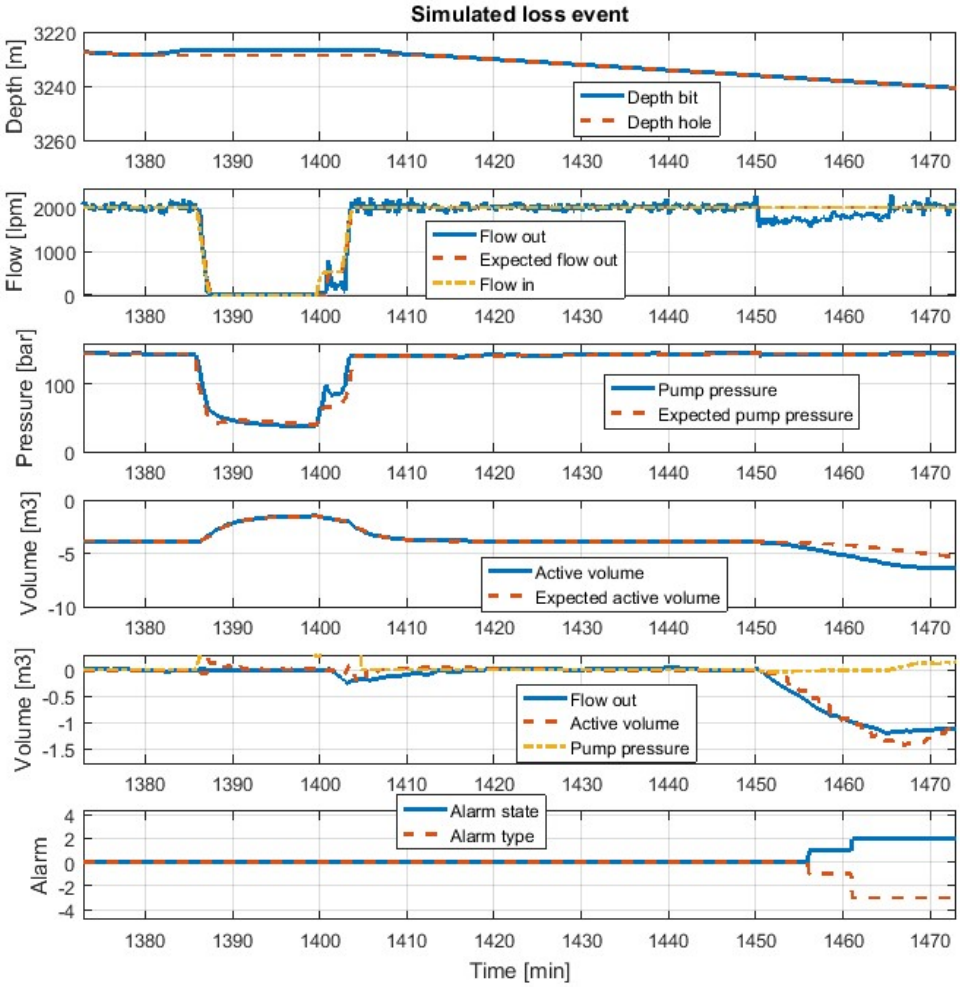

Figure 5: Simulated loss situation.

make a connection. The second plot shows the flow in rate, the noisy flow out, and the expected flow out from the model. The third plot shows how well the measured and the expected pump pressure are aligned. The lowest plot shows the very good alignment between the measured and expected flow back in the active volume. In Figure 5, the pressure drops almost 4 bar and the flow out rate drops with about 400 lpm at about 1450 minutes. The active volume starts to drop shortly after and the alarm goes off after 11 minutes later.

4 Conclusion

An overview of the drilling process has been given showing how multidisciplinary drilling automation is with application in both robotics, process control and mechanical systems control. The challenge of controlling the drilling fluid mixing has been outlined and an ongoing project on kick and loss detection has been described. The kick and loss detection falls in the category of machine learning, not using neural nets, but more a classical approach now referred to as feature engineering, where process knowledge is utilized in the learning. The drilling process is a batch process, unlike e.g. production. The well is extended, different kinds of drilling fluids are used, and new types of rock are exposed as you get deeper. The authors believe that this is a good case for using data driven methods during the operations opposed to the 1st principles models that are being used during planning.

Control-Oriented Modeling and Model Order Reduction for Managed Pressure Drilling Systems

S. Naderi Lordejani[1], B. Besselink[2], M. H. Abbasi[3], G.-O. Kaasa[4]
W. H. A. Schilders[3], N. van de Wouw[1,5]

[1]Department of Mechanical Engineering, Eindhoven University of Technology, Eindhoven, The Netherlands (s.naderilordejani@tu.nl, n.v.d.wouw@tue.nl)
[2]Johann Bernoulli Institute for Mathematics and Computer Science, University of Groningen, Groningen, The Netherlands (b.besselink@rug.nl)
[3]Department of Mathematics and Computer Science, Eindhoven University of Technology, The Netherlands (m.h.abbasi@tue.nl, w.h.a.schilders@tue.nl)
[4]Kelda Drilling Controls, Porsgrunn, Norway (gok@kelda.no)
[5]Department of Civil, Environmental & Geo-Engineering, University of Minnesota, Minneapolis, USA; Delft Center for Systems and Control, Delft University of Technology, Delft, The Netherlands

1 Introduction

Managed Pressure Drilling (MPD) is a method for fast and accurate pressure control in drilling operations. It has been introduced to overcome drawbacks of conventional pressure control methods, such as the incapability of rejecting transient pressure fluctuations [14]. In MPD, the annulus is sealed off at the top with a rotating control device and the mud is circulated out of the well through a choke valve. This combination provides a surface back pressure that can be controlled by manipulating the choke. In automated MPD systems, the surface pressure, and thereby the Bottom-Hole Pressure (BHP), is controlled by an automatic control system [13, 6]. The achievable accuracy and efficiency by this control system is dependent not only on the control design method, but also on the hydraulics model used for designing the control system. This model should be accurate enough to capture the essential dynamics of the system and, at the same time, the complexity of the model should be limited to allow for the use of established system-theoretic analysis and design techniques.

This research has been carried out in the HYDRA project, which has received funding from the European Union's Horizon 2020 research and innovation program under grant agreement No 675731

In principle, hydraulics models for MPD systems come in the form of high-fidelity Partial Differential Equations (PDE). From a control perspective, these models are too complex to be used directly for model-based controller design and, thus, further simplification/reduction is needed. Complexity-reduction approaches for these systems may be split into three groups. Firstly, the approximation of high-fidelity models by low-order Ordinary Differential Equation (ODE)/PDE models based on a time-scale separation has been proposed in [6, 2]. Such models are, however, incapable of capturing essential transients such as the propagation of pressure waves. Ignoring such phenomena in modeling and control design can cause a failure in the accomplishment of control objectives, such as the effective rejection of transient pressure fluctuations. It can even cause instability, which is especially probable in the case of long wells [10]. Secondly, model reduction can also be achieved by using low-resolution discretization of the PDE model based on, for example, a staggered-grid approach [10]. This, however, suffers from the lack of a quantitative measure on the achieved accuracy. Thirdly, model reduction can be performed based on a combination of a fine discretization, reducing the PDE model into a high-order ODE model, and automatic model order reduction techniques. Such an idea has been used in [12] for complexity-reduction of an MPD control system, and in [9] for deriving a control-oriented model for MPD systems. However, the high-complexity models in both cases were linear and the reductions were performed without providing any guarantee on accuracy.

In this paper, the third type of approach is pursued to obtain a control-oriented model for a nonlinear single-phase MPD system. Given 1) the spatially discretized ODE model combined with 2) (local) nonlinear boundary conditions, the resulting model is a nonlinear system comprising high-order linear dynamics with local nonlinearities. For this class of systems, a model order reduction procedure has been recently developed in [3]. This method, unlike many other model order reduction methods for nonlinear systems, preserves key system properties (such as $\mathcal{L}_2$ stability, a form of input-output stability). Moreover, it provides a computable error bound on the error induced by the reduction.

The remainder of this paper is organized as follows. Section 2 is devoted to the mathematical modeling of the system. In Section 3, the nonlinear model order reduction procedure is described. Illustrative simulation results are presented in Section 4 and, finally, conclusions are presented in Section 5.

2 Modeling of MPD system

An MPD system, as in Fig. 1, can be regarded as two equivalent long pipes, which are connected through a bit in the middle. One of these pipes models

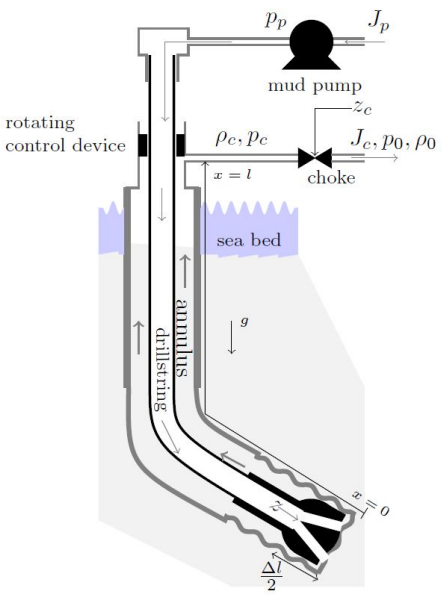

Figure 1: A simplified schematic diagram of an MPD system.

the drillstring and the other one the annulus. Moreover, the inlet and outlet of the connected pipes are connected to the pump and choke, respectively. A single-phase laminar flow, which is the case in many drilling scenarios, in a pipe can be accurately described by a linear PDE system [1]

$$\frac{\partial q}{\partial t} + \Psi \frac{\partial q}{\partial x} = -F(x)q, \tag{1}$$

with

$$q = \begin{bmatrix} q_1 \\ q_2 \end{bmatrix} := \begin{bmatrix} \rho \\ \rho v \end{bmatrix}, \Psi = \begin{bmatrix} 0 & 1 \\ c_l^2 & 0 \end{bmatrix}, F = \begin{bmatrix} 0 & 0 \\ g\sin(\theta(x)) & \frac{32\mu_m}{\rho_0 d^2} \end{bmatrix},$$

and where $x \in [0, l]$ and t are the spatial and time variables, respectively, and l it the length of the pipe. The liquid density, velocity, and pressure are denoted by $\rho(x,t)$, $v(x,t)$ and $p(x,t)$, respectively, whereas μ_m, d, $\theta(x)$, g and c_l are the liquid viscosity, the hydraulic diameter of the pipe, the pipe inclination, gravitational acceleration, and sound velocity in liquid, respectively. The equation of state, describing the relation between the pressure and density, is chosen as [6]

$$p = c_l^2 (\rho - \rho_0) + p_0, \tag{2}$$

where p_0 and ρ_0 are the reference pressure and density, respectively.

The MPD system is modeled by a series connection of two pipe models of the form (1) and a number of the boundary condition which are introduced in the sequel. The first boundary equation imposed by the pump equation is given as

$$J_p(t) - \phi^d q_2^d(0,t) = 0, \tag{3}$$

where ϕ is the cross-sectional area and J_p is the pump mass flow rate, see Fig. 1. In this context, a sub/superscript a refers to the annulus and d to the drillstring. The second and the third boundary equations describe the outlet of the drillstring and the inlet of the annulus. Those are derived using the bit equation and read

$$z(t) - \phi^d q_2^d(l,t) = 0, \quad z(t) - \phi^a q_2^a(0,t) = 0, \tag{4}$$

where $z(t)$ represents the mass flow rate through the bit. The latter is given by the nonlinear bit model

$$\dot{z} = \begin{cases} -\beta_1 z^2 - \beta_2 z + \beta_3 \Delta\rho_{dh}, \text{ for} & z > 0, \\ \max(0, -\beta_1 z^2 - \beta_2 z + \beta_3 \Delta\rho_{dh}), \text{ for} & z = 0, \end{cases} \tag{5}$$

where $\Delta\rho_{dh} = q_1^d(l,t) - q_1^a(0,t)$, and the parameters β_1, β_2 and β_3 are dependent on the well parameters and the bit parameters C_d and A_n, which are the bit constant and bit nozzle area, respectively. The last boundary equation is given by the choke equation

$$J_c(q_2^a(l,t)) - k_c c_l G(z_c) f_c\left(q_1^a(l,t)\right) = 0, \tag{6}$$

where J_c, k_c, $z_c(t)$ and $G(z_c)$ are the choke mass flow rate, the choke flow factor, the choke opening and the choke characteristic equation, respectively. Also, $f_c(q_1^a(l,t)) = sgn(r)\sqrt{|r|}$, where $r = 2q_1^a(l,t)(q_1^a(l,t) - \rho_0)$.

2.1 Finite-dimensional model

As mentioned before, in this modeling approach the PDE model (1) needs to be spatially discretized. Here, we use a so-called Kurganov-Tadmor scheme [8] for spatial discretization and a characteristics-based method [5] for treating the nonlinear implicit boundary conditions of the system. After performing the discretization and some algebraic manipulation, one arrives at an ODE model in a Lur'e-type form [7], composed of an interconnection of a linear subsystem and a nonlinear static mapping. Most of the drilling time is spent on the drilling ahead operation, during which the pump flow rate is kept constant at some

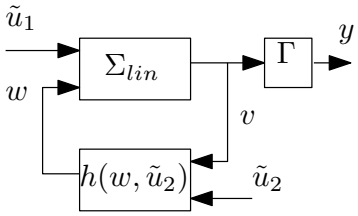

Figure 2: A block diagram of the finite-dimensional model in a Lur'e-type form.

nominal value J_p^* and the choke opening may have just small variations around a nominal value z_c^*, to compensate for transient pressure fluctuations. Thus, it is reasonable to change the origin of the resulting Lur'e-type system to an operating point that corresponds to the inputs $u_1^* = \frac{J_p^*}{2\phi^d}$ and $u_2^* = \frac{k_c c_l G(z_c^*)}{2\phi^a}$. The value z_c^* is designed such that the resulting surface pressure is larger than the reference pressure p_0 for normal drilling operations, thereby keeping the system controllable in practice. We finally obtain the Lur'e-type system

$$\Sigma_{lin} : \begin{cases} \dot{X} = AX + B_u\tilde{u}_1 + B_w w, \\ v = C_v X + D_{vu}\tilde{u}_1 + D_{vw} w, \\ y = \Gamma v, \end{cases} \tag{7}$$

$$\Sigma_{nl} : \quad w = h(v, \tilde{u}_2), \tag{8}$$

where $X \in \mathbb{R}^{n_c}$ is the high-dimensional state vector, $v \in \mathbb{R}^2$ and $w \in \mathbb{R}^2$ are internal inputs and outputs of the linear sub-system Σ_{lin}, connecting it to the nonlinear sub-system Σ_{nl}, and $y \in \mathbb{R}$ is the system output. Also, a tilde " ˜ " indicates the difference between a variable and its operational (steady-state) value denoted by *. The mapping $h(\cdot, \cdot)$ is nonlinear function that stems from the nonlinear boundary conditions. A simple block diagram of the model is shown in Fig. 2.

It should be mentioned that we choose the pressure upstream the choke, p_c as in Fig. 1, as the output y here, since it is the output that is typically used for feedback control [6]. This output is obtained by passing v through a linear mapping Γ, as in Fig. 2.

3 Nonlinear Model Order Reduction

3.1 Model Order Reduction procedure

The nonlinear model (7) and (8), denoted by $\Sigma = (\Sigma_{lin}, \Sigma_{nl})$, is in the form of a feedback interconnection of a high-order linear subsystem Σ_{lin} and low-order

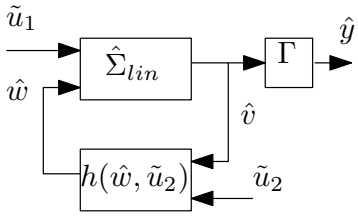

Figure 3: A block diagram of the reduced nonlinear model.

nonlinear subsystem Σ_{nl}. This particular structure enables us to reduce the model complexity by only reducing the linear subsystem using existing model order reduction techniques for linear systems, such as balanced singular perturbation [4, 11], which preserves the steady-state response. This leads to a reduced-order linear subsystem $\hat{\Sigma}_{lin}$ of the following form

$$\hat{\Sigma}_{lin} : \begin{cases} \dot{\hat{X}} = \hat{A}\hat{X} + \hat{B}_u\tilde{u}_1 + \hat{B}_w\hat{w}, \\ \hat{v} = \hat{C}_v\hat{X} + \hat{D}_{vu}\tilde{u}_1 + \hat{D}_{vw}\hat{w}, \\ \hat{y} = \Gamma\hat{v}, \end{cases} \tag{9}$$

where $\hat{X} \in \mathbb{R}^k$, $k < n_c$, and the dimensions of the inputs and outputs remain unchanged. Balancing-based model order reduction methods preserve stability and minimality, and provide a bound on the reduction error of the linear subsystem, such that for the H_∞-norm of the difference between Σ_{lin} (with v as output) and $\hat{\Sigma}_{lin}$, we have

$$\left\| \Sigma_{lin} - \hat{\Sigma}_{lin} \right\|_{H_\infty} \leq \epsilon_{lin}, \quad \epsilon_{lin} = 2 \sum_{j=k+1}^{n_c} \sigma_j, \tag{10}$$

where σ_j is the j^{th} Hankel singular value of Σ_{lin} [11].

Finally, the interconnection of the original nonlinear Σ_{nl} subsystem and the reduced linear subsystem $\hat{\Sigma}_{lin}$ leads to the reduced-order nonlinear system $\hat{\Sigma} = (\hat{\Sigma}_{lin}, \Sigma_{nl})$, a block diagram of which is shown in Fig. 3.

3.2 Properties of original and reduced-order systems

If a number of conditions hold [3], it can be guaranteed that the described model order reduction technique preserves stability properties and provides a computable bound on the reduction error in terms of $\mathcal{L}_2$-induced system norm for the reduced-order nonlinear system $\hat{\Sigma}$. These conditions are: 1) the linear subsystem Σ_{lin} is asymptotically stable and 2) the small-gain condition

$$\mu_{wv}\gamma_{vw} < 1, \tag{11}$$

holds, with γ_{vw} the (incremental) $\mathcal{L}_2$-gain of Σ_{lin} corresponding to w as input and v as output, and μ_{wv} is an upper bound for the incremental $\mathcal{L}_2$-gain of Σ_{nl} from v to w.

If Σ satisfies all the aforementioned conditions, then it has a bounded incremental $\mathcal{L}_2$ gain (from input $\tilde{u} = \begin{bmatrix} \tilde{u}_1 & \tilde{u}_2 \end{bmatrix}^T$ to y) with bound

$$\gamma_{yu} = \sqrt{2} \max\left(\gamma_{yu_1}, \gamma_{yu_2}\right). \tag{12}$$

Moreover, the origin is locally asymptotically stable. Here, the gains γ_{yu_1} and γ_{yu_1} are given as $\gamma_{yu_1} = \frac{\gamma_{yv}\gamma_{vu_1}}{M}$, $\gamma_{yu_2} = \frac{\gamma_{yv}\gamma_{vw}\mu_{wu_2}}{M}$, respectively, with $M = 1 - \mu_{wv}\gamma_{vw}$, γ_{yv} the $\mathcal{L}_2$ gain from v to y, γ_{vu_1} the incremental $\mathcal{L}_2$ gain from $\tilde{u}_1$ to v and μ_{wu_2} the $\mathcal{L}_2$ gain from $\tilde{u}_2$ to w.

Also, if Σ satisfies all the aforementioned conditions, the feedback interconnection $\hat{\Sigma} = (\hat{\Sigma}_{lin}, \Sigma_{nl})$ is well-posed and $\hat{\Sigma}_{lin}$ is asymptotically stable, the following statements hold:

1. The reduced-order system $\hat{\Sigma}$ has a bounded incremental $\mathcal{L}_2$ gain and the origin is asymptotically stable for $\tilde{u} = 0$ when

$$\mu_{wv}(\gamma_{vw} + \epsilon_{lin}) < 1 \text{ with } \epsilon_{lin} \text{ in (10).} \tag{13}$$

2. Let (13) hold. Then, the output error $y - \hat{y} =: \delta y$ is bounded as $\|\delta y\|_2 \leq \epsilon \|\tilde{u}\|_2$, with $\|.\|_2$ denoting the $\mathcal{L}_2$ norm and

$$\epsilon = \sqrt{2}\frac{\gamma_{yv}\epsilon_{lin}}{\hat{M}} \max\left(\gamma_1, \gamma_2\right), \tag{14}$$

where $\hat{M} = 1 - \mu_{wv}(\gamma_{vw} + \epsilon_{lin})$, $\gamma_1 = 1 + \frac{\mu_{wv}\gamma_{vu_1}}{M}$, $\gamma_2 = \frac{\mu_{wu_2}}{M}$ and γ_{yv} is the $\mathcal{L}_2$ gain from v to y.

4 An illustrative case study

To evaluate the accuracy of the reduced-order model obtained by the procedure discussed in Section 3, simulations are performed with the parameters listed in Table 1. The nominal inputs are taken as $J^*_{pump} = 54$ kg/s and $z^*_c = 0.3$.

In Fig. 4, the singular values σ_i of the high-order linear subsystem are shown. Clearly, a relatively fast decay begins around $j = 20$. Here, we choose $k = 41$, for which $\epsilon_{lin} = 0.0194$ and the condition (13) holds with $\hat{M} = 0.111$. In Fig. 5, a comparison is performed between the 2×2 transfer function matrices G_{vw} of Σ_{lin} from w to v and $\hat{G}_{vw}$ of $\hat{\Sigma}_{lin}$ from $\hat{w}$ to $\hat{v}$. Clearly, at low frequencies there is good match between the two linear subsystems and the resonance frequencies are also well captured by the reduced subsystem.

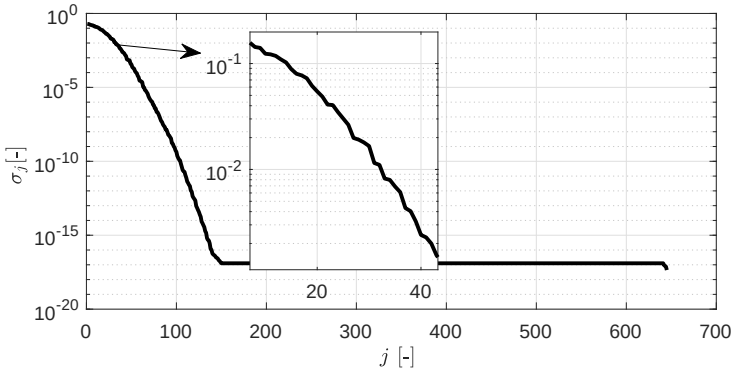

Figure 4: The singular values σ_i of the linear subsystem Σ_{lin}.

Remark: The normal drilling operations are performed so slowly that the high-frequency modes of the system are seldomly exited. But, there are undesirable scenarios, such as choke plugging and heave motion, that excite these high-frequency modes and cause transient and periodic pressure fluctuations. Thus, for effective compensation of such fluctuations by means of control, it is important that the hydraulics model is capable of capturing the major resonance frequencies of the system, which indeed approximate the wave propagation phenomenon.

In time-domain simulations in Fig. 6, the choke opening is decreased from its nominal value z_c^* to $z_c = 0.15$ with a step change at $t = 15$ s and the pump mass flow rate is reduced to 50% at $t = 35$ s. With these extreme inputs, which indeed resemble a choke plugging scenario, a comparison is performed between the original model Σ (M1), the reduced nonlinear model $\hat{\Sigma}$ (M2) and a model obtained from performing a coarse discretization of the PDE with $n_c = 41$ (M3). Note that M3 has the same order as M2. The response of the model presented in [6], shown by M4, is also added as it has a good steady-state accuracy. The

Table 1: The simulation parameters.

Par.	Value	Par.	Value	Par.	Value
l	1817 m	c_l	745 m/s	μ_m	0.04 kg/sm
$\theta(x)$	61.7^o	ρ_0	1800 kg/m^3	C_d	0.8
ϕ^a	0.026 m^2	p_0	1 bar	A_n	7.46×10^{-4} m^2
ϕ^d	0.01 m^2	k_c	0.0032	Δl	40 m
		n_c	645	g	9.81 m/s^2

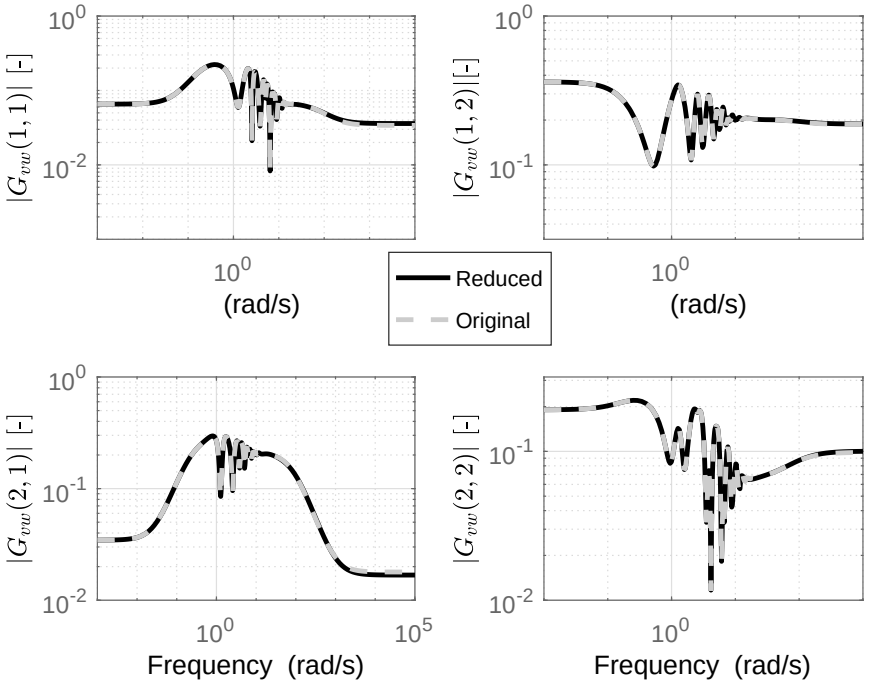

Figure 5: A comparison between the frequency responses of Σ_{lin} and $\hat{\Sigma}_{lin}$.

results are reported in Fig. 6. This figure shows that the reduced-order model M2 gives far more accurate response approximation compared to the discretized model M3 of the same order, indicating the usefulness of model order reduction for MPD systems. Moreover, M3 has a better performance in preserving the fast dynamics of the system compared to M4, but it suffers from inaccuracy in steady-state, while M4 has a good steady-state performance. The reduced-order model obtained by the reduction procedure proposed here captures both the steady-state behaviour and the transients accurately, with a moderate model order.

5 Conclusion

A nonlinear model order reduction method has been presented for a single-phase managed pressure drilling system. By using a high-resolution discretization scheme a new nonlinear control-oriented hydraulics model has been derived for

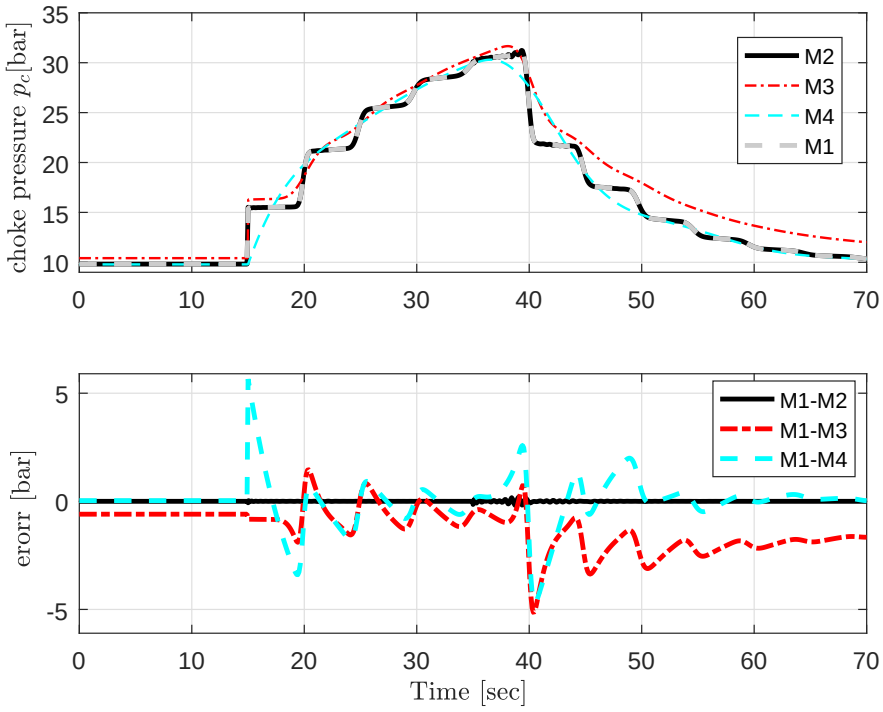

Figure 6: A time response comparison between M1 the original model Σ, M2 the reduced model $\hat{\Sigma}$, M3 the model with $n_c = 41$ and M4 by [6].

the system. The resulting model has been decomposed into a feedback interconnection of a high-order linear and low-order nonlinear subsystem, permitting a model reduction procedure that guarantees preservation of key system (stability) properties and provides a computable reduction error bound in terms of $\mathcal{L}_2$ norm. Simulations illustrate the effectiveness of the presented model order reduction method for managed pressure drilling applications.

References

[1] U. J. F. Aarsnes, O. M. Aamo, and A. Pavlov. Quantifying error introduced by finite order discretization of a hydraulic well model. In *2nd Australian Control Conference*, pages 54–59, Sydney, NSW, Australia, November 2012.

[2] U. J. F. Aarsnes, F. Di Meglio, R. Graham, and O. M. Aamo. A Methodology for Classifying Operating Regimes in Underbalanced-Drilling Opera-

tions. *SPE Journal*, 21(02):423–433, April 2016.

[3] B. Besselink, N. van de Wouw, and H. Nijmeijer. Model reduction for nonlinear systems with incremental gain or passivity properties. *Automatica*, 49(4):861–872, April 2013.

[4] K. Fernando and H. Nicholson. Singular perturbational model reduction of balanced systems. *IEEE Transactions on Automatic Control*, 27(2):466–468, April 1982.

[5] K. K. Fjelde and K. H. Karlsen. High-Resolution Hybrid Primitive-Conservative Upwind Schemes for the Drift Flux Model. *Computers & Fluids*, 31(3):335 – 367, 2002.

[6] G. O. Kaasa, Ø. N. Stamnes, O. M. Aamo, and L. S. Imsland. Simplified Hydraulics Model Used for Intelligent Estimation of Downhole Pressure for a Managed-Pressure-Drilling Control System. *SPE Drilling & Completion*, 27(01):127–138, March 2012.

[7] H. K. Khalil. *Nonlinear Systems*. Pearson New International Edition. Pearson, Harlow, United Kingdom, 2014.

[8] A. Kurganov and E. Tadmor. New High-Resolution Central Schemes for Nonlinear Conservation Laws and Convection-Diffusion Equations. *Journal of Computational Physics*, 160(1):241–282, May 2000.

[9] I. S. Landet, H. Mahdianfar, A. Pavlov, and O.M. Aamo. Modeling for MPD Operations With Experimental Validation. In *IADC/SPE Drilling Conference and Exhibition*, Society of Petroleum Engineers, San Diego, California, March 2012.

[10] I. S. Landet, A. Pavlov, and O. M. Aamo. Modeling and Control of Heave-Induced Pressure Fluctuations in Managed Pressure Drilling. *IEEE Transactions on Control Systems Technology*, 21(4):1340–1351, July 2013.

[11] Y. Liu and B. D. O. Anderson. Singular perturbation approximation of balanced systems. *International Journal of Control*, 50(4):1379–1405, 1989.

[12] H. Mahdianfar, O. M. Aamo, and A. Pavlov. Suppression of Heave-Induced Pressure Fluctuations in MPD. *IFAC Proceedings Volumes*, 45(8):239 – 244, 2012.

[13] H. Mahdianfar and A. Pavlov. Adaptive output regulation for offshore managed pressure drilling. *International Journal of Adaptive Control and Signal Processing*, 31(4):652–673, April 2017.

[14] Ø. N. Stamnes, J. Zhou, G. O. Kaasa, and O. M. Aamo. Adaptive observer design for the bottomhole pressure of a managed pressure drilling system. In *2008 47th IEEE Conference on Decision and Control*, pages 2961–2966, Cancun, Mexico, Dec 2008.

Nonlinear Modeling of Directional Drilling

Fahim Shakib[1], Emmanuel Detournay[2] and Nathan van de Wouw[1,2,3]

[1] Dep. of Mechanical Eng., Eindhoven, University of Technology, The Netherlands
[2] Dep. of Civil, Environmental, and Geo- Eng., University of Minnesota, USA
[3] Dep. of Mechanical, Maritime and Materials Eng., Delft, University of Technology

1 Introduction

Directional drilling allows for the drilling of curved boreholes, which are needed to exploit unconventional reservoir of oil, gas and mineral resources. 1a shows a sketch of a directional drilling system. The drillstring can be typically a few kilometers in length. It is supported at the rig where the rotary speed and the axial force (hook-load) are imposed. Most of the drillstring is in tension under its own weight, except for the bottom hole assembly (BHA), which is in compression to induce a sufficient weight on the bit. The BHA is usually about one hundred meters long and consists of drill collars, stabilizers ensuring centering of the BHA in the borehole, a bit penetrating the rock formation, and a rotary steerable system (RSS). The RSS is a downhole robotic actuator that steers the BHA in the desired direction. The work presented here considers the family of tools called push-the-bit RSS. Such a RSS is located between the bit and the first stabilizer and uses a set of extensible pads to induce a lateral force on the borehole wall, and thereby on the BHA.

In practice, drilling with such directional drilling technology often results in self-excited borehole oscillations, called borehole spiraling. An illustration of borehole spiraling and its two-dimensional equivalent, borehole rippling, is depicted in 1b. Borehole spiraling has negative effects on the drilling process and the borehole quality. First of all, it makes it harder to insert a casing after the borehole is drilled. Secondly, it decreases the drilling efficiency in terms of a low rate-of-penetration and high drilling costs due to increased drag forces, which in turn accelerate bit wear. Furthermore, it reduces the accuracy of reaching a desired target position. Finally, it could induce instability of the obtained borehole, which, consequently, makes the borehole more likely to collapse.

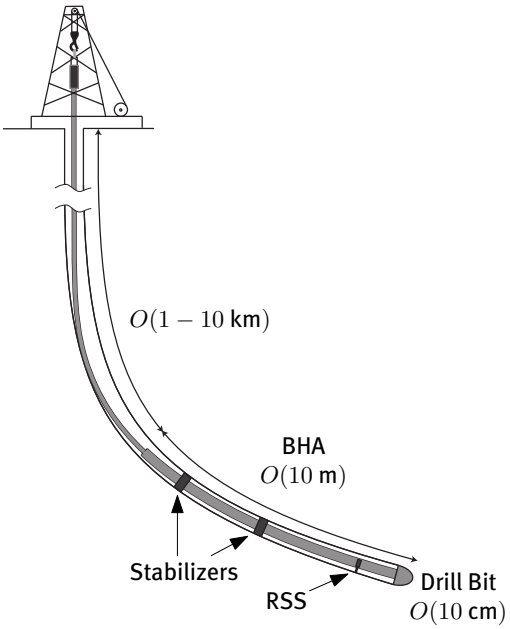

(a)

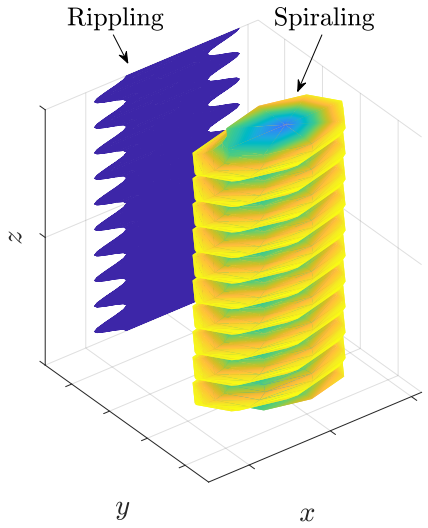

(b)

Figure 1: (a) Overview of a directional drilling system. (b) Illustration of borehole rippling and spiraling.

Many numerical directional drilling models exist, see [8, 12, 13, 4, 1, 3, 20, 5, 17]. These models do not lead to a closed-form model description for borehole propagation in directional drilling. As a consequence, such models do not provide insight into the effects of model parameters and RSS actuation on the borehole propagation and are not suitable for controller design. A closed-form model description was first developed by Neubert and Heisig [14, 15] and later by Downton and Ignova [6]. The model of Neubert and Heisig is only applicable for an actuation mechanism based on the eccentricity of an adjustable stabilizer, i.e., a point-the-bit RSS, while the model developed by Downton and Ignova is restricted to small rotations of the borehole evolution.

More advanced analytical models are developed by Detournay, Perneder and Marck [19, 18, 10]. These models are described by (nonlinear) delay differential equations, where the states are chosen to be the inclination and the azimuth of the borehole. These models are able to determine the conditions leading to oscillatory behavior in the borehole via a linear stability analysis. In [10, 18], an extension of this model is given which incorporates a saturation of the bit tilt, as documented in [16, 7]. The bit tilt is defined as the orientation difference

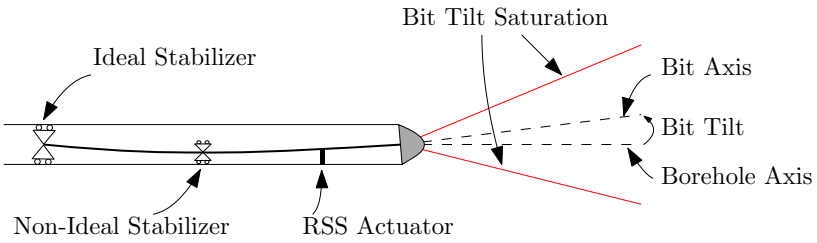

Figure 2: Non-ideal stabilizers and the bit tilt saturation.

between the bit and the borehole at the bit. 2 gives an illustrative interpretation of this nonlinearity. In fact, such a saturation of the bit tilt occurs when the bit gauge contacts a borehole wall. This saturation prevents oscillations to grow unbounded and naturally leads to steady-state borehole rippling and spiraling. The model extended with bit tilt saturation in [10, 18] is not given in a closed-form description.

Another nonlinearity is introduced when considering non-ideal stabilizers, which are stabilizers that have a diameter smaller than the borehole. Commonly in modeling directional borehole propagation, it is assumed that stabilizers have the same diameter as the borehole. However, in practice, this assumption seldomly holds due to bit over-gauging and whirling of the bit and the BHA. This implies that there is some clearance between the stabilizers and the borehole wall(s) [10], see 2 for an illustration.

In [21], we introduce a modeling framework, based on linear complementarity systems, that is able to deal with non-ideal stabilizers and also supports modeling the bit tilt saturation previously used in [10, 18]. The resulting mathematical model, restricted to planar borehole propagation, is analyzed in order to obtain insights into key model parameters that control the directional capabilities of directional drilling systems and the stability of trajectories. In particular, we are interested in finding conditions leading to borehole rippling. Such insight can then be used to select the drill bit and improve the design of the BHA such that borehole spiraling is prevented. Furthermore, this model can serve as a basis for the development of model-based controllers, which have the objective to accurately track an intended (predefined) well path [9].

2 Borehole Propagation Model

The evolution of the bit trajectory, and thus the geometry of the borehole, is a result of the interaction between the drilling structure, being a mechanical object, and the borehole itself, being a geometrical object. The borehole propagation

model involves three components, namely (i) a static (beam) model of the BHA of the drillstring, (ii) a model of the bit-rock interaction, and (iii) a kinematic model relating the motion of the bit into the rock formation to geometric variables for the borehole evolution. See 3, for an overview of the components and their interaction.

Next, we will treat each model component in more detail. The model of the BHA aims at statically fitting the drillstring inside the already drilled borehole using the Euler-Bernoulli beam theory. By doing so, we yield expressions for the forces and the moment experienced by the bit. Signorini's contact law is employed to formulate a linear complementarity problem of which the solution is the contact force experienced by the non-ideal stabilizers and the clearance between each non-ideal stabilizer and the borehole walls.

The forces and the moment at the bit can be related to penetration variables using the bit-rock interaction law. These penetration variables relate to the amount of rock removed by the bit over one bit revolution and, therefore, relate to the movement of the bit through the rock formation. The bit tilt saturation is involved in this model component; it constrains the removal of rock in certain directions when saturated. The linear complementarity problem is extended to take into account the saturation of the bit tilt as well. This extended linear complementarity problem returns both the contact forces at the non-ideal stabilizers as well as those associated to the bit tilt.

The kinematic model relates these penetration variables to geometric variables. These geometric variables represent the evolution of the bit inclination and, thereby, the borehole inclination over the length of the borehole. The length of the borehole is taken as the independent parameter.

By combining the three model components, an analytically closed-form description of the borehole propagation model is derived. The derived model is in the class of delay complementarity systems [2]. The delay nature of this model stems from the delayed influence of the borehole geometry on the deformation of the BHA through the stabilizers. Complementarity relations are used to describe the unilateral contact of non-ideal stabilizers with the borehole walls and to model the bit tilt nonlinearity. The modeling framework allows for a compact notation of the hybrid model, whose dynamics are governed by continuous dynamics of borehole propagation and discrete events of unilateral contact of the non-ideal stabilizers and the saturation of the bit tilt. For the sake of brevity, we do not provide the mathematical model description here, but rather focus on illustrating the effect of the non-linearities on the directional response. For details on the model we refer to [21].

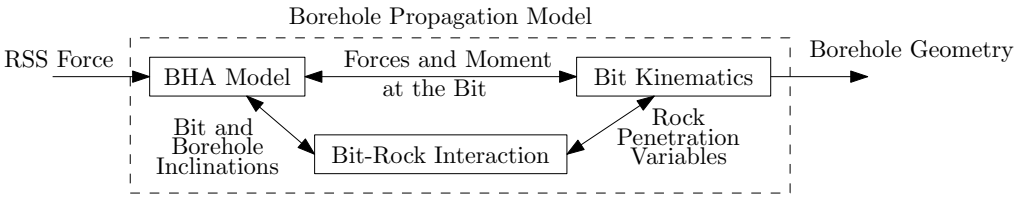

Figure 3: Borehole propagation model and its three model components.

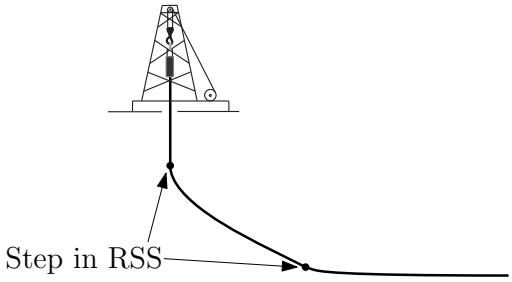

Figure 4: Response to multiple steps in RSS force.

3 Steady-State Solutions of Propagating Boreholes

The analytical form of the derived borehole propagation model allows for a comprehensive analysis. This analysis involves the response of the model to a step in RSS force, which is motivated by the fact that such an actuation technique is used in practice in directional drilling processes. A typical response of the drilling system on a step in RSS force is depicted in 4. On a length scale sufficiently large compared to the length of the BHA, such a constant actuation leads to a borehole evolving with a uniform curvature, when viewed at the scale of the BHA length. The borehole curvature however changes slowly over the increasing length of the borehole. Under appropriate drilling parameter settings, such a step in RSS actuation leads asymptotically to a straight inclined borehole where a balance between the RSS force and the gravity forces exist. These two length scales are hence associated to two types of stationary solutions, which are given analytically as a function of the RSS actuation and model parameters in [21].

In such analysis, we identify a key dimensionless group $\eta\Pi$ [10, 18] which controls both the directional capabilities of directional drilling systems as well as the stability of the response. This group represents the active weight on the bit (being the part of the weight on bit associated with rock cutting), the flexural stiffness of the drillstring, position of the stabilizers behind the bit, the bit bluntness, and parameters characterizing the steering resistance of the bit.

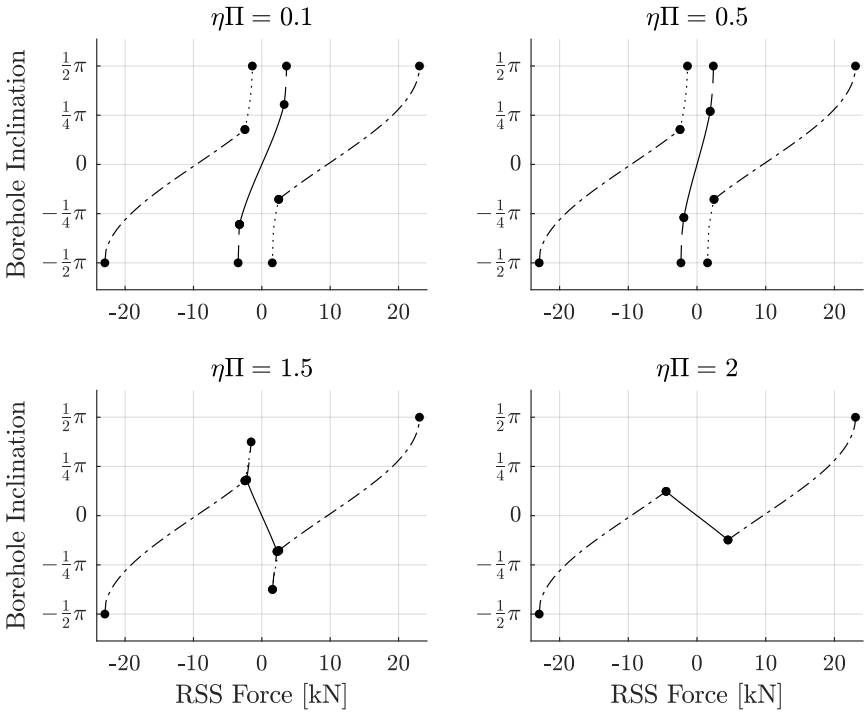

Figure 5: Map of the inclination of stationary solutions versus the step applied in RSS force for the parameter group $\eta\Pi = \{0.1, 0.5, 1.5, 2\}$.

This parameter group can be interpreted as a pseudo stiffness contrasting the flexural stiffness of the BHA with the 'stiffness' of the rock formation. In words, if the bit is tilted, then the drillstring tends to deform back to its undeformed shape due to the flexural stiffness of the drillstring, however, this is counteracted by the rock formation disallowing the bit to change its orientation.

On account of conciseness, we only focus on the second kind of stationary solutions here, i.e., straight inclined boreholes that evolve along a straight line. A two-stabilizer BHA is considered, where the last stabilizer is ideal and the stabilizer between the bit and the last stabilizer is non-ideal, like the BHA setting in 2. The borehole inclination versus the applied RSS force is depicted in 5 for several values of the parameter group $\eta\Pi$. Due to the inclusion of the nonlinearities, i.e., the non-ideal stabilizers and the bit tilt saturation, the borehole propagation model exhibits multiple modes, where in each mode significantly different dynamics are active. As a direct consequence, branches of steady-state solutions exist, where the line style in 5 corresponds to the branch starting and ending at

the circular marks. The line styles are defined as follows: solid represents the non-ideal stabilizer being cleared from both walls and the bit tilt not saturating; dashed corresponds to the non-ideal stabilizer touching one of the walls and the bit tilt not saturating; dashed dotted represents the non-ideal stabilizer being cleared from the walls and the bit tilt saturating; and dotted corresponds to the non-ideal stabilizer contacting one of the walls and the bit tilt saturating.

Evaluating over $\eta\Pi$, we can observe that branches of solutions for which the bit tilt saturates (partly) exist independently of $\eta\Pi$. This can be explained by the dependency on $\eta\Pi$ vanishing when the bit tilt saturates. Another observation is the occurrence of non-minimum phase behavior, where, the borehole evolves, counter-intuitively, in the opposite direction as the applied RSS force. This is due to the existence of multiple drilling regimes, where the drilling tendency in one regime is in the direction of the bit axis and in the other regime along the lateral force experience by the bit. Furthermore, we can observe that multiple solutions coexist for the same applied RSS force. This is again directly related to the inclusion of the nonlinearities.

Recall that each mode has different dynamics and, therefore, induces distinct stability properties of the stationary solutions in that mode. We utilize a method based on the spectrum of the underlying delay differential equations [11], to conclude on the local stability of each solution. The stability classification is valid as long as the trajectory stays sufficiently close to the examined solution and the mode during the trajectory does not change. In our analysis, we observed that within a mode (a branch), all the solutions have the same stability properties. This allows us to do a the stability analysis for branches of solutions rather than for a single solution.

In 6, we give a parametric stability analysis for the case where the bit tilt is not saturated. Here, we analyze the parameter group $\eta\Pi$ and the dimensionless BHA length λ, which is scaled with the distance between bit and the stabilizer closest to the bit. In this diagram, we distinguish between two modes, namely the non-ideal stabilizer contacting one of the borehole walls and the non-ideal stabilizer being cleared from both walls. The solutions can exhibit two types of instabilities: a drift-type instability and an oscillatory-type instability. The drift-type instability is related to a real pole entering the complex right half plane, stemming from the influence of gravity, which reverses for specifically $\eta\Pi^*_{\mathrm{nc}}$ and $\eta\Pi^*_{\mathrm{c}}$, for the no contact and contact mode, respectively. These are the gray areas in 6. The oscillatory-type instability is related to the geometric feedback of the borehole sensed through the stabilizers and being amplified at the bit. These are the red areas in 6. This is a result of complex pole pairs entering the complex right half plane. For this type of instability, we see stability lobes, which were also observed in [10, 18]. For the case where the bit tilt is saturated, we do not

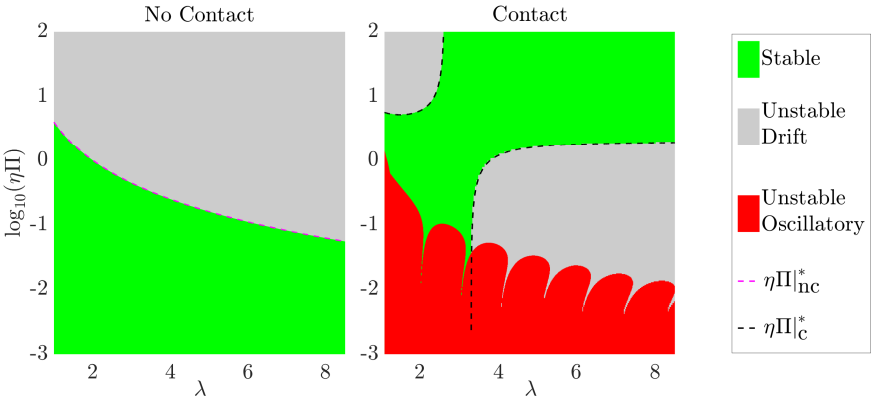

Figure 6: Stability diagram for a two-stabilizer model.

observe the oscillatory-type instability. However, we do observe the drift-type instability which, again, stems from gravitational effects.

4 Borehole Rippling

Naturally, we can see this parameter group $\eta\Pi$ as a bifurcation parameter since it controls the right-most poles (in the complex-plane) of the linearized dynamics of the borehole propagation model around stationary solutions. In practice, the parameter group $\eta\Pi$ is uncertain and might change for example when transitioning between two rock layers. We can see that for certain $\eta\Pi$ and λ values, in the no contact mode, stable dynamics are active (green areas), implying that perturbations will die and the borehole evolves according to the nominal stationary solution. For the same $\eta\Pi$ in the contact mode, we observe complex pole pairs in the right half plane, implying that perturbation will grow in an oscillatory fashion.

The combination of such stable and unstable dynamics being active in different modes results in steady-state borehole oscillation which we can relate to borehole rippling. This is illustrated in the following numeric simulation, for which a two-stabilizer BHA is used where the distance between the bit and the first stabilizer is identical to the distance between the first and last stabilizer. The nominal clearance between the borehole and the non-ideal stabilizers is set to 1 mm and the saturation of the bit tilt is set to 2 degrees. These values are common in practical situations. As the initial condition, a straight, vertical borehole under a small inclination is taken. We do not apply a RSS force, which implies that if the dynamics were stable, then the stationary solution would

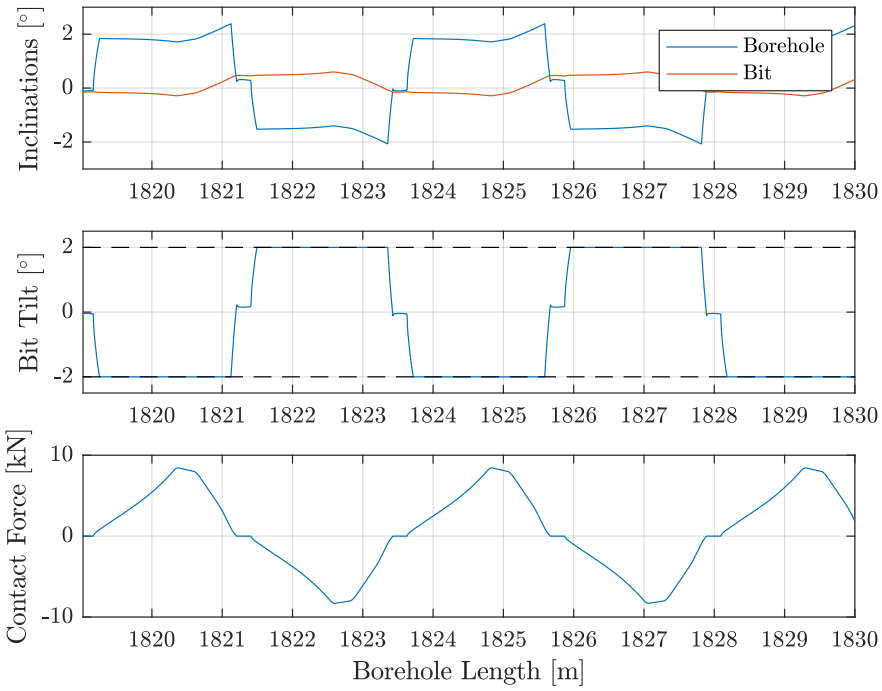

Figure 7: Steady-state borehole rippling.

converge to a straight vertical borehole.

7 contains the results of this simulation in steady-state. The top plot shows the bit and borehole inclination in degrees. It can be seen that the bit and borehole oscillate near the stationary solution, i.e., a vertical borehole corresponding to zero degrees. The oscillations in the borehole are essentially a reflection of the oscillations undergone by the bit. The middle plot shows that the bit tilt oscillates between the two saturation boundaries. The bottom plot shows the contact force experienced at the non-ideal stabilizer. Here, we can observe that the non-ideal stabilizer moves from one side of the borehole to the other side and back. The short intervals where the contact force is zero represent the intervals where the non-ideal stabilizer is cleared from both walls.

We have thus shown using this numerical study that the proposed model can predict steady-state borehole rippling. Furthermore, we have identified for which model parameters this phenomenon occurs, namely those that trigger this type of bifurcation.

5 Conclusions

We presented a non-smooth borehole propagation model for planar directional borehole propagation. This model incorporates non-ideal stabilizers and the bit tilt saturation. A group of model parameters is identified which dominates the directional capabilities of directional drilling systems and the stability of borehole trajectories. Using a numerical study, we have shown that this model is capable of predicting borehole rippling and thus provides valuable insight in this undesired phenomenon.

References

[1] M.H. Amara, *Use of Drillstring Models and Data Bases for the Scientific Control of Vertical and Directional Hole Paths*, Proc. SPE/IADC Drilling Conf., SPE-13495-MS, New Orleans, Louisiana, USA, March 1985.

[2] J.J.B. Biemond, W. Michiels, N. van de Wouw, *Stability analysis of equilibria of linear delay complementarity systems*, IEEE Control Systems Letters, Vol. 1, Issue 1, pp. 158–163, July 2017.

[3] M. Birades, R. Fenoul, *A Microcomputer Program for Prediction of Bottomhole Assembly Trajectory*, SPE Drilling Engineering, Vol. 3, Issue 2, pp. 31–38, SPE-15285-PA, Silver-Creek, CO, USA, June 1988.

[4] N.P. Callas, R.L. Callas, *Boundary value problem is solved*, Oil Gas J., Vol. 78, No. 50, pp. 62–66, 1980.

[5] D.C.K. Chen, M. Wu, *State-of-the-Art BHA Program Produces Unprecedented Results*, Proc. Int. Petroleum Technol. Conf. (IPTC), Kuala Lumpur, Malaysia, December 2008.

[6] G.C. Downton, M. Ignova, *Stability and Response of Closed Loop Directional Drilling System using Linear Delay Differential Equations*, Proc. IEEE Int. Conf. Control Appl. (CCA), pp. 893–898, Denver, CO, USA, September 2011.

[7] S. Ernst, P.E. Pastusek, P.J. Lutes, *Effects of RPM and ROP on PDC Bit Steerability*, SPE/IADC Drilling Conference, No. SPE/IADC 105594, Amsterdam, The Netherlands, February 2007.

[8] F.J. Fischer, *Analysis of Drillstrings in Curved Boreholes*, Proc. 49th Annu. Fall Meeting Soc. Petroleum Eng. of AIME, p. SPE 5071, Dallas, Texas, USA, October 1974.

[9] N.A.H. Kremers, E. Detournay, N. van de Wouw, *Model-based Robust Control of Directional Drilling Systems*, IEEE Transactions on Control Systems Technology, Vol. 24, No. 1, pp. 226–239, June 2015.

[10] J. Marck, *A Nonlinear Dynamical Model of Borehole Spiraling*, PhD dissertation, Faculty of the Graduate School of the University of Minnesota, Minneapolis, Minnesota, USA, December 2015.

[11] W. Michiels, S.-I. Niculescu, *Stability and Stabilization of Time-Delay Systems: An Eigenvalue-Based Approach*, SIAM, 2007.

[12] K. Millheim, *The Effect Of Hole Curvature On The Trajectory Of A Borehole*, Proc. 52nd Annu. Fall Tech. Conf. Exhibit. Soc. Petroleum Eng. AIME, Denver, CO, USA, pp. 1–8, October 1977.

[13] K. Millheim, S. Jordan, C.J. Ritter, *Bottom-Hole Assembly Analysis Using the Finite-Element Method*, J. Petroleum Technol., Soc. Petroleum Eng. vol. 30, no. 2, pp. 256–274, February 1978.

[14] M. Neubert, G. Heisig, *Mathematical description of the directional drilling process and simulation of directional control algorithm*, Zeitschrift Angew. Math. Mech., Vol. 76, No. 5, pp. 361–362, January 1996.

[15] M. Neubert, G. Heisig, *Advanced trajectory simulation of directional wellbores*, Proc. Energy Week Conf. Exhibit., p. 336, Houston, Texas, USA, July 1997.

[16] P.E. Pastusek, V.J. Brackin, P.J. Lutes, *A Fundamental Model for Prediction of Hole Curvature and Build Rates With Steerable Bottomhole Assemblies*, SPE Annual Technical Conference and Exhibition, No. SPE 95546, Dallas, Texas, USA, October 2005.

[17] P.E. Pastusek, V.J. Brackin, *A Model for Borehole Oscillations*, SPE Annual Technical Conference and Exhibition, No. SPE 84448, Denver, Colorado, USA, October 2003.

[18] L. Perneder, J. Marck, E. Detournay, *A Model of Planar Borehole Propagation*, SIAM J. Appl. Math., Vol. 77, Issue 4, pp. 1089–1114, 2017.

[19] L. Perneder, *A Three-Dimensional Mathematical Model of Directional Drilling*, Ph.D. dissertation, Faculty of the Graduate School of the University of Minnesota, Minneapolis, Minnesota, USA, January 2013.

[20] S. Rafie, H.S. Ho, and U. Chandra, *Applications of a BHA Analysis Program in Directional Drilling*, Proc. IADC/SPE Drilling Conf., pp. 345–354, Dallas, TX, USA, February 1986.

[21] M.F. Shakib, *Nonlinear Modeling for Dynamic Analysis of Directional Drilling Processes*, M.Sc. dissertation, Eindhoven University of Technology, The Netherlands, November 2017.

Effects of latency, motor inertia and filtering on stick-slip mitigation control

Roman J. Shor[1], Ulf Jakob F. Aarsnes[2] and Florent di Meglio[3]

[1]University of Calgary, Calgary, Canada
[2]International Research Institute of Stavanger (IRIS), Oslo, Norway
[3]Mines ParisTech, Paris, France

1 Introduction

Exploration and production of oil and gas in the deep subsurface, where hydrocarbon reservoirs are found at depths between 2,000 and 20,000 feet, requires that a narrow borehole, between 4 and 24 inches in diameter, be drilled using a slender drill string through a varied downhole environment and along an often snaking wellpath. Drill string vibrations, and their negative consequences on ROP and equipment, is a well known phenomenon when drilling for hydrocarbons. In particular, the torsional oscillations known as stick slip, which are considered to be the most destructive vibrations, are to be avoided.

Significant literature exists which seeks to explain the incidence of stick slip through various implementations of bit-rock interaction and various complexities of drill string dynamic models. The simplest models impose bit-rock interaction as a discontinuous frictional force at the bit and abstract the drill string as a lumped mass, representing the bottom hole assembly (BHA) inertia, and a torsional spring, representing the drill-string stiffness [5, 6]. These models may be confounded by introducing higher complexity dynamics at the bit-rock interaction or through higher order models along the drill-string [12, 13], but still assume that stick slip is incided due to the non-linearity of the frictional force at the bit. pAll these models have used to demonstrate the occurrence of the limit cycle which exhibits itself as stick-slip and may be used to various types of stick-slip mitigation controllers, including simple tuned PID controllers [11, 15], impedance matching controllers [7], H-infinity controllers [16], sliding mode controllers [14], and others.

2 Model

We use a distributed model, similar to [4, 3, 8] and described in detail in [2], where we consider only the torsional dynamics of the drill string. For angular motion, angular velocity and torque are denoted as as $\omega(t,x), \tau(t,x)$, respectively, with $(t,x) \in [0,\infty) \times [0,L]$. See Fig. 1 for a schematic indicating locations. For an infinitesimal element dx, the torque is found as the shear strain, or twist per unit length. Letting ϕ denote the angular displacement in the string s.t. $\frac{\partial \phi(t,x)}{\partial t} = \omega(t,x)$, we have $\tau(t,x) = JG\big(\phi(t,x) - \phi(t,x+dx)\big)/dx$, where J is the polar moment for inertia and G is the shear modulus. Hence the equations for the angular motion are given by

$$\frac{\partial \tau(t,x)}{\partial t} + JG\frac{\partial \omega(t,x)}{\partial x} = 0 \tag{1}$$

$$J\rho\frac{\partial \omega(t,x)}{\partial t} + \frac{\partial \tau(t,x)}{\partial x} = S(\omega,x), \tag{2}$$

where the source term S is modeled as

$$S(\omega,x) = -k_t\rho J\omega(t,x) - \mathcal{F}(\omega,x), \tag{3}$$

where k_t is a damping constant representing the viscous shear stresses and $\mathcal{F}(\omega)$ is a differential inclusion, to be described, representing the Coulomb friction between the drill string and the borehole. The viscous shear stress coefficient k_t represnts the combined damping effects of the viscous shear of the drilling mud and the rolling contact between drill string and the cuttings bed.

The lowermost section of the drill string is typically made up of drill collars which may have a great impact on the drill string dynamic due to their added inertia. In particular, the transition from the pipes to collars in the drill string will cause reflections in the traveling waves due to the change in characteristic line impedance [4]. We split the drill string into a pipe section with polar moment of inertia and lengths J_p, L_p and a collar section with the same parameters given as J_c, L_c.

2.1 Coulomb friction as an inclusion

The Coulomb friction is modeled as an inclusion

$$\begin{cases} \mathcal{F}(\omega,x) = F_d(x), & \omega > \omega_c, \\ \mathcal{F}(\omega,x) \in [-F_c(x), F_c(x)], & |\omega| < \omega_c, \\ \mathcal{F}(\omega,x) = -F_d(x), & \omega < -\omega_c, \end{cases} \tag{4}$$

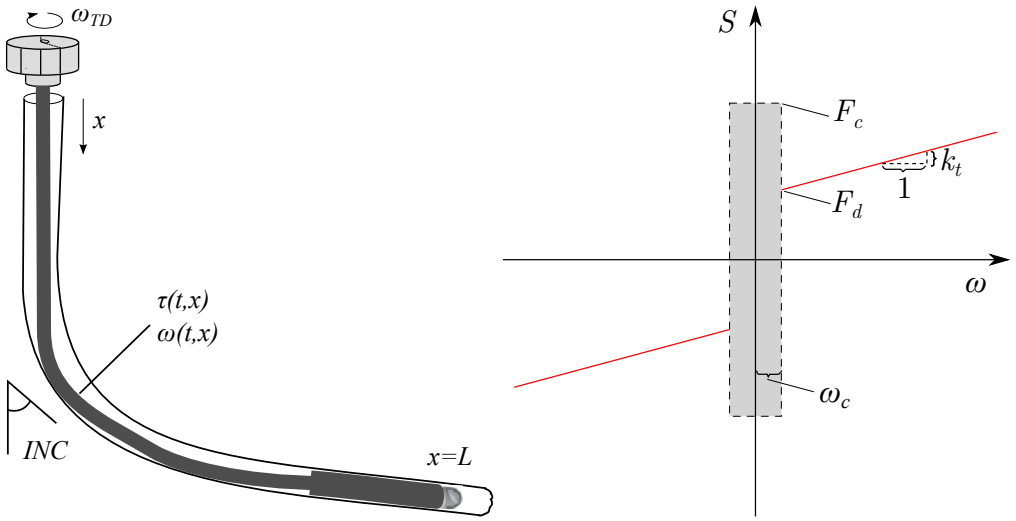

Figure 1: Schematic indicating the distributed drill string lying in deviate borehole (left). Schematic illustrating the four parameters determining the friction: the coulomb friction parameters ω_c, F_c, F_d and the viscous friction coefficient k_t, with the shaded region indicating the region of static torque, and the red curve the dynamic torque (right).

where ω_c is the threshold on the angular velocity where the Coulomb friction transitions from static to dynamic, F_d is the dynamic Coulomb torque, F_c is the static Coulomb torque, and $\mathcal{F}(\omega) \in [-F_c, F_c]$ denotes the inclusion where

$$\mathcal{F}(\omega, x) = -\frac{\partial \tau(t,x)}{\partial x} - k_t \rho J \omega(t,x) \in [-F_c(x), F_c(x)], \tag{5}$$

and take the boundary values $\pm F_c(x)$ if this relation does not hold. We define the non-dimensional coefficient $f_{rat} = F_c/F_d$ to help characterize the magnitude of the oscillations. The shape of the friction source term is illustrated in Fig. 1.

3 Model comparison with field data

To validate the modeling approach taken in the present work, a simulation study was undertaken to compare the behavior of the model to that of recorded field data. A field comparison is presented which exhibits inerita dominated oscillations, as categorized in [2]. Field data for a deviated well, the survey of which is shown in Figure 2, is considered. Rotational data – rotary rpm and torque – is recorded at 100 Hz and includes both setpoints and realized values. The

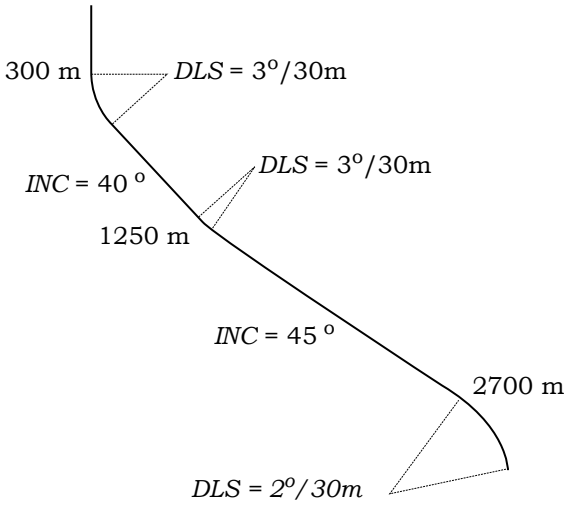

Figure 2: Wellbore survey of the field well

drill-string starts at rest with zero torque at the surface. However, the stored torsional energy within the drill-string is not known. The drill-string design is a

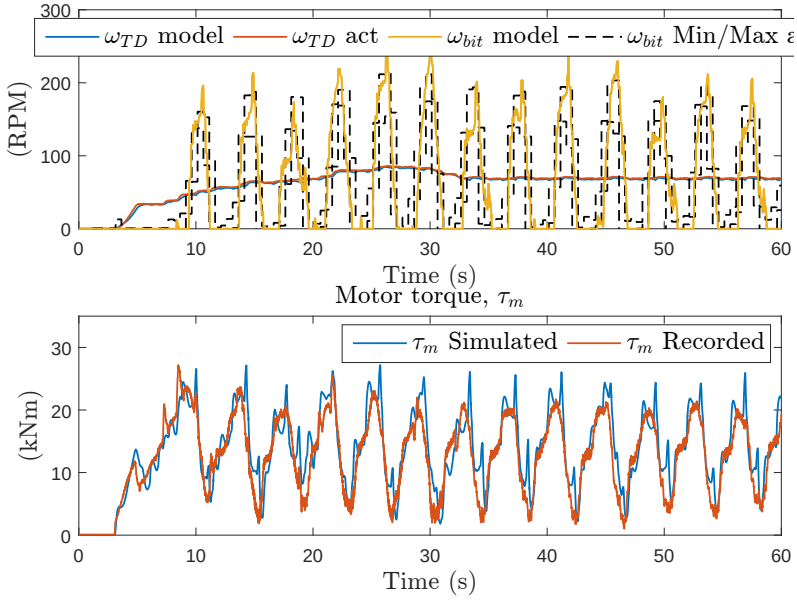

Figure 3: Recorded and simulated drill-string response at a bit depth of 1,733 m, using fitting parameters: $\mu = 0.34, f_{rat} = 0.55, \omega_c = 19$ (RPM).

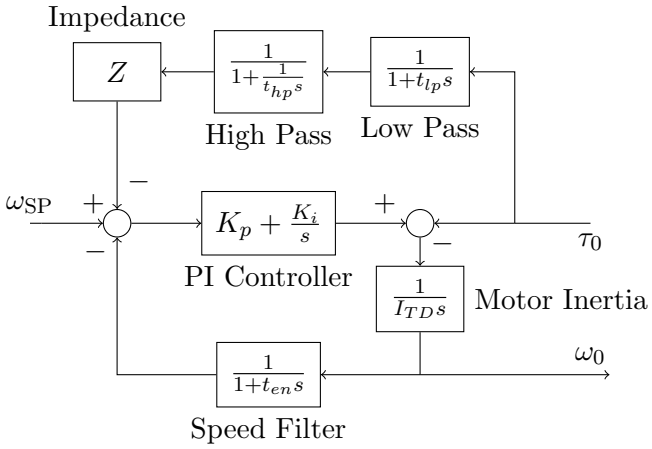

Figure 4: Control diagram for a ZTorque system with direct pipe torque measurement. For ZTorque $Z = 1/\zeta_p$ is used. If $Z = 0$, the control diagram is equivalent to a SoftTorque or stiff speed controller system.

simple directional assembly which is simplified to a 230 meter $5\frac{3}{4}$" OD BHA and monodiameter drillpipe to the surface. Downhole rpm and vibration data was collected for drilling performance improvement and control system verification and included continuous low frequency (0.5Hz) data as well as occasional burst sequences of high frequency data (125 Hz).

Recorded field data and a model fit for 1,733 m depth is shown in Figure 3. The top plot shows the surface (in red) and downhole (dashed) recorded data as well as the modeled data (in blue and yellow, respectively). The bottom plot shows surface torque, with recorded data in red and simulated data in blue.

4 Stick-slip Mitigation Controllers

A majority of drilling rigs in the field utilize AC electric top drives controlled using a variety of variable frequency drives – or inverters – which are capable of highly accurate, and often high frequency (> 20 Hz), rotary speed control. A majority of these controllers are simple stiff PI controllers, but two types of stick-slip mitigation controllers are widely deployed – the older SoftTorque / SoftSpeed systems and the newer ZTorque systems.

The behavior of a control system may evaluated through the use of a top-side reflection coefficient – a reflection of '1' indicates all energy is reflected back downhole, while a reflection of '0' means all energy is absorbed by the topdrive. Assuming for the moment a constant set-point, and defining the controller trans-

fer function $C(s) \equiv \frac{\tau_m}{\omega_0}$ we obtain the relation:

$$\frac{\tau_0(s)}{\omega_0(s)} = C(s) + I_{TD}s \equiv \bar{C}(s), \tag{6}$$

while the topside reflection coefficient is given as [11]

$$R(\omega) = \left| \frac{\bar{C}(s) - \zeta_p}{\bar{C}(s) + \zeta_p} \right|_{s=j\omega}. \tag{7}$$

4.1 Stiff controller

The industry standard controller that is most often used is a high gain PI control to ensure rapid tracking of the top drive set-point. For this study, we use the gains

$$K_p = 100\zeta_p, \qquad K_i = 5I_{TD}. \tag{8}$$

which is similar to gains typically used in the field.

4.2 SoftTorque

The current industry standard in handling torsional vibrations are the two products NOV's SoftSpeed [11, 9] and Shell's SoftTorque [7, 15]. The essential approach of all these solutions is to reduce the reflection coefficient at the top drive in a certain key frequency range [10].

The approach of SoftSpeed [11] is to set the proportional action to

$$K_p = 4\zeta_p, \tag{9}$$

and then tune the integral gain according to

$$K_i = (2\pi f_c)^2 I_{TD}^2, \tag{10}$$

where f_c is the frequency (in Hertz) where the minimum of $R(\omega)$ is achieved. Since the transfer funciton of an ideal PID controller writes $C(s) = K_p + \frac{K_i}{s} + K_d s$, the minimum of the reflection coefficient is obtained at

$$\underset{\omega}{\operatorname{argmin}}\, R(\omega) = \sqrt{\frac{K_i}{I_{TD} + K_d}} \equiv f_c 2\pi. \tag{11}$$

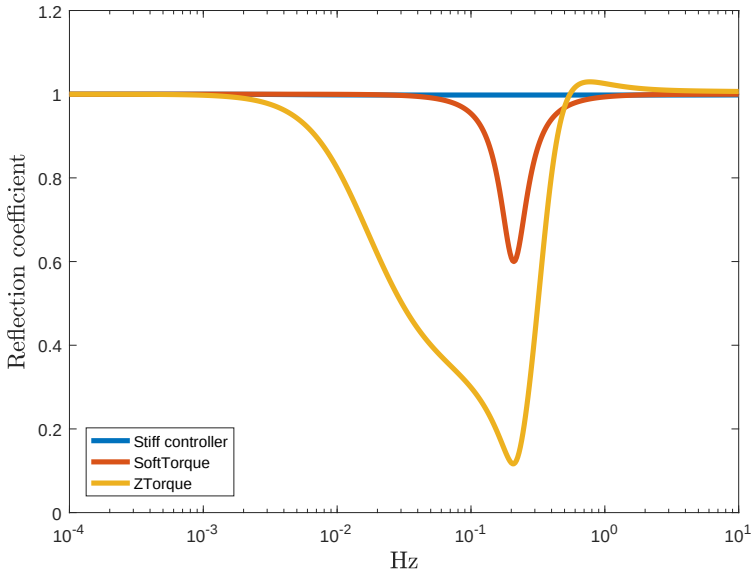

Figure 5: Topside reflection coefficient of the three considered controllers.

4.3 ZTorque

A newer embodiment of stick-slip mitigation control developed by Shell, *ZTorque*, seeks to minimize the reflection coefficient of the top drive for a wider range of frequencies by measuring the torque from between the drill string and top-drive τ_0, and using this in the feedback controller to "artificially" have the top-drive match the impedance of the drill-pipe ζ_p. The drill pipe impedance is given as $\zeta_p = J_p\sqrt{G_p\rho}$ where ζ_p is the characteristic line impedance of the drill string.

For a given pipe torque, the instantenous top drive rotary velocity necessary to match the pipe impedance is given by:

$$\omega_0(t) = \frac{1}{\zeta_p} \cdot \tau_0(t) \tag{12}$$

To ensure set point tracking, the control system uses a bandpass filter on the impedance matching rotary velocity – to exclude high frequency noise and low frequency set point changes – by combining a high-pass and low pass filter. Therefore, the PI controller acts on a combination of the tracking error $\omega_{\mathrm{SP}-\omega_0}$, and the band-pass filtered measured pipe torque $Z\frac{1}{s+\frac{1}{t_{hp}s}}\frac{1}{s+t_{lp}s}\tau_0$, i.e. the input

to the PI controller is

$$e_{PI} = \omega_{\mathrm{SP}} - \omega_0 - Z\frac{s}{(s+\frac{1}{t_{hp}})(1+t_{lp}s)}\tau_0 \tag{13}$$

where t_{hp}, t_{lp} are the high pass, low pass filter time constants. Note that the ω_0 measurement passes through an encoder, illustrated in Fig. 4 as a low-pass filter with time constant t_{en}. Typically, t_{lp} and t_{en} are around 1 to 10 milliseconds and t_{hp} is around 2 to 10 seconds but must be greater than the period of the first mode of stick-slip. The implementation studied in this talk assumes the presence of a torque sensor between the top drive and drillstring which is capable of real-time measurement of pipe torque, τ_0.

Topside reflection coefficient of the three considered controllers is shown in Fig. 5. The SoftTorque controller uses $K_p = 4\zeta_p, f_c = 0.2(\mathrm{Hz})$ and the ZTorque controller a 1 ms speed and low pass filters and a 10 second high pass filter.

5 Simulation study

We consider a rotation startup such as is required after each pipe connection procedure while drilling a well. In this scenario the stationary drill string is initially kept in place by the Coulomb friction until enough torque is built up to overcome it. At which point, pipe-rotation is initiated and the Coulomb friction is reduced as it changes from static to dynamic. The resulting release of the stored energy potentially pushes the drill string into a destructive stick slip limit cycle. We refer to [2] for a more detailed description of this phenomena, where it is shown that the simulation model used in the present talk is capable of effectively replicating this type of stick-slip phenomenon.

Figure 6 depicts time series of the bottom rotational velocity and topside torque for two sets of friction parameters μ and f_{rat}. It is clear from these simulations that ZTorque yields a much slower controller, but one that effectively avoids reflections in the relevant frequency range, thus mitigating the tendency of stick slip. The length of time necessary to reach the setpoint rotation speed is directly related to the time costant of the high pass filter in the ZTorque system. It is also clear that the severity of the stick slip, and the tendency of such oscillation to be initiated, is highly dependent on the friction parameters μ, f_{rat}. A thorough treatise of the topic is presented in [1].

6 Sensitivity to filtering and latency

Latency and filtering in rig systems may be included directly in the control system model presented above, and by evaluating the topside reflectivity as a

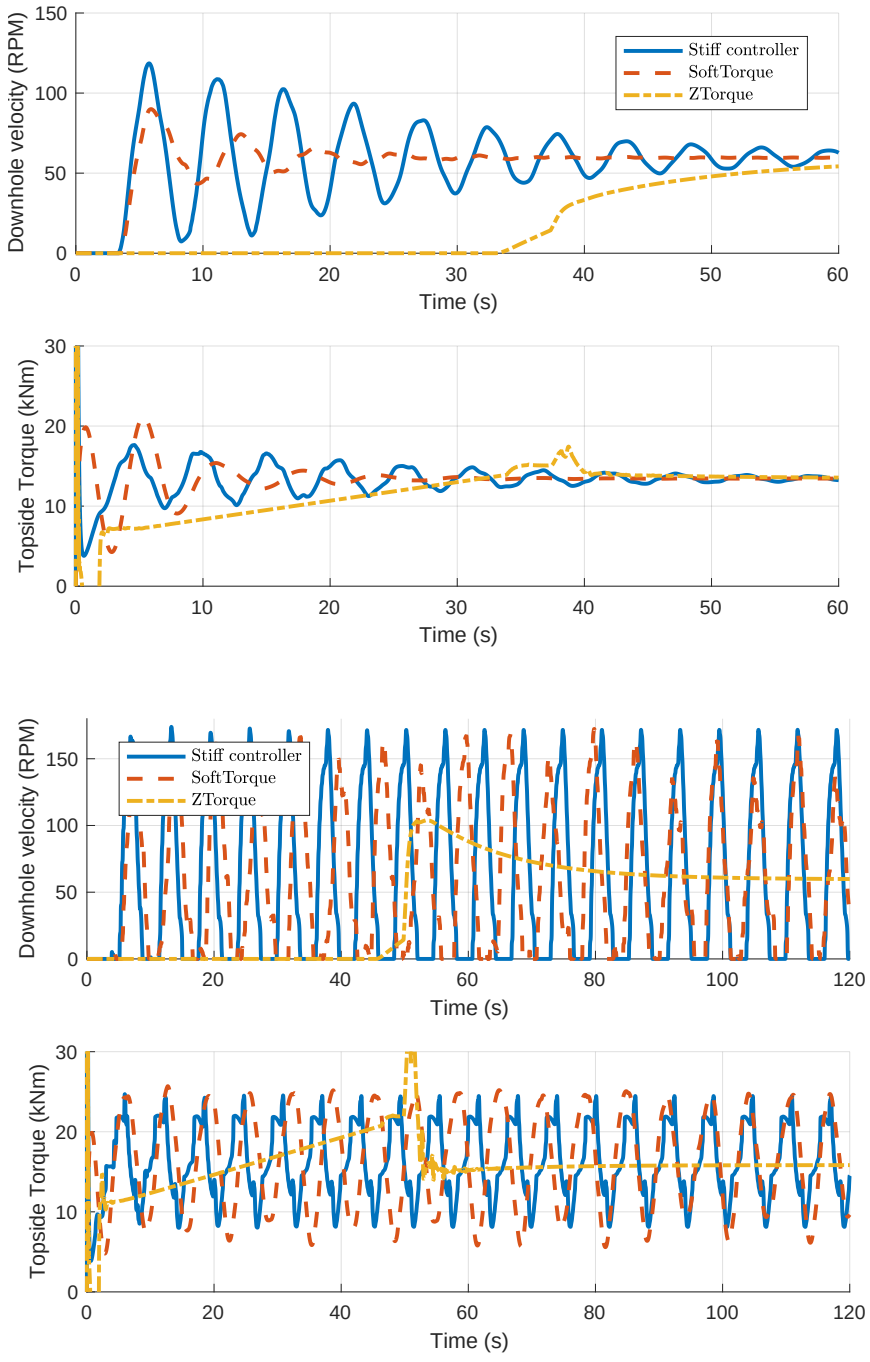

Figure 6: Bottom velocity (top) and topside torque (bottom) as a function of time, for $\mu = 0.2$ and $f_{rat} = 0.75$ (top) and $\mu = 0.3$ and $f_{rat} = 0.85$ (bottom), for each of the three controllers.

function of frequency, their effects on performance may be quantified. During this talk, a series of examples will be presented which will include the effects of top drives with large inertias, highly filtered torque or speed sensors and delays in inverter - control system communication. Every increase in filtering or latency leads to a decrease in system performance, but this performance degradation may still yield an effective system in certain scenarios.

References

[1] Ulf Jakob F Aarsnes, Florent Meglio, and Roman J Shor. Benchmarking of Industrial Stick-Slip Mitigation Controllers. In *IFAC Workshop on Automatic Control in Offshore Oil and Gas Production*, 2018.

[2] Ulf Jakob F. Aarsnes and Roman J Shor. Torsional vibrations with bit off bottom: Modeling, characterization and field data validation. *Journal of Petroleum Science and Engineering*, 163:712–721, apr 2018.

[3] Ulf Jakob F. Aarsnes and Nathan van de Wouw. Dynamics of a distributed drill string system: Characteristic parameters and stability maps. *Journal of Sound and Vibration*, 417:376–412, mar 2018.

[4] Ulf Jakob Flø Aarsnes and Ole Morten Aamo. Linear stability analysis of self-excited vibrations in drilling using an infinite dimensional model. *Journal of Sound and Vibration*, 360:239–259, jan 2016.

[5] J J Bailey and I. Finnie. An Analytical Study of Drill-String Vibration. *Transactions of the American Society of Mechanical Engineers*, (May 1960):122–127, 1960.

[6] Dmitriy Dashevskiy, Jens Rudat, and Linus Pohle. Model-Based Stability Analysis of Torsional Drillstring Oscillations. In *Proceedings of 2011 IEEE International Conferencce on Control Applications*, Denver, CO, 2011.

[7] Sicco Dwars. Recent Advances in Soft Torque Rotary Systems. In *Proceedings of 2015 SPE/IADC Drilling Conference*, number March, pages 17–19, London, United Kingdom, 2015.

[8] Christophe Germay, Vincent Denoël, and Emmanuel Detournay. Multiple mode analysis of the self-excited vibrations of rotary drilling systems. *Journal of Sound and Vibration*, 325(1-2):362–381, aug 2009.

[9] G.W. Halsey, A Kyllingstad, and A Kylling. Torque Feedback Used to Cure Slip-Stick Motion. In *SPE Annual Technical Conference and Exhibition*, pages 277–282. Society of Petroleum Engineers, apr 1988.

[10] Aage Kyllingstad. A Comparison of Stick-Slip Mitigation Tools. In *SPE/IADC Drilling Conference and Exhibition*, number March, pages 14–16. Society of Petroleum Engineers, mar 2017.

[11] Åge Kyllingstad and Pål Jacob Nessjøen. A New Stick-Slip Prevention System. In *Proceedings of SPE/IADC Drilling Conference and Exhibition*, number March, pages 17–19, 2009.

[12] R. I. Leine, D. H. van Campen, and W. J. G. Keultjes. Stick-slip Whirl Interaction in Drillstring Dynamics. *Journal of Vibration and Acoustics*, 124(2):209, 2002.

[13] K. Nandakumar and Marian Wiercigroch. Stability analysis of a state dependent delayed, coupled two DOF model of drill-string vibration. *Journal of Sound and Vibration*, 332(10):2575–2592, 2013.

[14] Eva M. Navarro-Lopez, Domingo Cort, and Domingo Cortes. Sliding-mode control of a multi-DOF oilwell drillstring with stick-slip oscillations. In *Proceedings of the 2007 American Control Conference*, pages 3837–3842, New York City, jul 2007. IEEE.

[15] D. John Runia, Sicco Dwars, and Ivo Petrus Jozef Maria Stulemeijer. A brief history of the Shell "Soft Torque Rotary System" and some recent case studies. In *SPE/IADC Drilling Conference*, pages 69–76. Society of Petroleum Engineers, mar 2013.

[16] Muhittin Yilmaz, Salman Mujeeb, and Naren Reddy Dhansri. A H-infinity control approach for oil drilling processes. *Procedia Computer Science*, 20:134–139, 2013.

ADVANCES IN CONTROL OF HYPERBOLIC PARTIAL DIFFERENTIAL EQUATIONS: OPPORTUNITIES FOR DRILLING

Florent Di Meglio[1], Ulf Jakob Aarsnes[2], Roman Shor[3]

[1]Centre Automatique et Systèmes, Mines ParisTech, Paris, France
[2]International Research Institute of Stavanger (IRIS), Oslo, Norway
[3]University of Calgary, Calgary, Canada

1 Introduction

The drilling process involves transport phenomena: mechanical deformation waves, pressure waves propagating into the drilling fluid, or simply the transport of mud, cuttings, and oil and gas in UnderBalanced Operations (UBO). These dynamics are often coupled and take a growing importance when the length of the well increases.

From a systems and control perspective, the industrial needs related to these phenomena span the whole field: set point tracking and disturbance rejection for pressure control in Managed Pressure Drilling (MPD), disturbance estimation for kick management, state estimation in UBO to monitor the amount of gas in the well, parameter estimation to perform reservoir characterization, or stabilization for severe slugging and mechanical vibrations. All of these problems have in common their distributed nature and, most importantly, high uncertainty.

Although the distributed nature of the transport phenomena is not necessary the bottleneck for all of these questions, it appears that some cases require the associated delays and wave propagation to be taken into account. We review here advances in boundary control and estimation of hyperbolic Partial Differential Equations that could bring solutions to some of these issues. We believe that the methods developed the past few years have the potential to be successfully applied to problems in drilling. Towards this end, we illustrate an application to friction estimation during stick-slip oscillations.

2 Torsional vibrations dynamics

To motivate the theoretical developments and illustrate their potential, we describe here a control problem representative of the class we tackle. Consider the drill-string depicted on Figure 1. It undergoes lateral, torsional and axial vibrations that propagate as

This work has been partially supported by the ANR project MACS-Drill ANR-15-CE23-0008-01.

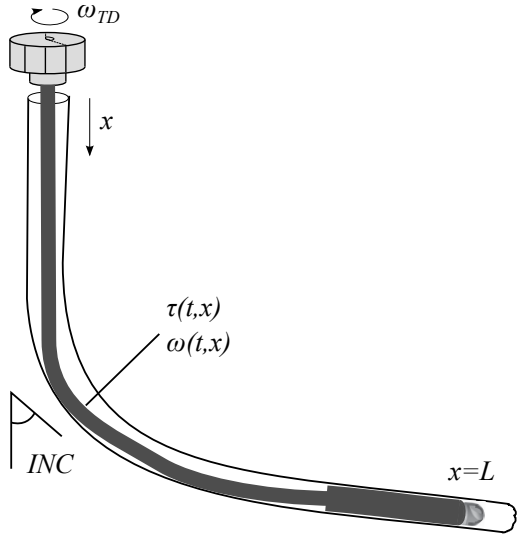

Figure 1: Schematic view of a drillpipe.

waves along its whole length. The causes for these detrimental oscillatory phenomena are many, generally associated with side forces [1] or cutting effects [12]. Importantly, the distributed nature of the wave propagation can play a predominant role, as illustrated in [4]. In [1], a model describing torsional dynamics is compared with field data, showing excellent accuracy. This result comes at the price of a careful tuning of the model parameters. More precisely, the model takes the form of a 1-D wave equation along the linear spatial dimension x, where the source term is due to frictional contact with the borehole and is modeled as

$$S(\omega,x) = -k_t \rho J \omega(t,x) - \mathscr{F}(\omega,x), \tag{1}$$

where k_t is a damping constant representing the viscous shear stresses between the pipe and drilling mud, $\omega(t,x)$ is the angular velocity at time t and position x, ρ is the pipe density and J its polar moment of inertia. The term $\mathscr{F}(\omega)$ is a differential inclusion, to be described, representing the Coulomb friction between the drill string and the borehole,

$$\begin{cases} \mathscr{F}(\omega,x) = F_d(x), & \omega > \omega_c, \\ \mathscr{F}(\omega,x) \in [-F_c(x), F_c(x)], & |\omega| < \omega_c, , \\ \mathscr{F}(\omega,x) = -F_d(x), & \omega < \omega_c, \end{cases} \tag{2}$$

where ω_c is the threshold on the angular velocity where the Coulomb friction transitions from static to dynamic, F_d is the dynamics Coulomb torque, and $\mathscr{F}(\omega) \in [-F_c, F_c]$

denotes the inclusion where

$$\mathscr{F}(\omega,x) = -\frac{\partial \tau(t,x)}{\partial x} - k_t \rho J \omega(t,x) \in [-F_c(x), F_c(x)], \tag{3}$$

and take the boundary values $\pm F_c(x)$ if this relation does not hold.

There is a large uncertainty in the distributed Coulomb friction terms $F_c(x)$, $F_d(x)$. In the next section, we design observers for hyperbolic PDEs in view of estimating these on-line from topside measurements only.

3 Control design for Hyperbolic PDEs: backstepping design

Backstepping is a control and observer design method first introduced for boundary control and observer design for PDEs in [13] and described in details in [8]. It relies on a change of variables such that control (resp. observer) design is "simple" in the new system of coordinates. We give here an example corresponding to the boundary control of two coupled transport equations which model, e.g., channel flow [3] or single-phase liquid flow, e.g. the annulus in Managed Pressure Drilling (MPD) [7]. Consider the following system of PDEs

$$\begin{pmatrix} u_t(t,x) \\ v_t(t,x) \end{pmatrix} + \begin{pmatrix} \lambda(x) & 0 \\ 0 & -\mu(x) \end{pmatrix} \begin{pmatrix} u_x(t,x) \\ v_x(t,x) \end{pmatrix} = \Sigma(x) \begin{pmatrix} u(t,x) \\ v(t,x) \end{pmatrix} \tag{4}$$

with the following boundary conditions

$$u(t,0) = d_0 v(t,0), \qquad u(t,1) = d_1 v(t,1) + U(t) \tag{5}$$

The variables u and v represent quantities (e.g. pressure waves) being transported along the spatial domain $x \in [0,1]$. The quantity u travels left to right while v travels in the opposite direction, i.e. we have $\lambda(x), \mu(x) > 0$. At the boundaries of the spatial domain, the waves are reflected with coefficients d_0 and d_1, with $|d_0 d_1| < 1$[1]. Inside of the domain, the two states are coupled through the matrix $\Sigma(x)$ typically representing friction and gravity effects. These coupling terms are responsible for poor transient performance and sometimes instability. Note that these equations usually stem from linearizing conservation laws around an equilibrium profile. Consider now the following change of coordinates

$$\begin{pmatrix} \alpha(t,x) \\ \beta(t,x) \end{pmatrix} = \begin{pmatrix} u(t,x) \\ v(t,x) \end{pmatrix} + \int_0^x K(x,y) \begin{pmatrix} u(t,y) \\ v(t,y) \end{pmatrix} dy \tag{6}$$

[1] This is a necessary assumption for the system to be robustly stabilizable [10].

Provided the kernel $K(x,y)$ is appropriately chosen, as described in [5], the equations satisfied by the new variables α and β read

$$\begin{pmatrix}\alpha_t(t,x)\\ \beta_t(t,x)\end{pmatrix}+\begin{pmatrix}\lambda(x) & 0\\ 0 & -\mu(x)\end{pmatrix}\begin{pmatrix}\alpha_x(t,x)\\ \beta_x(t,x)\end{pmatrix}=0 \tag{7}$$

with the following boudary conditions

$$\alpha(t,0)=d_0\beta(t,0),\qquad \beta(t,1)=d_1\alpha(t,1)+U(t)+\int_0^x L(x,y)\begin{pmatrix}\alpha(t,y)\\ \beta(t,y)\end{pmatrix}dy \tag{8}$$

for a certain known kernel $L(x,y)$. Notice that the coupling terms have been moved from the right-hand-side of the PDE to the controlled boundary of the domain. This suggests the following control law

$$U(t)=-k\alpha(t,1)-\int_0^x L(x,y)\begin{pmatrix}\alpha(t,y)\\ \beta(t,y)\end{pmatrix}dy \tag{9}$$

where k is a design parameter used to trade-off performance versus robustness. Controller (9) ensures convergence of the solutions of (7)–(8) and, equivalently of (5)–(**??**) with a decay rate $\frac{1}{d_1-k}$. Imposing $k=d_1$ leads to finite-time convergence to zero in theory, but with vanishing robustness margins, as detailed in [10, 6, 2]. Transformation (6) serves as the basis for many extensions. In particular, in [5], a Luenberger observer is designed, relying on boundary measurements. In [11], a slightly more general state-feedback controller is obtained through a Port-Hamiltonian approach.

In [9], an integrator is added to (9) to reject constant disturbances, along with a boundary observer design with added design parameters. This result in an implementable output-feedback control law with three degrees of freedom that have an intuitive impact on set point tracking performance, robustness to noise and uncertainty and stability. In the next section, we show how these results can be extended to the more industry-relevant model described in Section 1.

4 Application to friction estimation

4.1 State and parameter observer design

To estimate unmeasured states and uncertain friction terms, we consider the following observer, based on an approximation of the model of [1] plus linear output error injec-

tion terms

$$\dot{\hat{\omega}}_0 = -a_0\hat{\omega}_0 + b_0\hat{v}(0,t) + B_U U(t) - p_0(\hat{\omega}_0 - y(t)) \tag{10}$$
$$\hat{u}(0,t) = c_0\hat{\omega}_0(t) + d_0\hat{v}(0,t) - P_0(\hat{\omega}_0 - y(t)) \tag{11}$$
$$\hat{u}_t(x,t) = -\lambda(x)\hat{u}_x(x,t) + \sigma^{++}(x)\hat{u}(x,t) + \sigma^{+-}(x)\hat{v}(x,t) - p_u(\hat{\omega}_0 - y(t)) \tag{12}$$
$$\hat{v}_t(x,t) = \mu(x)v_x(x,t) + \sigma^{-+}(x)\hat{u}(x,t) + \sigma^{--}(x)\hat{v}(x,t) - p_v(\hat{\omega}_0 - y(t)) \tag{13}$$
$$\hat{v}(1,t) = c_1\hat{\omega}_1(t) + d_1\hat{u}(1,t) - P_1(\hat{\omega}_0 - y(t)) \tag{14}$$
$$\dot{\hat{\omega}}_1 = -a_1\hat{\omega}_1 + b_1\hat{u}(1,t) + \hat{d}(t) - p_1(\hat{\omega}_0 - y(t)) \tag{15}$$

with

$$\begin{cases} d(\omega) = \hat{d}_d, & \hat{\omega}_1 > \omega_c, \\ d(\omega) \in [-\hat{d}_c, \hat{d}_c], & |\hat{\omega}_1| < \omega_c, \\ d(\omega) = -\hat{d}_d, & \hat{\omega}_1 < -\omega_c. \end{cases} \tag{16}$$

and where $\hat{u}$, $\hat{v}$ are defined as

$$u = \hat{\omega} + \frac{c_t}{JG}\hat{\tau}, \quad \hat{v} = \hat{\omega} - \frac{c_t}{JG}\hat{\tau}, \tag{17}$$

where $c_t = \sqrt{\frac{\rho}{J}}$ is the velocity of the torsional wave. This model is obtained by writing the equations in Riemann coordinates and lumping the Bottom Hole Assembly (BHA) into a single inertial element of rotational velocity ω_1. Moreover, we have lumped the inclusion representing the Coloumb friction at the ODE giving the downhole boundary condition. This approximation is typically amenable given either of the following two assumptions:

- Stabilizers located at the BHA ensures that a significant part of the total torque on the drill-string from side forces is acting on the BHA.
- The inertia of the BHA is sufficiently large so as to ensure that the torque from the BHA is large compared to that of the distributed side forces on the pipe. This is a qualitative observation seen from simulations.

However, if both these points do not hold, the approximation could cause the approach described in this paper to fail. The parameters $\hat{d}_d$ and $\hat{d}_c$ are chosen to satisfy the following update laws

$$\begin{pmatrix} \dot{\hat{d}}_d(t) \\ \dot{\hat{d}}_c(t) \end{pmatrix} = \begin{cases} \begin{pmatrix} k_1(\omega_0 - y(t)) \\ k_2(\omega_0 - y(t)) \end{pmatrix} & |\hat{\omega}_1| > \omega_c \\ \begin{pmatrix} k_1(\omega_0 - y(t)) \\ -k_2(\omega_0 - y(t)) \end{pmatrix}, & |\hat{\omega}_1| < \omega_c, \end{cases} \tag{18}$$

with $k_1, k_2 > 0$. Using a transformation similar to (6), one can find values of the observer gains and update gains such that when the observer velocity is non-zero, i.e. the observer state is in slip mode (rather than sticking), then (10)–(15),(18) converges to the true state. Although no proof of convergence is available for the full nonlinear observer, this approach yields promising results when applied to field data, as described in Section 3.2.

4.2 Field data validation

We have validated the approach by applying it to a data set corresponding to a 1733 meter-long well with an inclination pattern similar to the one schematically depicted on Figure 1. Since no bottom velocity measurement is available for this dataset, we evaluate the performance of the observer using the following two metrics

- we use, as the plant, the simulation model of [1]. The result of this comparison is depicted on Figure 2: the BHA velocity is accurately estimated and the friction parameter estimates converge to constant values.
- we use field data and vary the initial condition of the friction parameter estimates. These results are depicted on Figure 3. One can readily check that the estimates converge to roughly the same value, regardless of the initial condition, suggesting some form of robustness of the proposed approach.

References

[1] Ulf Jakob F. Aarsnes and Roman J Shor. Torsional vibrations with bit off bottom: Modeling, characterization and field data validation. *Journal of Petroleum Science and Engineering*, 163:712–721, apr 2018.

[2] Jean Auriol and Florent Di Meglio. Minimum time control of heterodirectional linear coupled hyperbolic pdes. *Automatica*, 71:300–307, 2016.

[3] Georges Bastin and Jean-Michel Coron. On boundary feedback stabilization of non-uniform linear $2\times$ 2 hyperbolic systems over a bounded interval. *Systems & Control Letters*, 60(11):900–906, 2011.

[4] Eric Cayeux, Roman Shor, Adrian Ambrus, Parham Pournazari, Pradeepkumar Ashok, and Eric van Oort. From shallow horizontal drilling to ERD wells: How scale affects drillability and the management of drilling incidents. *Journal of Petroleum Science and Engineering*, 160(October 2017):91–105, jan 2018.

[5] Jean-Michel Coron, Rafael Vazquez, Miroslav Krstic, and Georges Bastin. Local exponential h^2 stabilization of a $2\times$ 2 quasilinear hyperbolic system using backstepping. *SIAM Journal on Control and Optimization*, 51(3):2005–2035, 2013.

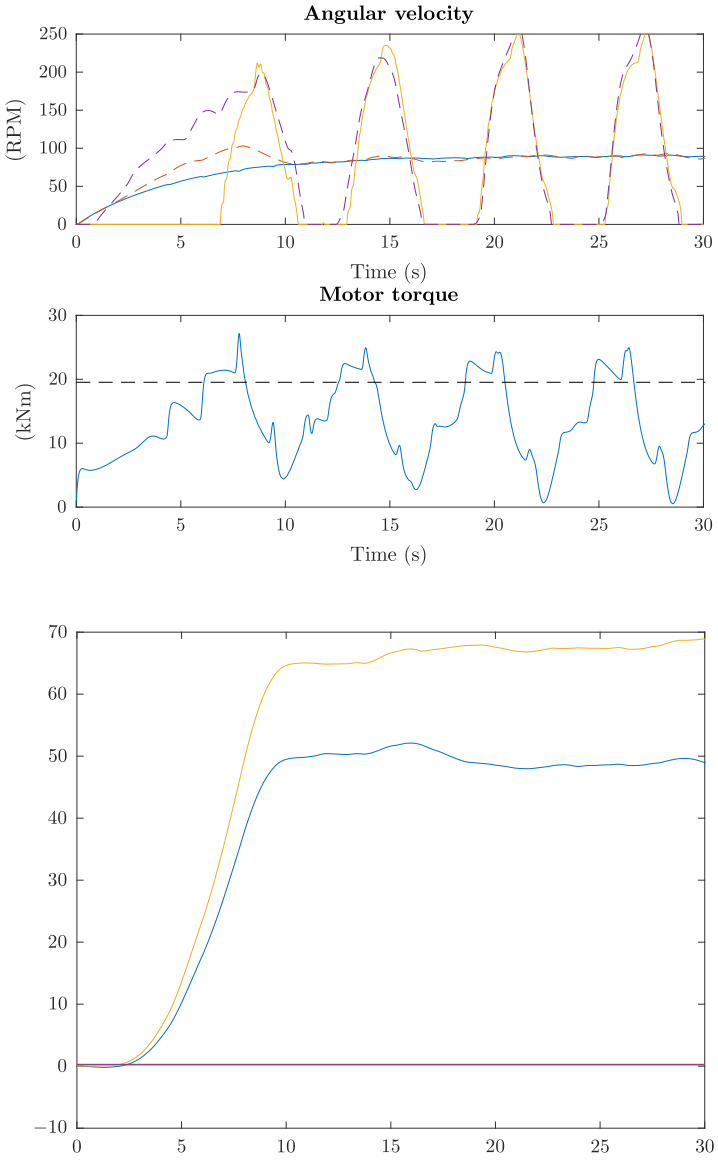

Figure 2: Plant (simulation model) and observer velocities and torque (top) and friction parameters estimates (bottom). Notice the large initial error in the latter.

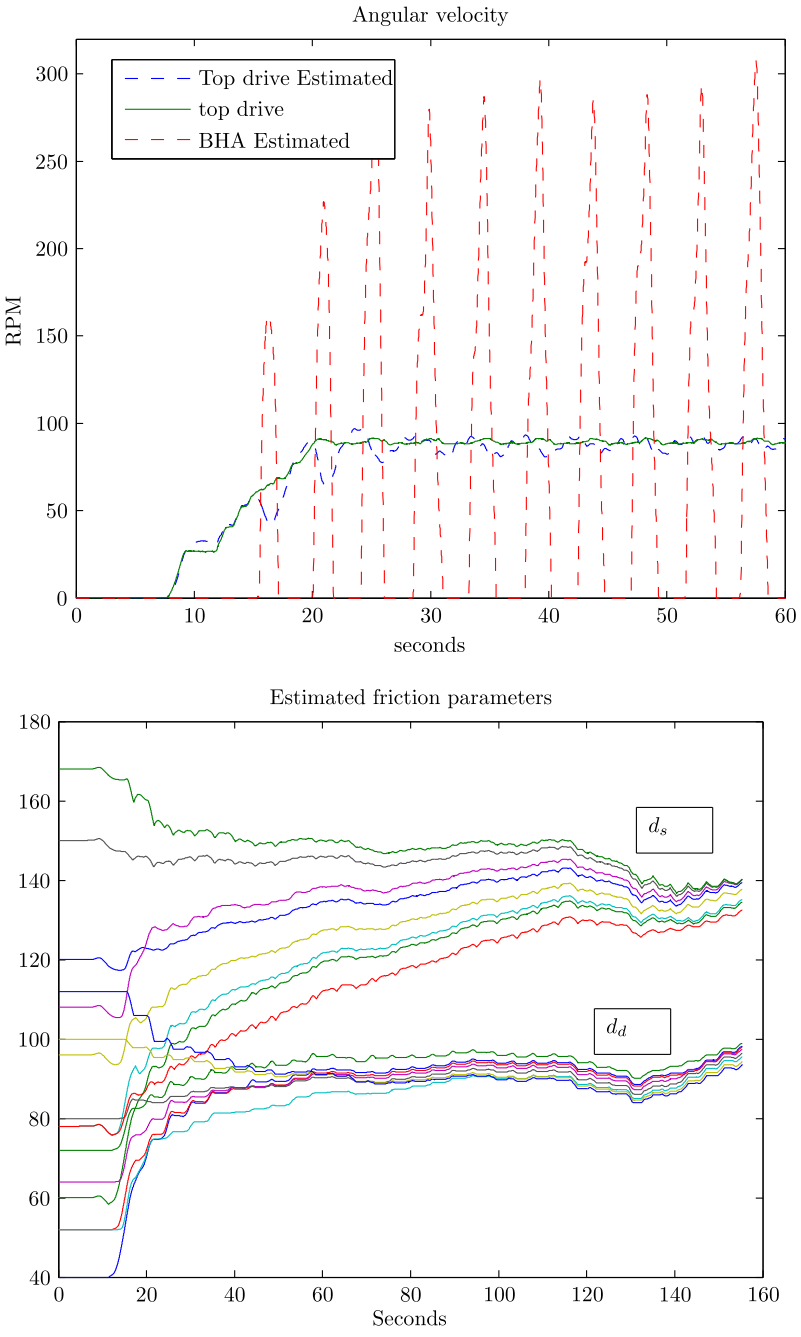

Figure 3: Plant (field data) and observer velocities and torque (top) and friction parameters estimates (bottom).

[6] Jack K Hale and Sjoerd M Verduyn Lunel. Strong stabilization of neutral functional differential equations. *IMA Journal of Mathematical Control and Information*, 19(1 and 2):5–23, 2002.

[7] Agus Hasan. Adaptive boundary control and observer of linear hyperbolic systems with application to managed pressure drilling. In *ASME 2014 Dynamic Systems and Control Conference*, pages V001T09A003–V001T09A003. American Society of Mechanical Engineers, 2014.

[8] Miroslav Krstic and Andrey Smyshlyaev. *Boundary control of PDEs: A course on backstepping designs*, volume 16. Siam, 2008.

[9] Pierre-Olivier Lamare, Jean Auriol, Florent Di Meglio, and Ulf Jakob F Aarsnes. Robust output regulation of 2 x 2 hyperbolic systems: Control law and input-to-state stability. In *American and Control Conference*, 2018.

[10] Hartmut Logemann, Richard Rebarber, and George Weiss. Conditions for robustness and nonrobustness of the stability of feedback systems with respect to small delays in the feedback loop. *SIAM Journal on Control and Optimization*, 34(2):572–600, 1996.

[11] Hector Ramirez, Hans Zwart, Yann Le Gorrec, and Alessandro Macchelli. On backstepping boundary control for a class of linear port-hamiltonian systems. In *Decision and Control (CDC), 2017 IEEE 56th Annual Conference on*, pages 658–663. IEEE, 2017.

[12] Thomas Richard, Christophe Germay, and Emmanuel Detournay. Self-excited stick-slip oscillations of drill bits. *Comptes Rendus Mécanique*, 332(8):619–626, aug 2004.

[13] Andrey Smyshlyaev and Miroslav Krstic. Closed-form boundary state feedbacks for a class of 1-d partial integro-differential equations. *IEEE Transactions on Automatic Control*, 49(12):2185–2202, 2004.

List of Participants

Bernt Sigve Aadnøy
Department of Energy and Petroleum Engineering
University of Stavanger
Stavanger Norway
bernt.aadnoy@uis.no

Ulf Jakob F. Aarsnes
International Research Institute of Stavanger
Oslo, Norway
ujfa@iris.no

Mohammad Hossein Abbasi
Centre for Analysis, Scientific Computing and Applications
Eindhoven University of Technology
Eindhoven Netherlands
m.h.abbasi@tue.nl

Adrian Ambrus
International Research Institute of Stavanger
Stavanger, Norway
Adrian.Ambrus@iris.no

Arviandy G. Aribowo
Department of Mechanical Engineering
Eindhoven University of Technology
Eindhoven, Netherlands
A.G.Aribowo@tue.nl

Bala Balachandran
Department of Mechanical Engineering
University of Maryland
College Park, MD, USA
balab@umd.edu

Bence Beri
Department of Applied Mechanics
Budapest University of Technology and Economics
Budapest, Hungary
beri@mm.bme.hu

Eric Cayeux
International Research Institute of Stavanger
Stavanger, Norway
eric.cayeux@iris.no

Shilin Chen
Halliburton Drill Bits & Services
Houston, TX, USA
Shilin.Chen@Halliburton.com

Robert Darbe
Sperry Drilling - Halliburton
Houston, TX, USA
Robert.Darbe@Halliburton.com

Emmanuel Detournay
Department of Civil Engineering
University of Minnesota
Minneapolis, MN, USA
emmanuel.detournay@gmail.com

Florent di Meglio
Centre Automatique et Systmes
MINES ParisTech
Paris, France
florent.di_meglio@mines-paristech.fr

John Morten Godhavn
Statoil
Trondheim, Norway
jmgo@statoil.com

Espen Hauge
Statoil
Trondheim, Norway
eshau@statoil.com

Sigve Hovda
Department of geoscience and petroleum
Norwegian University of Science and Technology
Trondheim, Norway
sigve.hovda@ntnu.no

Maja Ignova
Schlumberger
Cheltenham, Gloucestershire, United Kingdom
MIgnova@slb.com

Benjamin Jeffryes
Schlumberger Cambridge Research
Cambridge, United Kingdom
bpjeffryes@slb.com

Glenn-Ole Kaasa
Kelda
Porsgrunn, Norway
gok@kelda.no

Julien Marck
Sperry Drilling - Halliburton
Houston, TX, USA
Julien.marck@halliburton.com

Sajad Naderi
Department of Mechanical Engineering
Eindhoven University of Technology
Eindhoven, Netherlands
sj.lordejani@gmail.com

Paul Pastucek
ExxonMobil
Houston, TX, USA
paul.pastusek@exxonmobil.com

Alexei Pavlov
Department of geoscience and petroleum
Norwegian University of Science and Technology
Trondheim, Norway
alexey.pavlov@ntnu.no

Greg Payette
ExxonMobil
Spring, TX, USA
gregory.s.payette@exxonmobil.com

Nils Reimers
Tomax
Stavanger, Norway
Nils.Reimers@tomax.no

Fahim Shakib
Department of Mechanical Engineering
Eindhoven University of Technology
Eindhoven, Netherlands
m.f.shakib@student.tue.nl

Roman Shor
Department of Chemical and Petroleum Engineering
University of Calgary
Calgary, Canada
roman.shor@ucalgary.ca

Xianfeng Song
Department of Engineering Cybernetics
Norwegian University of Science and Technology
Trondheim, Norway
xianfeng.song@ntnu.no

Dan Sui
IEP, Department of Energy and Petroleum Engineering
University of Stavanger
University of Stavanger
Stavanger, Norway
dan.sui@uis.no

Herman Y. Sutarto
Pusat Riset Energi, PT. (PRE)
East Continent Energy Indonesia (ECEI)
Jakarta, Indonesia
hytotok@gmail.com

Torstein Thingnæs
National Oilwell Varco
Stavanger, Norway
Torstein.Thingnes@nov.com

Kaixiao Tian
Department of Civil Engineering
University of Minnesota
Minneapolis, MN, USA
tianx274@umn.edu

Nathan van de Wouw
Department of Mechanical Engineering
Eindhoven University of Technology
Eindhoven, Netherlands
n.v.d.wouw@tue.nl

Naveen Velmurugan
MINES ParisTech
Paris, France
naveen.velmurugan@mines-paristech.fr

Pankaj Wahi
Department of Mechanical Engineering
Indian Institute Of Technology Kanpur
Kanpur, Uttar Pradesh
wahi@iitk.ac.in
Dapeng Zhao
Sintef
Trondheim, Norway
dapeng.zhao@sintef.no